# Source Signatures of Fine Particulate Matter from Petroleum Refining and Fuel Use

Gerald P. Huffman[1], Frank E. Huggins[1], Naresh Shah[1], Artur Braun[1], Yuanzhi Chen[1], J. David Robertson[2], Joseph Kyger[2], Adel F. Sarofim[3], Ronald J. Pugmire[3], Henk L.C. Meuzelaar[3], and JoAnn Lighty[3]
[1]University of Kentucky
[2]University of Missouri
[3]University of Utah

Contact: Gerald P. Huffman, (859) 257-4027; huffman@engr.uky.edu

**July 31, 2003**

**Final report on research supported by the by the U.S. Department of Energy (FE/NPTO) under contract No. DE-AC-99BC15220. Support was also provided by the National Science Foundation under CRAEMS grant CHE-0089133.**

UNIVERSITY OF KENTUCKY

CFFS

# Source Signatures of Fine Particulate Matter from Petroleum Refining and Fuel Use

## Abstract

The molecular structure and microstructure of a suite of fine particulate matter (PM) samples produced by the combustion of residual fuel oil and diesel fuel were investigated by an array of analytical techniques. Some of the more important results are summarized below.

*Diesel PM (DPM):* A small diesel engine test facility was used to generate a suite of diesel PM samples from different fuels under engine load and idle conditions. C XANES, $^{13}C$ NMR, XRD, and TGA were in accord that the samples produced under engine load conditions contained more graphitic material than those produced under idle conditions, which contained a larger amount of unburned diesel fuel and lubricating oil. The difference was enhanced by the addition of 5% of oxygenated compounds to the reference fuel. Scanning transmission x-ray micro-spectroscopy (STXM) was able to distinguish particulate regions rich in C=C bonds from regions rich in C-H bonds with a resolution of ~50 nm. The former are representative of more graphitic regions and the latter of regions rich in unburned fuel and oil. The dominant microstructure observed by SEM and TEM consisted of complex chain-like structures of PM globules ~20-100 nm in mean diameter, with a high fractal dimension. High resolution TEM revealed that the graphitic part of the diesel soot consisted of onion-like structures made up of graphene layers. Typically 3-10 graphene layers make up the "onion rings", with the layer spacing decreasing as the number of layers increases.

*ROFA PM:* Residual oil fly ash (ROFA) PM has been analyzed by a new approach that combines XAFS spectroscopy with selective leaching procedures. ROFA $PM_{2.5}$ and $PM_{2.5+}$ produced in combustion facilities at the U.S. EPA National Risk Management Research Laboratory (NRML) were analyzed by XAFS before and after leaching with water, acid (1N HCl), and pentane. Both water and acid leaching removed most of the metal sulfates, which were the dominant phase present for most metals (V, Ni, Zn, etc.). This allowed conclusive identification in the leaching residue of important secondary sulfide and oxide phases, including Ni sulfide, a toxic and carcinogenic phase observed in the leached $PM_{2.5+}$ samples. Other significant secondary phases identified included $V_2O_4$, V sulfide, and $NiFe_2O_4$.

**Table of contents**

# Source Signatures of Fine Particulate Matter from Petroleum Refining and Fuel Use

**DOE (FE/NPTO) Contract No. DE-AC26-99BC15220**

## Executive Summary

Prepared by Gerald P. Huffman, Principal Investigator
Consortium for Fossil Fuel Science & Dept. of Chemical & Materials Engineering, University of Kentucky, 107 Whalen Building, 533 S. Limestone St., Lexington, KY 40506
Contact information: (859) 257-4027; huffman@engr.uky.edu

### Introduction

Numerous studies [1-4] have demonstrated a correlation between the concentration of airborne particulate matter (PM) <2.5 μm in mean diameter ($PM_{2.5}$) and human morbidity and mortality due to cardiovascular disease. As summarized in a recent review [5], the combustion of fossil fuels for the generation of electrical power and for transportation is a major source of $PM_{2.5}$. This investigation has been focused on determining the molecular structure and microstructure of combustion aerosols derived from petroleum. The principal objective of the research is to identify structural source signatures for $PM_{2.5}$ derived from petroleum refining and combustion of petroleum-derived fuels, particularly diesel fuel. An important secondary objective is to identify structural features that may be important for human health considerations.

### Experimental Approach

The combustion of petroleum-based fuel fuels produces a complex array of PM products. Therefore, we are employing an array of powerful analytical techniques to determine their molecular structure and microstructure. These techniques are briefly summarized below.

- X-ray absorption fine structure (XAFS) spectroscopy provides information on the molecular structure, valence states, and speciation of both major and trace elements.
- Scanning x-ray microspectroscopy (SXM) is used to image and obtain XAFS spectra of individual particles, with a resolution of approximately 50 nm.
- X-ray ray fluorescence (XRF), high-resolution inductively coupled plasma – mass spectrometry (ICP-MS), and instrumental neutron activation analysis (INAA) provide major, minor and trace element concentrations.
- ICP-MS is being used to measure measurement of sulfur isotopic and ratios to determine the percentage of ammonium sulfate in $PM_{2.5}$ derived from different fossil fuels.
- Accelerator MS is being used to investigate the use of $^{14}C$ as a marker to distinguish between petrogenic and biogenic sources of carbon in $PM_{2.5}$.
- Thermal desorption (TD) GC/MS provides information on the structure of volatile organic compounds.
- $^{13}C$ NMR and C K-shell XANES are used to determine the molecular and skeletal structure of carbon.
- Computer-controlled scanning electron microscopy (CCSEM) provides particle size distributions (PSD), morphologies, and composition diagrams for particles down to ~ 0.2 μm in diameter.

- High resolution transmission electron microscopy (HRTEM) and electron energy loss spectroscopy (EELS) is used to investigate the microstructure and molecular structure of ultrafine particles (1 nm - 0.2 μm in diameter).
- Mössbauer spectroscopy provides quantitative iron phase distributions.

These techniques have been used to characterize the structure of variety of petroleum-based combustion PM samples in this investigation. These included residual oil fly ash (ROFA) PM prepared in combustion experiments at the U.S. Environmental Protection Agency (EPA) National Risk Management Research Laboratory (NRMRL) in Research Triangle Park, NC, a suite of diesel emission PM samples generated in experiments at the University of Utah using a small diesel engine test facility, PM emissions from a jet engine test facility at the Air Force Research Laboratory at Wright Patterson Air Force Base in Dayton, Ohio, and ambient PM samples collected in several locations. The results are briefly summarized below.

## Results and Discussion

***Diesel PM:***

A suite of six diesel PM samples was generated in a small diesel engine test facility at the University of Utah. The samples were produced with the engine running under either load or idle conditions using a reference diesel fuel and the reference fuel plus 5% of two oxygenate additives. The structure of this suite of diesel PM samples has been thoroughly investigated by a range of different analytical techniques. The principal results obtained for the structural properties of this suite of diesel PM samples are briefly summarized below.

1. Carbon x-ray absorption near edge spectra (XANES) demonstrated that the ratio of graphitic carbon to unburned diesel fuel and lube oil was higher in diesel PM produced when the diesel engine was running under load than under idle conditions. The difference was increased substantially for diesel fuels containing 5% of oxygenate additives, which also significantly reduce the total amount of diesel PM emitted.
2. Scanning x-ray transmission microspectroscopy (STXM) was able to identify carbon with rich in C=C or C-H bonds with a resolution of ~50 nm. The former were associated primarily with graphitic soot and the latter with unburned diesel fuel or lubricating oil.
3. STXM measurements on diesel soot was shown to be capable of distinguishing rich in graphitic soot from regions rich in unburned diesel fuel or lubricating oil with a resolution of ~100 nm.
4. High resolution TEM provides significant insight into the structure of carbonaceous PM emitted from diesel engines. Two significant observations should be emphasized.
   - Diesel PM exhibits a distinctive microstructure that consists primarily of three dimensional chain-like structures of 20-100 nm primary PM globules.
   - High magnification, high resolution TEM reveals that the primary globules consist of onion-like structures made up of graphene layers. Typically 3-10 graphene layers make up the “onion rings”, with the layer spacing decreasing from approximately 4.5 to 3.4 nm as the number of layers increases.
5. A method of correlating sample conductivity with graphene layering in diesel soot samples was developed. The method relies on measuring a graphite conductance factor from the change in the Q value of an RF coil when a measured amount of sample is placed in the coil.

The technique is useful for determining the amount of graphitic carbon in diesel PM. The results correlate well with $^{13}C$ NMR linewidths and with XRD data.

6. X-ray diffraction (XRD) established a graphitic crystallite width parameter that correlated well with the graphite conductance factor established by Pugmire and co-workers using $^{13}C$ NMR.
7. Small angle x-ray scattering (SAXS) was used to determine several important parameters for diesel soot. These included the mean diameter of the primary diesel particulates, the mean size of diesel PM aggregates, and the fractal dimensions of the diesel PM aggregates.
8. Thermogravimetric analysis (TGA) results were consistent with the conclusion that the diesel PM consisted of a graphitic soot plus unburned diesel fuel and lubricating oil, and that the latter component was smaller under engine load than under engine idle conditions.
9. An aromaticity factor for diesel PM was established from the intensity of aliphatic sidebands in the XRD patterns.

***Jet PM:***

TEM was used to examine PM collected during jet engine tests conducted at the Air Force Research Laboratory (AFRL) at the Wright Patterson Air Force Base. The preliminary results are as follows.

1. With the jet engine running under cruise conditions, chain-like structures of 20-100 nm primary PM globules very similar to the diesel PM are observed. Under idle conditions, larger, more rounded, agglomerates are observed.
2. Attempts to observe graphitic structures at higher magnification were unsuccessful, due to the growth of unusual fibrous carbon structures. Such structures could arise from the volatilization and re-deposition of unburned fuel and lube oil.

***ROFA PM:***

The combination of leaching using aqueous or acid solutions with XAFS spectroscopy has revealed a wealth of information about minor phases present in residual oil fly ash (ROFA) PM samples. These studies have significantly augmented our earlier studies based solely XAFS examination of the original bulk material. Some of the conclusions are given below.

It has shown conclusively that sulfates are the dominant form of occurrence of most metals in ROFA PM and that most metals exhibit minor sulfide and oxide occurrences. The major exceptions to this overall scheme are (i) iron, which appears not to form significant sulfates; and (ii) base metals such as lead and copper, which appear not to form oxides. The sulfide occurrences constitute a higher fraction of the metal in the coarse (>2.5 μm) PM fractions compared to the fine (<2.5 μm) PM fractions. In contrast, oxide phases tend to be found only in the finest PM < 2.5 um fractions. We suspect that these differences relate to the combustion process and that the oxide is formed as burn-out goes closer to completion, whereas sulfide is preserved in the more carbon-rich coarser particulate. It is worth noting that at least one of the sulfides identified, Ni sulfide, is a toxic compound.

***Other results for carbonaceous PM:***

Upgrades to the small diesel engine test facility at the University of Utah enable better engine control, temperature sensing, air- flow control, and monitoring of brake-specific fuel

consumption and horsepower. With this improved engine control installed, a test matrix has been devised that will systematically investigate diesel PM as a function of engine load, cetane number, and fuel composition.

Factor analysis was performed on TD/GC/MS data obtained from PM samples collected along the US/Mexican boarder near Juarez, Mexico and El Paso, Texas. The results show a clear demarcation between high concentrations of PAH's (associated with brick kilns) and animal fatty acids (associated with cooking) on the Mexican side of the border, and of fossil terpenoids (associated with incomplete combustion of petroleum-derived fuels) plus alcohols and ketones (associated with automotive catalytic converters) on the U.S. side.

Fractal dimension analysis based on SEM or TEM particle shapes appears to be a useful new method to quantitatively characterize carbonaceous particles from combustion sources.

Collaboration has been initiated with the Center for Accelerator Mass Spectrometry to investigate the use of $^{14}C$ as a marker to distinguish between petrogenic and biogenic sources of carbon in $PM_{2.5}$.

One of the primary goals of this CRAEMS project is to develop new and better source signature variables that can be used to identify source emissions. For example, most source-receptor models assign the sulfate observed in ambient particulate to sulfur dioxide produced by coal combustion or emitted from vehicle exhaust. This model may, however, be overestimating the contribution of fossil fuel to the sulfate component of ambient particulate. We have developed a method for determining sulfur isotope ratios and are now investigating the possibility of combining isotope ratio data with trace-element and mode-of-occurrence data to determine what fraction of the sulfate in $PM_{2.5}$ originates from coal combustion versus, for example, combustion of fossil fuels for transportation.

Since lead was removed from gasoline, there has not been an adequate elemental signature for gasoline vehicle emissions and researchers have had to rely upon challenging and lengthy organic compound analysis. We have developed analytical methods for measuring the platinum group elements in fine air particulate samples and are working with Environment Canada to investigate how this source signature varies from in-use light duty gasoline motor vehicles.

## Conclusions

Significant progress has been made towards the goal of identifying structural source signatures of $PM_{2.5}$ derived from petroleum refining and fuel use. Some of the more useful results with regard to source attribution and possible effects on human health are summarized below.

*Diesel PM:*

Measurements by carbon XANES and STXM, $^{13}C$ NMR, XRD, and GC/MS establish that diesel PM is a mixture of graphitic soot and unburned or partially reacted diesel fuel and lubricating oil. Methods of determining the graphitic content of diesel PM were established using both XRD and a graphite conductance factor measured by the electrical response of an RF coil.

TEM and SEM studies established that diesel PM exhibits a distinctive microstructure that consists primarily of three dimensional chain-like structures of 20-100 nm primary PM globules. High resolution, high magnification TEM established that the graphitic component of the diesel PM consists of "onion-like" structures that typically consist of approximately 3-10 concentric graphene layers.

*ROFA PM:*
Most of the ROFA PM investigated was prepared in a 732 kW boiler typical operations in refineries or other industrial settings. As reported earlier [6,7], the ROFA PM produced in this boiler was highly carbonaceous, containing ~60-90% carbon that was essentially all graphitic, with the balance consisting primarily of metals, sulfur, and oxygen. XAFS spectroscopy established that the sulfur was primarily a mixture of sulfate and thiophenic sulfur and that the metallic components were dominated by sulfates, particularly vanadyl sulfate ($VO{\cdot}SO_4{\cdot}xH_2O$) and nickel sulfate ($NiSO_4$). However, the XAFS spectra also indicated the presence of additional metal compounds (sulfides and oxides) in small amounts.

In our more recent work, discussed in this report, XAFS spectroscopy has conclusively identified Ni and V sulfides and Ni and V oxides in PM subjected to aqueous or acid (1N HCl) leaching. Essentially all of the metal sulfates are removed by either aqueous or acid leaching, leaving metal sulfides as the dominant components of the spectra for the PM > 2.5μm, which is more carbon-rich, and metal oxides as the dominant components for the PM < 2.5μm ($PM_{2.5}$). This is an important observation since Ni sulfides are known to be toxic and carcinogenic [8,9]. It is found that 20-25% of the nickel in some ROFA PM samples is in the form of Ni sulfide.

These and other results are summarized in more detail in the individual project reports in the remainder of this report and in a number of publications (see Appendix).

## Future Work

As noted in our previous report on this contract, we have received a new grant from the National Science Foundation to investigate PM derived from the combustion of fossil fuels entitled "Molecular Structure and Microstructure of $PM_{2.5}$ Derived from Stationary and Mobile Fossil Fuel Sources", NSF CRAEMS (collaborative research activity on environmental molecular science) grant CHE-0089133. This grant will enable us to continue and expand our research program on fine airborne particulate matter. Much of our work on this topic during the next 2-3 years will be focused on carbonaceous PM and will include a significant amount of research on emissions from diesel jet, and automobile engines. We will be investigating PM samples generated in full-scale engine and automotive test facilities at the Ford Motor Scientific Research Laboratory, the Air Force Research Laboratory, the EPA NRMRL, and the Lovelace Respiratory Research Institute, in addition to new samples prepared in our small diesel engine test facility at the University of Utah.

Additional work will also be conducted on PM derived from residual oil combustion. One goal of this work will be to more conclusively identify the nickel sulfide phases present in ROFA PM.

Finally, we will increase our investigation of PM collected from the ambient atmosphere. The primary goal will be to identify in ambient PM the structural features we have observed in our source PM research.

**References:**


1. Dockery, D.W.; Pope III, A.; Xu, X.; Spengler, J.D.; Ware, J.H.; Fay, M.E.; Ferris, Jr., B.G.; Speizer, F.E. *J. Medicine*, **1993**, *329*, 1753-1759.
2. Pope III, C.A.; Thun, M.J.; Namboodiri, M.M.; Dockery, D.W.; Evans, J.S.; Speizer, F.E.; Heath, Jr. C.W. *Am. J. Respir. Crit. Care Med.*, **1995,** *151*, 669-674.
3. Wolff G. T. *Closure by the Clean Air Scientific Advisory Committee (CASAC) on the staff paper on particulate matter, EPA-SAB-CASAC-LTR-96-008,* US EPA Science Advisory Board, Washington, DC, **1996**, June 13.
4. Bachmann, J.D.; Damberg, R.J.; Caldwell, J.C.; Edwards, C.: Koman, P.D. *Review of the National Ambient Air Quality Standards for Particulate Matter: Policy Assessment of Scientific and technical Information*; EPA-452/R-96013 (NTIS PB97-115406); U.S. EPA, Office of Air Quality Planning and Standards, Research Triangle Park, NC, 1996.
5. Lighty, J. M.; Veranth, J. M.; Sarofim, A. F. *J. Air Waste Manage. Assoc.* **2000**, *50*, 1565-1618.
6. Huffman, G.P.; Huggins, F.E.; Shah, N.; Huggins, R.; Linak, W.P.; Miller, C.A.; Pugmire, R.J.; Meuzelaar, H.C.; Seehra, M.; and Manivannan, A. *J. Air & Waste Manage. Assoc.*, **2000**, *50*, 1106-1114.
7. G.P. Huffman, F.E. Huggins, N. Shah, R.J. Pugmire, H.L.C. Meuzelaar, M. Seehra, and A. Mannivannan, " Source Signatures of Fine Particulate Matter ($PM_{2.5}$) from Petroleum Refining and Fuel Use", 18 month progress report on U.S. DOE Contract No. DE-AC26-99BC15220; available at http://www.cffs.uky.edu/PM/Pubs/pubs.htm .
8. Sunderam, Jr., F. W. in: *Toxicology of Metals*; Brown S. S., Kodama, Y. Eds.; Ellis Horwood, Ltd.; Chichester, U.K., pp. 355-365, 1987.
9. Lee, S. D. in: *Toxicology of Metals*, Brown S. S., Kodama, Y. Eds.; Ellis Horwood, Ltd.; Chichester, U.K., pp. 347-353, 1987.

# Investigation of diesel particulate matter using several analytical x-ray techniques

Artur Braun, Naresh Shah, Frank E. Huggins, and Gerald P. Huffman, University of Kentucky, Consortium for Fossil Fuel Science, Dept. of Chemical and Materials Engineering, 107 Whalen Building, 533 S. Limestone St., Lexington, KY 40506
Adel Sarofim and Kerry Kelley, University of Utah, Department of Chemical and Fuels Engineering, Salt Lake City, Utah

## Introduction

We have investigated the structure of a suite of diesel soot samples prepared in the combustion laboratory at the University of Utah using a variety of x-ray techniques. The samples were generated by a small diesel test engine under idle and load conditions, using one reference diesel fuel and two diesel fuels that consisted of the reference fuel plus 5% of oxygenate additives [1]. These samples have been analyzed using traditional analytical x-ray techniques as well as state-of-the-art synchrotron radiation techniques in experiments conducted at the National Synchrotron Light Source at Brookhaven National Laboratory and the Advanced Photon Source at Argonne National Laboratory. The techniques included x-ray diffraction (XRD), x-ray absorption fine structure (XAFS) spectroscopy, scanning transmission x-ray microspectroscopy (STXM), small angle x-ray scattering (SAXS), thermogravimety analysis (TGA), and light scattering. Additionally, Naresh Shah and Yuanzhi Chen of our group have carried out extensive electron microscopy analyses of the samples and the results, which are complementary to the results in this section, are reported in a separate section of this report.

For all the techniques mentioned above, significant differences in the sample characteristics were found between idle and load soot for the oxygenated fuels. For the reference diesel fuel, only small differences were found. The differences in structure are discussed in the remainder of this report.

## General remarks about the soot samples

The soot samples were provided in amounts of ~100 milligrams each. This is sufficient material for all of the above-mentioned analytical techniques. They are in the form of a black powder, with highly dispersed particles ≤~1 micron in size. Figure 1 shows a light micrograph of a typical sample.

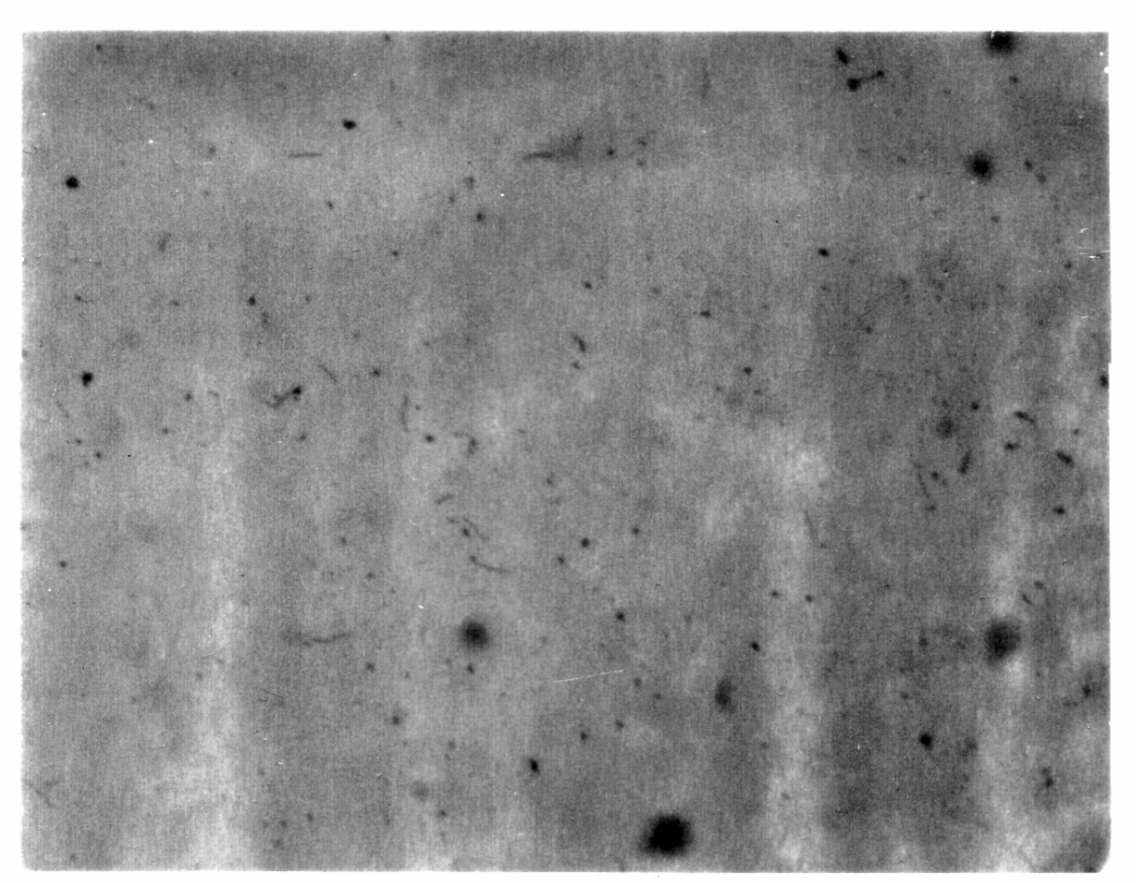

Figure 1: Optical microscopy image of diesel soot (load, not oxygenated). Magnification of 20X.

Soot generated with the engine running under idle conditions will be termed “idle soot” and with the engine running under load conditions, “load soot”. The idle tends to aggregate into large lumps more than the load soot. The idle soot is also fluffier than the load soot. We have pressed pellets from the soot to determine their mass densities and found that idle soot has a larger apparent density than load soot. On the other hand, the carbon skeletal density of the idle soots is found to be lower than their corresponding load soot counterparts.

**Light Scattering**

Light Scattering (LS) experiments were performed by CPS Company for two of our soot samples. The detection and separation power of this technique was enhanced with a disc centrifuge. Results were given as the relative weight (volume fraction)[%] vs. the particle diameter [micron], with the maximum at 110 nanometer for the “idle” soot and 140 nanometer for the “load” soot. Those data were transformed into particle fraction vs. particle radius to obtain average values for particle radius [2, 3].

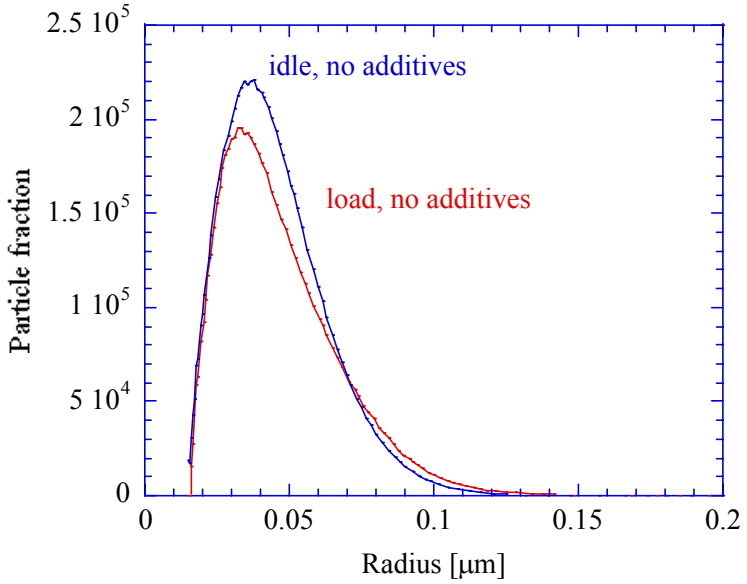


Figure 2: Particle size distribution of load and idle soot from non-oxygenated diesel fuel.

Figure 2 displays the particle size distribution for both soot samples. The particle sizes do not differ significantly from each other. Mean radii were <R>=45.5 nm for the load soot, and <R>=47.2 nm for the idle soot. From the shapes of the particle size distributions, it appears that the service company assumed a logarithmic normal size distribution. The LS technique appears to be reasonable for this type of particle size analysis.

**X-ray diffraction**

X-ray diffraction (XRD) is usually employed to study materials with long-range order and high crystallinity. Soot is not such a material. However, XRD has been also employed for many decades in the study of disordered carbonaceous material [4, 5] such as coal.

Unlike totally amorphous materials, poorly ordered carbon samples **do** exhibit Bragg diffraction peaks that allow for an at least semi-quantitative estimation of structural parameters. In this investigation, x-ray diffraction (XRD) was applied to determine the crystallite size and aromaticity (ratio between aliphatic and aromatic carbon) of the diesel soot. The XRD results were found to be in agreement with results on the degree of graphitization as determined by nuclear magnetic resonance by the group of Prof. Pugmire in Utah.

Diffractograms of all six samples were recorded using Cu K-alpha radiation. The soot powders were placed in a standard sample holder. The diffractograms exhibit Bragg reflection patterns (Figure 3) similar to that observed for graphite (2H reference graphite JCPDS 26-1079).

Figure 3 displays X-ray diffractograms of the idle and load soots from the reference diesel fuel (Fig. 3a.), the reference fuel with an additive of 1.5% diethyl carbonate (DEC) + 4.2% ethanol (Fig. 3b.), and the reference fuel with an additive of 5% DEC (Fig. 3c.). The most prominent peak is the (002) Bragg reflection, found at s=0.275, which corresponds to approximately 26° on the 2Θ scale. The (100) reflection is found at about s=0.45. The Bragg reflections of graphite (2H Graphite, JCPDS 41-1487) are plotted as vertical lines for reference.

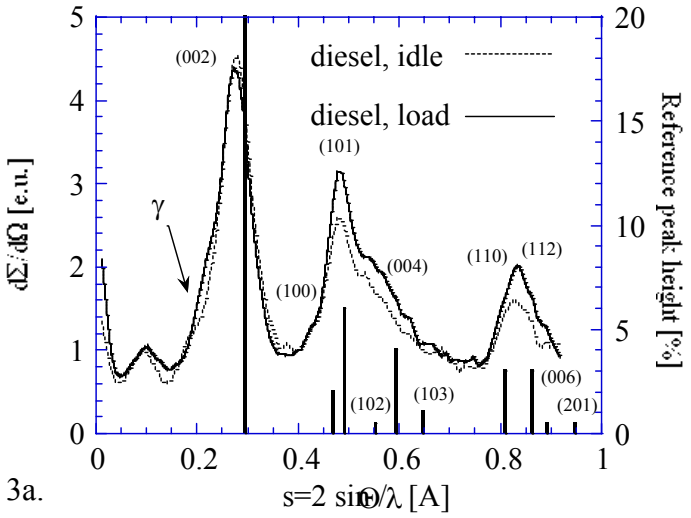


3a.

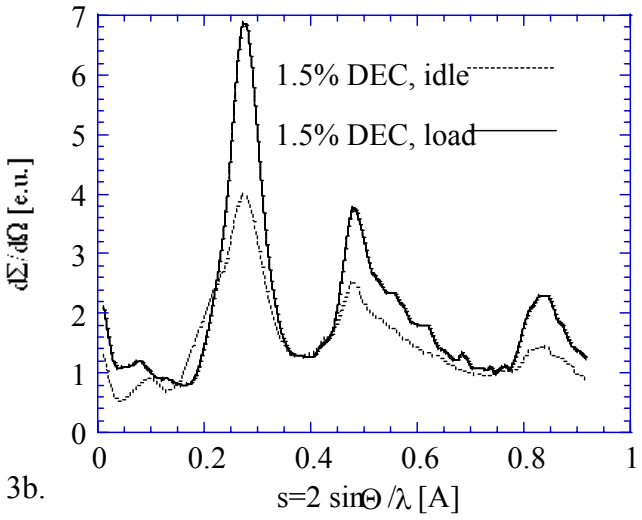


3b.

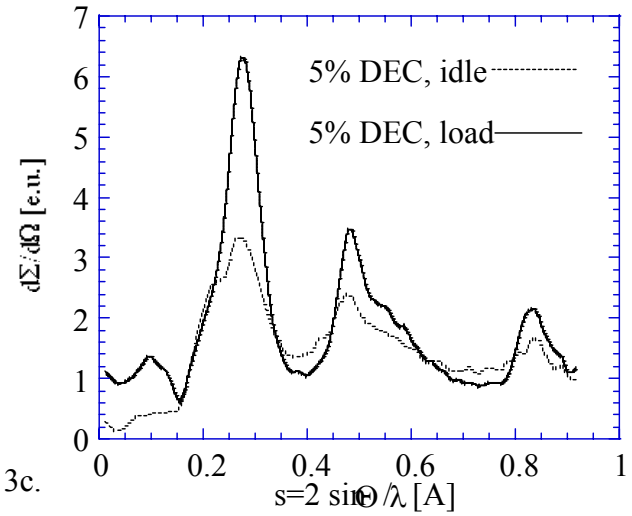


3c.

Figures 3a, 3b, and 3c: Comparison of XRD patterns from soot produced from various fuels at idle or load condition.

All these reflections are reasonably well resolved, indicating that the soot contains significant amounts of graphitic material. The idle and load soot diffractograms are of overall similar shape, although the idle soot diffractogram peaks are generally broader and weaker than those of the load soots. On the left side of the (002) reflection, the so-called γ-sideband is found at about s=0.2. This band is attributed to aliphatic side chains [6]. Figures 3b and 3c show the diffractograms of the idle and load soots obtained from oxygenated diesel fuels. We note that the full width at half maximum (FWHM) of the (002) reflection is wider for the idle soots than for the load soots. For the load samples, the intensity of the γ-band seems relatively suppressed compared to that of the idle samples.

We have fitted the (002) reflection and its γ-sideband with two Gaussian functions in order to determine the aromaticity of the soot by their relative scattering contributions. Figure 4 shows the corresponding peaks of the soot obtained from the reference diesel fuel under idle conditions, as well as the two Gaussian curves and the fit curve. The *aromaticity* can be defined as

$$f_a = \frac{C_{ar}}{C_{ar} + C_{al}} = \frac{A_{(002)}}{A_{(002)} + A_\gamma}$$

where $A_{(002)}$ and $A_\gamma$ are the areas the two Gaussian curves, which are assumed to be proportional to the number of aromatic and aliphatic carbon atoms per structural unit, $C_{ar}$ and $C_{al}$, respectively. Table 1 summarizes the results for the aromaticity of the soots.

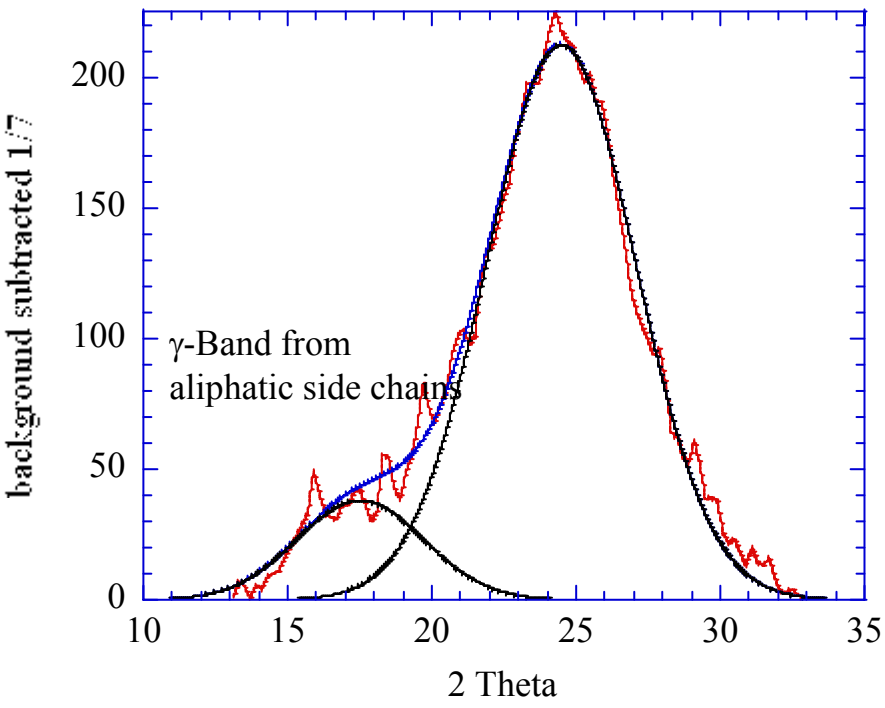


Figure 4: Deconvolution of graphite (002) Bragg reflection and γ-band .
This is reference diesel fuel, idle soot.

Visual inspection of the (002) peak positions of either samples as well as the fitting results reveal that the reflections are slightly shifted versus the 2Θ-axis, depending on fuel and operation conditions. We find for the oxygenated fuel that the *load* samples have (002) reflections at higher angles than the *idle* samples.

Table 1: Aromaticity f of diesel soot as determined by XRD.

| | Aromaticity *f* of diesel soot | | |
|---|---|---|---|
| Fuel type | regular diesel | diesel +5 % DEC | diesel + 4.2% ethanol + 1.5% DEC |
| idle | 0.868 | 0.765 | 0.745 |
| load | 0.821 | 0.930 | 0.868 |

The (002) peak position reflects the distance between the graphene sheets. From its width, the crystallite size $L_c$ and $L_a$ were estimated via the Scherrer formula

$$w = \frac{0.9 \times \lambda}{b \times \cos(\Theta)}$$

with the X-ray wavelength λ=1.54056 Å, the peak width b, and the peak position Θ. The empirical parameter *b* has values between 0.8<b<1.9, where *b* =0.89 (1.84) is chosen for the (002) reflection and b=1.84 for the (110) and (112) reflections.

Table 2: Comparison of crystallite sizes.

| Sample | $L_c$ (002) [Å] | $L_a$ (110) [Å] | $L_a$ (112) [Å] |
|---|---|---|---|
| Diesel, idle | 11.10 | 8.67 | 17.24 |
| Diesel, load | 11.78 | 10.48 | 16.68 |
| 4.2% ethanol +1.3% DEC idle | 10.18 | 6.96 | 13.24 |
| 4.2% ethanol +1.3% DEC load | 12.86 | 8.64 | 14.92 |
| +5% DEC, idle | 8.64 | 8.93 | 6.24 |
| +5%DEC, load | 10.78 | 16.30 | 11.19 |

The $L_c$ (002) width of the crystallites correlated well with the graphite factor determined from graphite conductance factor measurements by the Pugmire group [7], as shown in Figure 5.

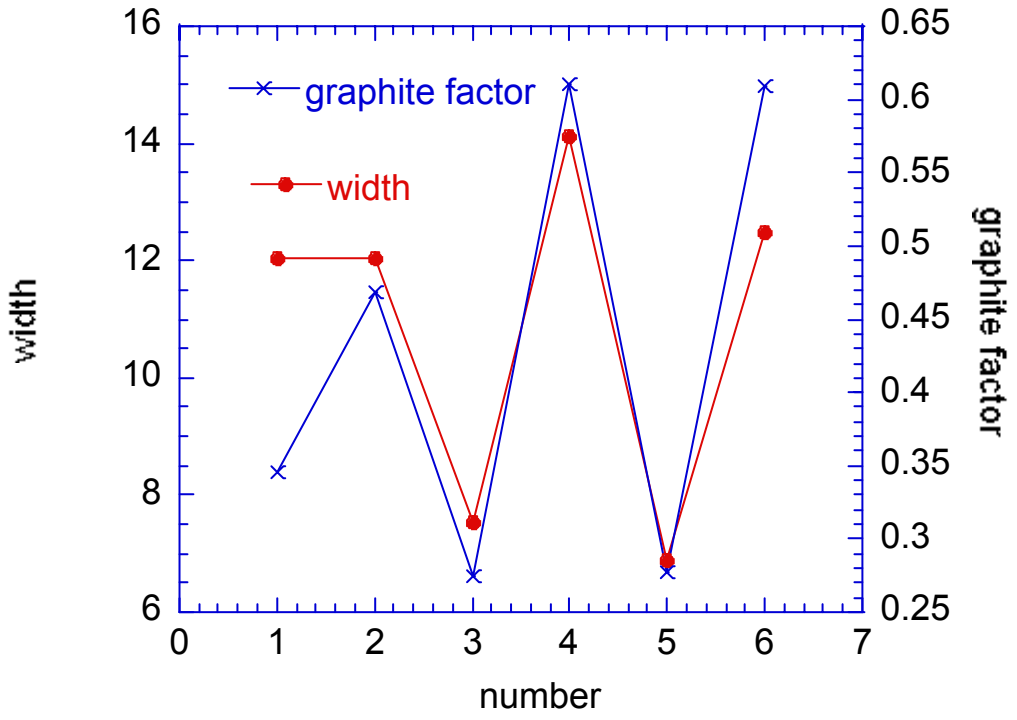


Figure 5: Comparison of crystallite width (from XRD) and graphite conductance factor (from NMR).

Thus, XRD and NMR both verify that diesel soots generated under load conditions are more graphitic than those produced at idle conditions.

We used the x-ray data to determine the x-ray density of the soot particles, this is, the density of the graphite-like skeleton, neglecting porosity.

$$\rho_x = \frac{3.33538\text{Å}}{d_{002}} \times 2.268 \frac{g}{cm^3}.$$

Note that 3.33538 Å is twice the lattice distance of graphite, and 2.268 g/cm$^3$ is the graphite density. The pressed sample density was obtained from the weight and dimension of pressed soot pellets.

Figure 6 displays the variation of skeleton density and press density, as obtained by measuring the dimension and weight of pellets. The values of the press density are given in arbitrary units only since no calibration was carried out yet.

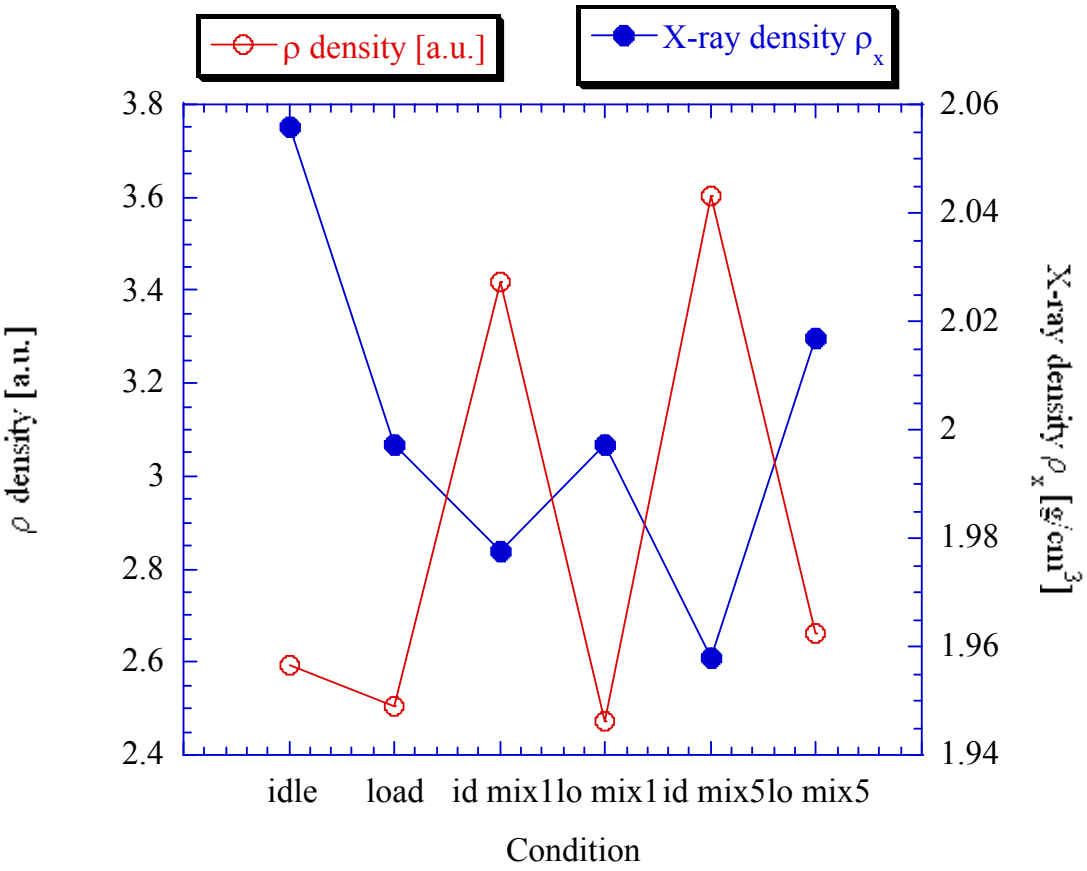


Figure 6: Comparison of X-ray density vs. press density.

Both densities seem to be inversely related. Load soot has a small press density but a high skeleton density, and idle soot has a high press density but a low skeleton density, with the exception of soot from regular diesel.

**Scanning Transmission X-ray Microspectroscopy**

Using Scanning Transmission X-ray Microspectroscopy (STXM) at Brookhaven National Laboratory, National Synchrotron Light Source, we were able to study single, sub-micron sized soot particles with a spatial resolution of approximately 50 nm. This enabled us to obtain x-ray absorption near edge spectra (XANES) from single soot particles. Characteristic and systematic differences were found for load/idle and oxygenated/conventional diesel soot.

This work was carried out at beamline X1A in collaboration with Christopher Jacobsen and Susan Wirick of the State University of New York (SUNY) at Stonybrook. A detailed discussion of this beamline and of the STXM technique is available at the X1A web site, http://xray1.physics.sunysb.edu/ . A manuscript summarizing our initial work on diesel PM using STXM has been submitted for publication to the journal *Fuel* [8].

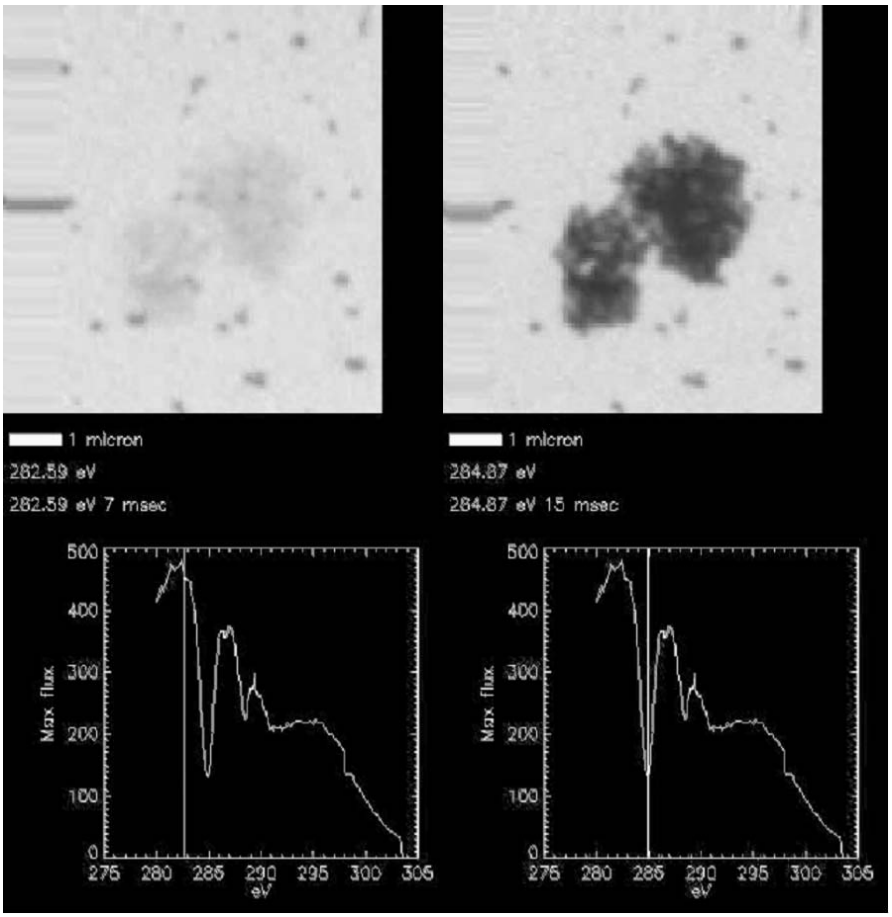


Figure 7. Sharply contrasting images of a diesel PM agglomeration at X-ray energies below (left) and above (right) the C K-shell absorption edge.

Since carbon is quite transparent to the X-ray beam at energies below its K-shell absorption edge, the diesel PM is essentially invisible in images obtained at such energies. A striking example is shown in Figure 7, which shows two images of a four-micron wide agglomeration of diesel soot particles, surrounded by a number of smaller non-carbonaceous particles. The image to the right was scanned below the absorption edge, and the image to the right was scanned

above the absorption edge. In the left hand image of Figure 7, only a very faint, diffuse indication of the soot agglomeration can be seen, while the smaller, sub-micron sized non-carbonaceous particles are easily visible. In contrast, the image on the right side shows the particle in the center with clear contrast versus the background, while the smaller non-carbonaceous particles appear the same in both images. Below each image, the transmitted X-ray intensity is plotted versus the X-ray energy. The vertical lines in the plot indicate the energies at which the images were scanned.

Figure 8 shows two STXM images, obtained from the same sample region at two different X-ray energies. The left image was scanned at a photon energy of 285 eV, and the right image was scanned at 288.2 eV. Both images show the same distribution of particles, dispersed over an area of about 7.5 x 7.5 microns square. However, the particles on the right image appear more diffuse and spread out then the ones in the left image, which appear smaller and sharper.

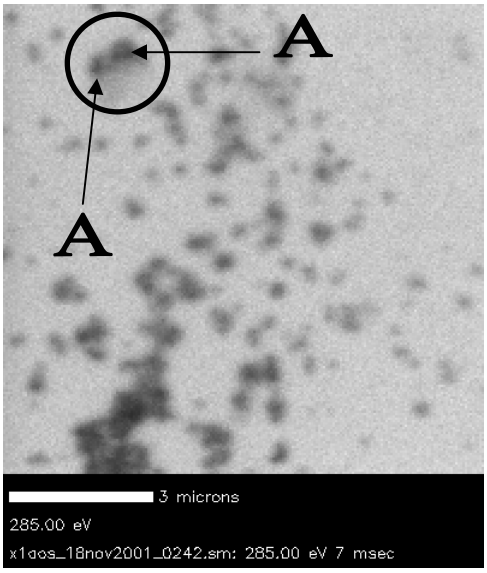


Fig. 8-a. STXM image of soot particles at 285 eV photon energy. “A” denotes selected areas for XANES.

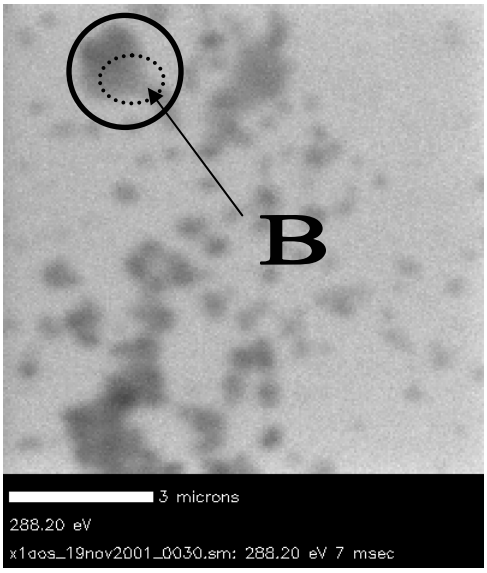


Fig. 8-b. STXM image of soot particles at 288.2 eV photon energy. “B” (dashed circle) denotes the selected area for XANES.

In both images, a circle is drawn to highlight a particle agglomeration of two particles indicated by the arrows labeled A with a size of about 0.5 microns each. Both particles are visible in the left image, but not in the right image where only a large diffuse shaded area can be seen. This diffuse region, exclusive the two mentioned particles, is labeled region “B”.

Figure 9 displays XANES spectra recorded from regions A (particle core) and B (diffuse ring). We will focus on the characteristic peaks at 285 eV, 287 and 288 eV. At 285 eV, carbon has a $\pi^*$ resonance due to C=C bonds. In the vicinity of 288 eV, there are two hydrocarbon resonances, indicative of C-H bonds. Figure 10 shows XANES obtained from the reference diesel fuel and from graphite. On the basis of these XANES, it is logical to conclude that the particle cores (region A) are rich in graphitic carbon, while the diffuse ring region B is rich in unburned diesel fuel and lubricating oil. Although these conclusions are somewhat quantitative, they are supported by the fact that peak intensity ratio of the C=C resonance to that of the C-H

resonance is about 1/10 for the diesel fuel, while the C-H resonance is absent in the graphite XANES spectrum.

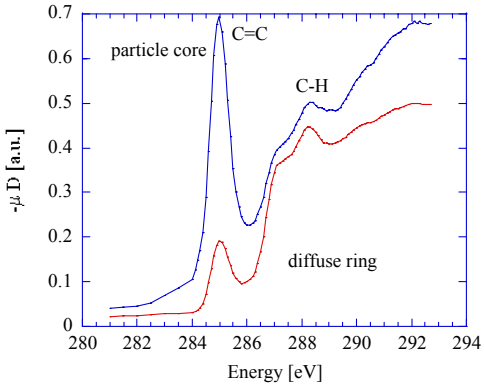


Fig. 9. XANES of particle core (region A) and diffuse ring area (region B).

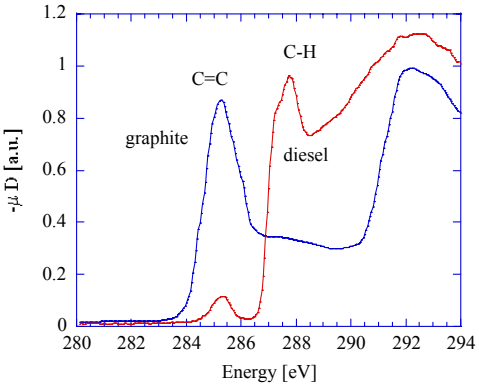


Fig. 10. Reference XANES of graphite and diesel fuel.

It should be noted that the diffuseness of region B may be due in part to a leaching effect of the acetone used in the sample preparation on diesel fuel and lube oil condensed on the graphitic particle cores.

Efforts to model the diesel PM spectra by building linear combinations of the two reference spectra have not yet been very successful. However, this is probably because we have used only a limited set of reference spectra. It is probable that additional hydrocarbon species are created during fuel combustion.

We have also studied single diesel PM particles and found that different XANES could be assigned to the particle cores and the particle boundary regions. It was found that C=C bonds were dominant in the particle core regions, and C-H resonances in the particle boundary regions. The separation of the two types of region may have been enhanced by the previously noted leaching effect of acetone on diesel fuel and lubricating oil condensed on the graphitic particle cores.

Additional STXM and complimentary experiments are in progress on this suite of diesel soots.

Finally, it is useful to compare the spatial and energy resolution of various techniques that are being used for $PM_{2.5}$ research. We are using both STXM/XANES and TEM/EELS, which give some similar type of information. Figure 11 compares the resolution of these and other techniques, as of the year 1997. There may have been some improvements in resolution during the intervening years. From our own experiments, it is evident that TEM has much better spatial resolution for morphological characterization, while comparison of XANES and EELS spectra show that STXM has the advantage of better energy resolution.

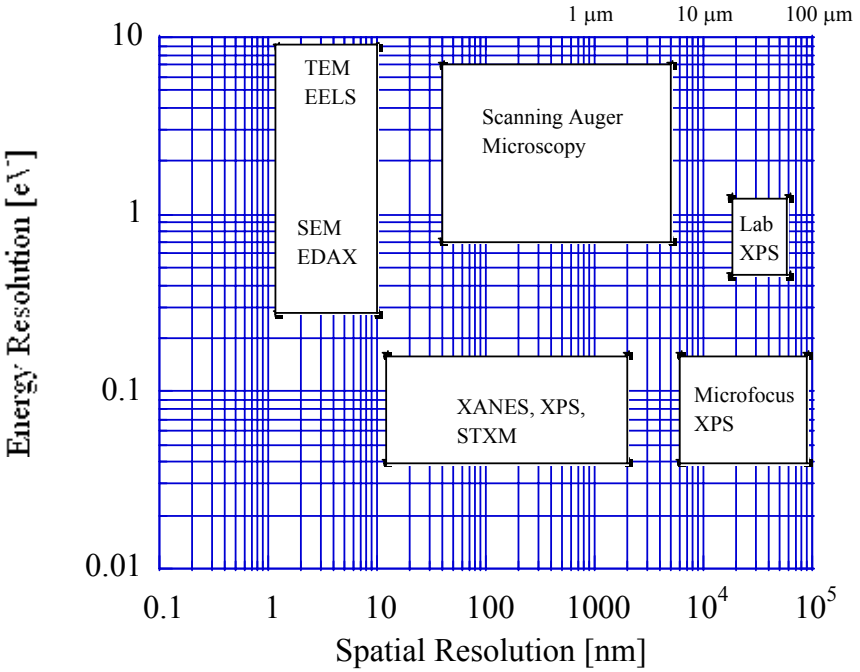


Figure 11: Resolution of microscopy/spectroscopy techniques [9].

**X-ray Absorption Near-Edge Spectroscopy (XANES)**

XANES were obtained using the STXM microscope as described in the previous subsection. This subsection concerns only results from single-particle analysis, but we plan to carry out future bulk XANES measurements on these soot samples in the near future.

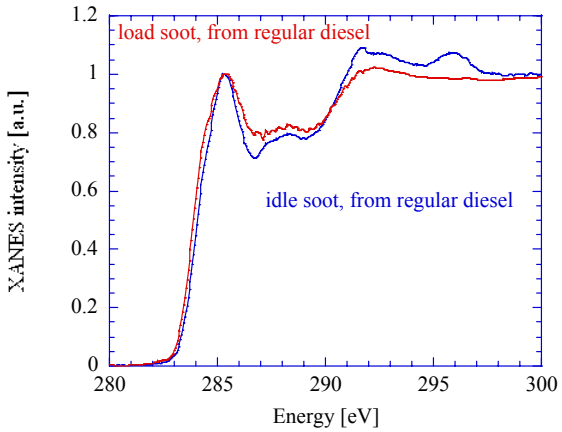

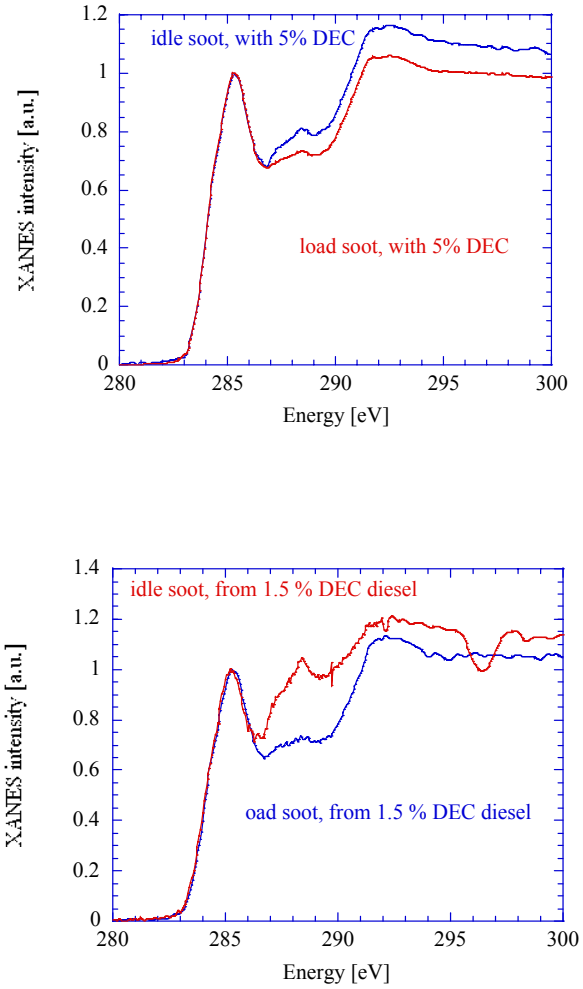


Figure 12: Comparison of XANES as obtained from single soot particles.

A huge body of literature and reference data exists on XANES of carbonaceous samples. Figure 12 displays the XANES spectra of representative particles in the six soot samples. The $\pi^*$ transitions at 285 eV that are characteristic of carbon-carbon double bonds (C=C) are well developed in all samples. Between 287 and 289 eV, there are further transitions, indicative of C-H bonds. The spectra have been normalized to unity at the primary C=C $\pi^*$ transition peak. While we have not modeled these spectra in detail yet, it is evident that the relative intensities of the C-H resonances to the C=C resonances is higher for the idle soots than it is for the load soots, particularly for the diesel fuels with oxygenate additives. Since the C-H resonances are attributed to unburned diesel fuel and lube oil and the DEC and ethanol + DEC additives promote more complete combustion of the fuel [1], this result seems logical. More detailed fitting of the XANES spectra to models is in progress.

**Small Angle X-ray Scattering (SAXS)**
Small angle x-ray scattering (SAXS) was used to study the soot powder, both in the form of pressed pellets and immersions of soot particles in water and acetone. SAXS is an inelastic scattering technique that focuses on the profile of the (000) (specular) Bragg reflection. Generally, particle size distributions, surface areas and volumes, porosities, and fractal dimensions of objects can be determined with SAXS. We were able to determine the fractal dimension of the soot aggregates and their particle size distribution. SAXS was carried out at two different synchrotron beamlines at the Advanced Photon Source in Argonne National Laboratory, BESSRC-CAT and UNI-CAT.

We were able to resolve three different size ranges in the soot, up to ~1 nm, 150-400 nm, and 800 – 1500 nm. This is in agreement with data published in [10]. Objects with size ~1 nm are most likely the graphite crystallites that were detected with XRD and observed by TEM. Objects with radii between 150 and 400 nm are the primary particles, as observed with electron microscopy. The large size of 800 – 1500 nm radius must be assigned to agglomerates of the primary particles, also observed with electron microscopy.

SAXS scattering curves are usually plotted in a double logarithmic representation of the scattered intensity versus the scattering vector ("log-log plot") to obtain a global picture of the structures resolved in the experiment. Figures 13-15 display log-log plots for idle and load soot powder for the three fuels used. Generally, we see a convolution of a power law intensity decay and broad bumps, which account for Bragg-like reflections resulting from a very diffuse coherence length distribution in the particles. The intensity bump in the middle at about q=0.005 is a signature from the primary particles. This structural feature is observed in all powder soot samples. While the soot from conventional diesel shows similar scattering curves for idle and load soot, the oxygenated samples show remarkable differences, i.e., for the idle soot samples derived from oxygenated fuels, the bump from the primary particles is overshadowed by the power law decay.

The position of the bump roughly tells us the size of the primary particles (there is a whole body of well established theory for accurate determination), while the power law decay provides information about the fractal dimensions of particle aggregates. Since for the idle soot, the bump is at a smaller q value than for the load soot, load primary particles are smaller than idle primary particles.

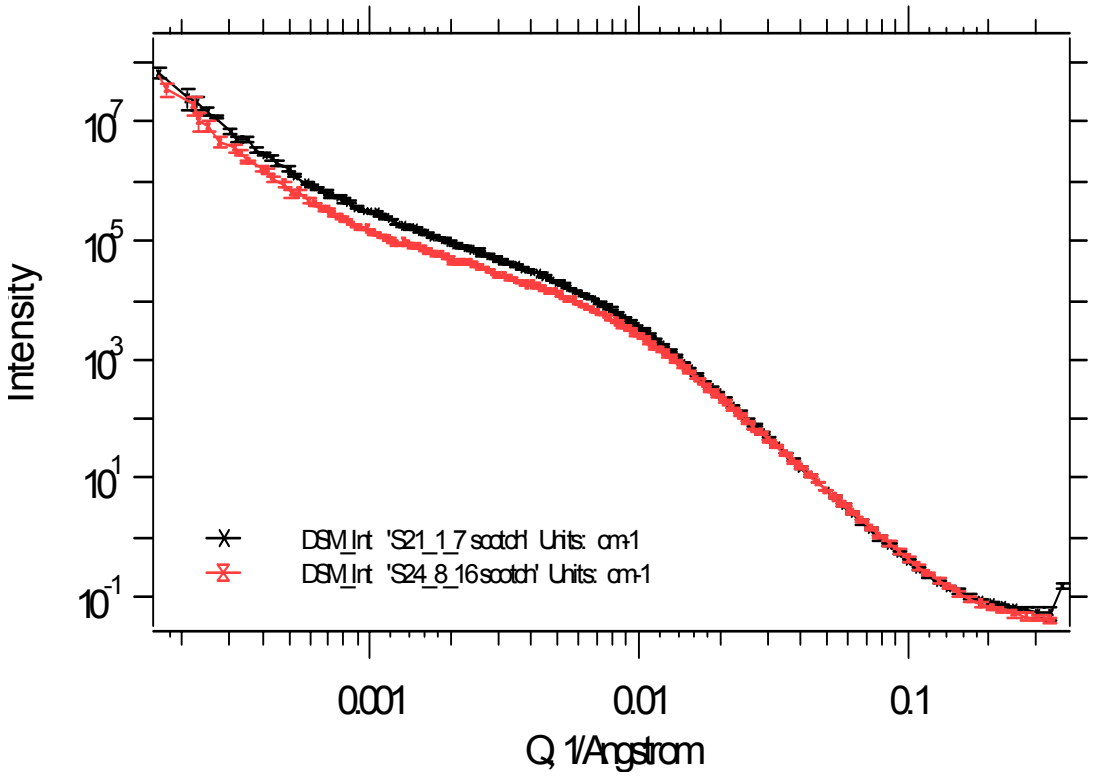


Figure 13: SAXS curves of idle (black) and load (red) soot.

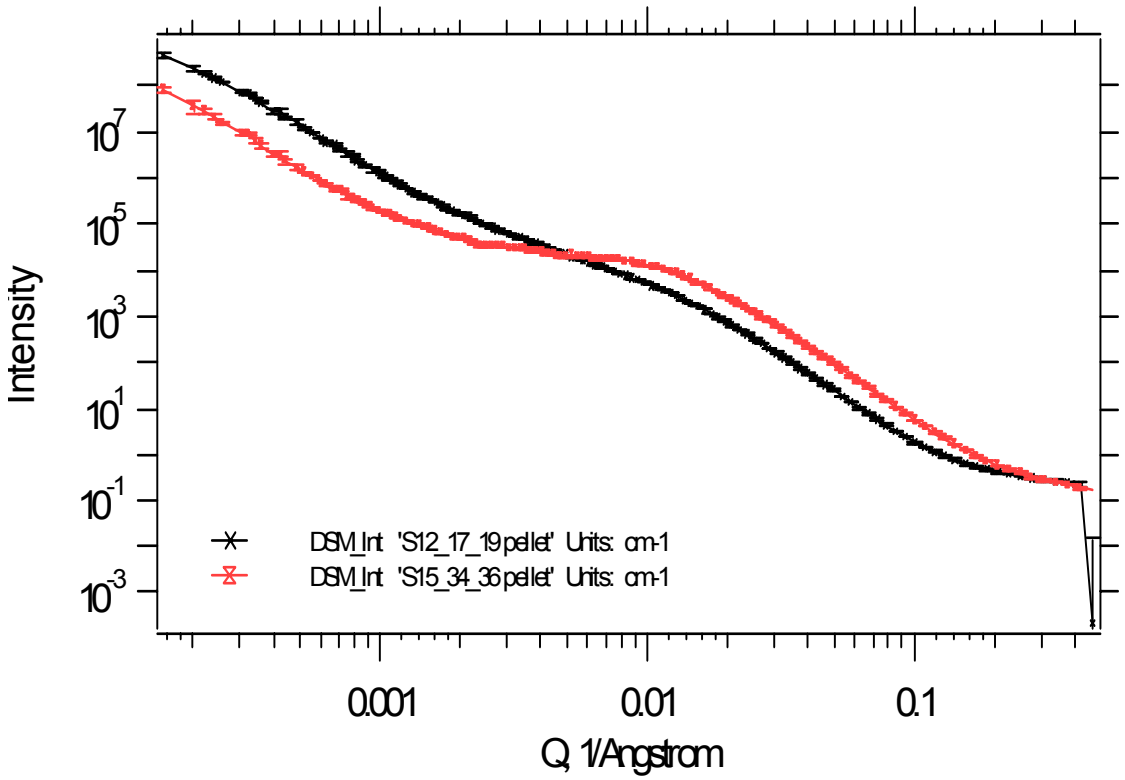


Figure 14: SAXS curves of idle (black) and load (red) soot, from diesel with 1.5 % DEC.

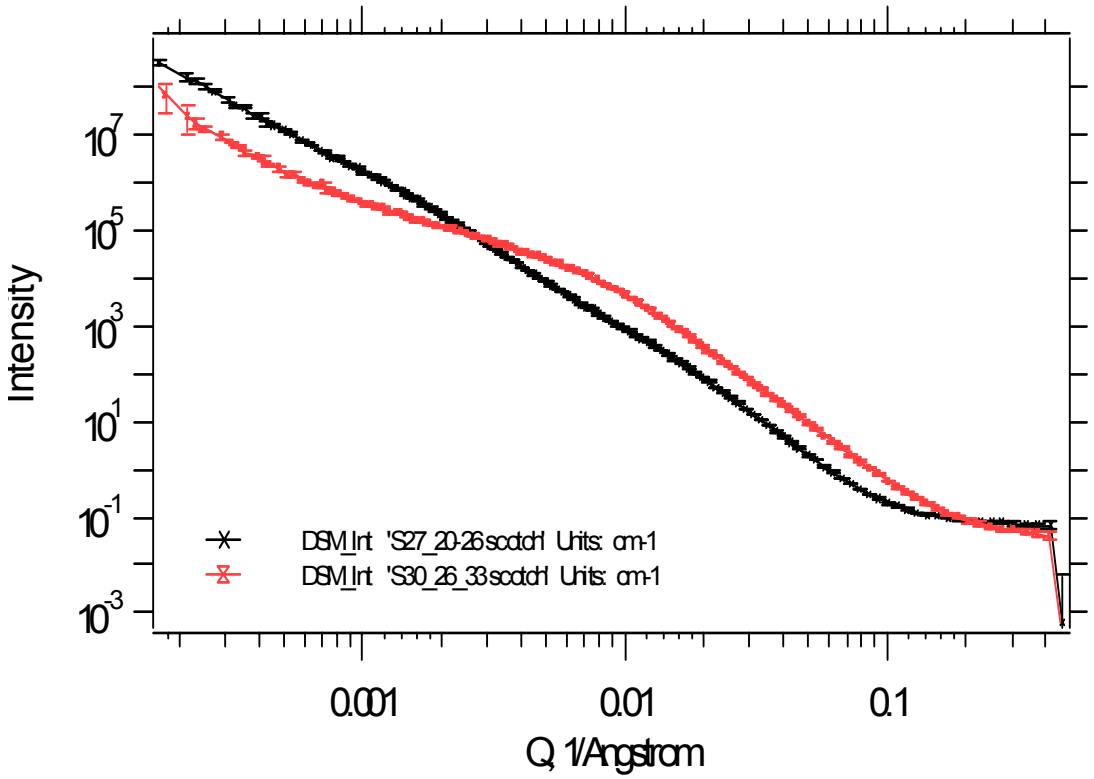


Figure 15: SAXS curves of idle (black) and load (red) soot, from diesel with 5 % DEC.

To separate the signal from the aggregates and the primary particles, we used a trick. Pellets were pressed (~10 metric tons load) from the soot powder so that the aggregates became compressed and insignificant compared to primary particle scattering. We also tried suspending the soot samples in acetone and ultra-sonicating as another approach to destroying the aggregates. Figure 16 shows the scattering curves of all samples; lose powders, pressed pellets, and acetone suspensions.

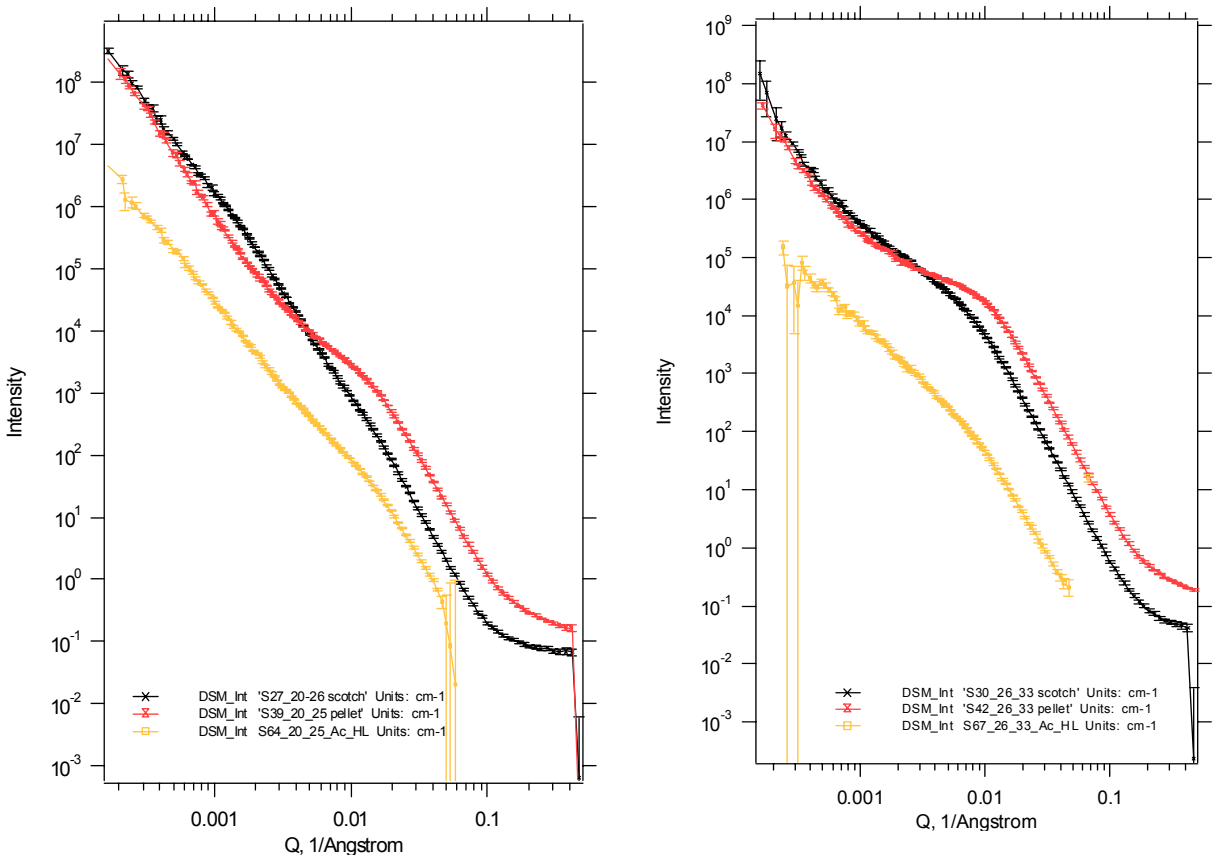


Figure 16: SAXS curves from soot in powder, pellet (curve with higher intensity at high Q values), and immersed in acetone (lower, short curves)).

We have attempted a detailed quantitative analysis by curve fitting this data to conventional SAXS models. In particular, we have determined the particle size and the fractal dimension. For the particle size, we have applied so-called Guinier fits, which give us radius of gyration with respect to the center of electron density of the particles. Assuming one particular particle shape, this can be translated into geometrical dimensions. Here we have assumed that the primary particles are spheres. Examples of the computer fitting procedures and the values obtained from them are shown in Figure 17.

Regarding the fractal dimension, we must distinguish volume/mass fractals and surface fractals. For mass fractals, the mass scales with

$$m \sim R^D$$

and "D" is the fractal dimension, which can be measured by the recording the decay of intensity versus Q. In fact, the exponent of decay "D" can be translated directly into the fractal dimension of the object measured:

$$\frac{d\sigma}{d\Omega}(Q) = NV^2\Delta\eta^2 Q^{-D} \ , \quad 1 \le D < 3$$

For surface fractals, the surface scales with

$$A \sim R^{D_S}$$

and for the intensity variation versus Q we find

$$\frac{d\sigma}{d\Omega}(Q) = NV^2 \Delta\eta^2 Q^{D_S - 6} \quad , \quad 2 < D_S < 3$$

For most samples and Q-ranges, the exponent of decay was between –3 and -4, which implies that we have to deal with fractal dimensions between those values. Those are surface fractals; that is, compact objects with rough surfaces.

For large Q, the fractal dimension $D_s$ was found to be in the range between 2 and 2.5. $D_s = 2$ actually means that the surface is smooth, and this is in fact observed more or less for the primary particles.

From SEM/TEM, we can also obtain information about fractal dimension of the soot. However, the microscopy techniques provide 2-dimensional data with a limited statistical significance, while the scattering results provide 3-dimensional information with a pronounced statistical significance.

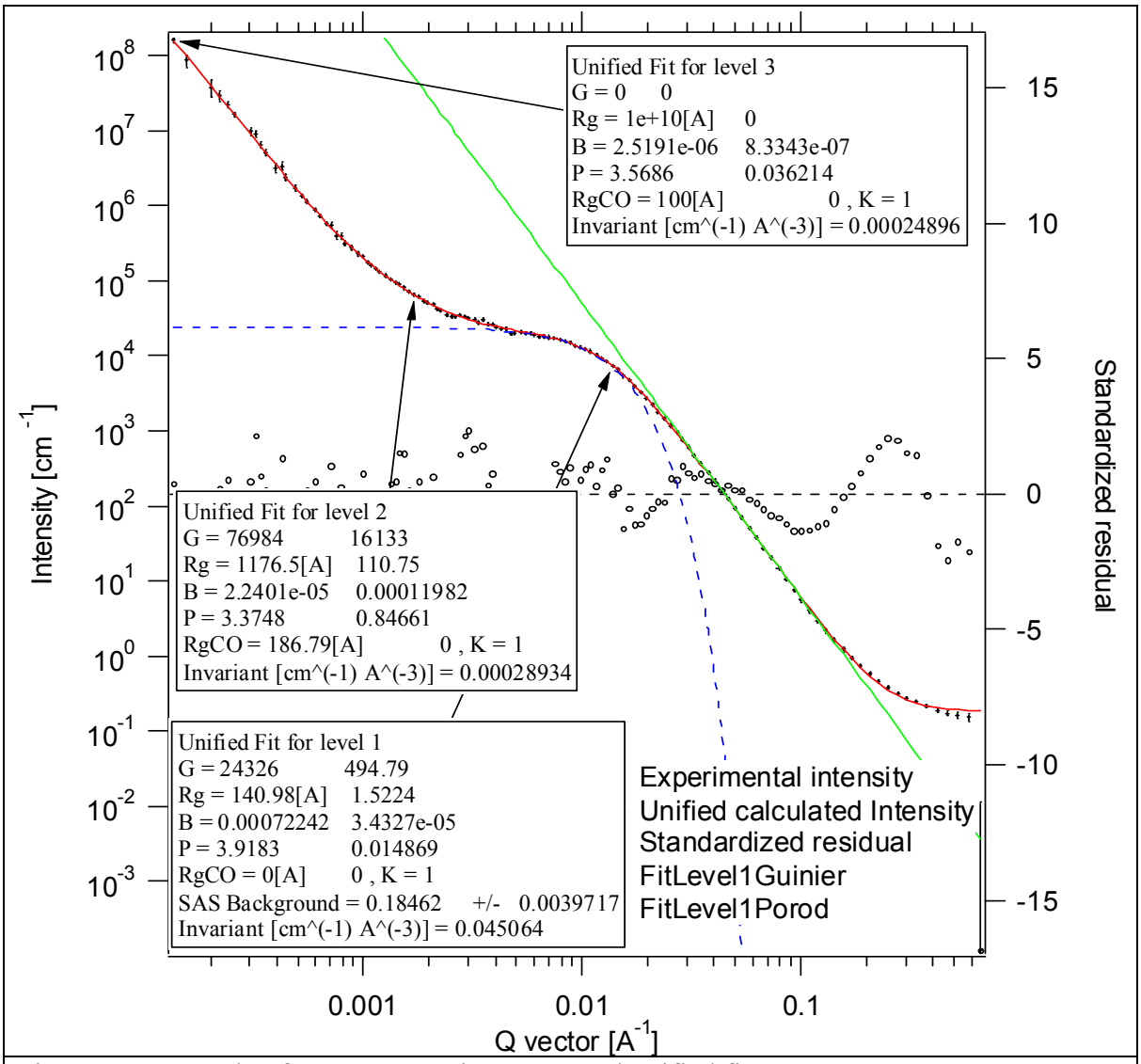

Figure 17: Example of SAXS scattering curve and unified fit.

**Thermogravimetry**

Thermogravimetric analysis was performed with a TA 2950 TGA instrument. The program used to analyze our samples was as following: increase temperature at a rate of 20 K/min in $N_2$ to 100°C and hold for 5 min.; increase at 50 K/min in $N_2$ to 750°C; hold at 750 °C for 15 min in $O_2$. The initial sample amount was always about 20 mg.

Figure 17 provides a typical example of TGA profiles for idle and load diesel soot. The axis for the mass is normalized to unity. On the time axis, the curves are shifted by some minutes to allow the temperature ramp between 100°C and 750°C. Numerical results are summarized in Table 3. We clearly find that idle soot contains more volatile matter than load soot and that the difference is increased by the oxygenate additives.

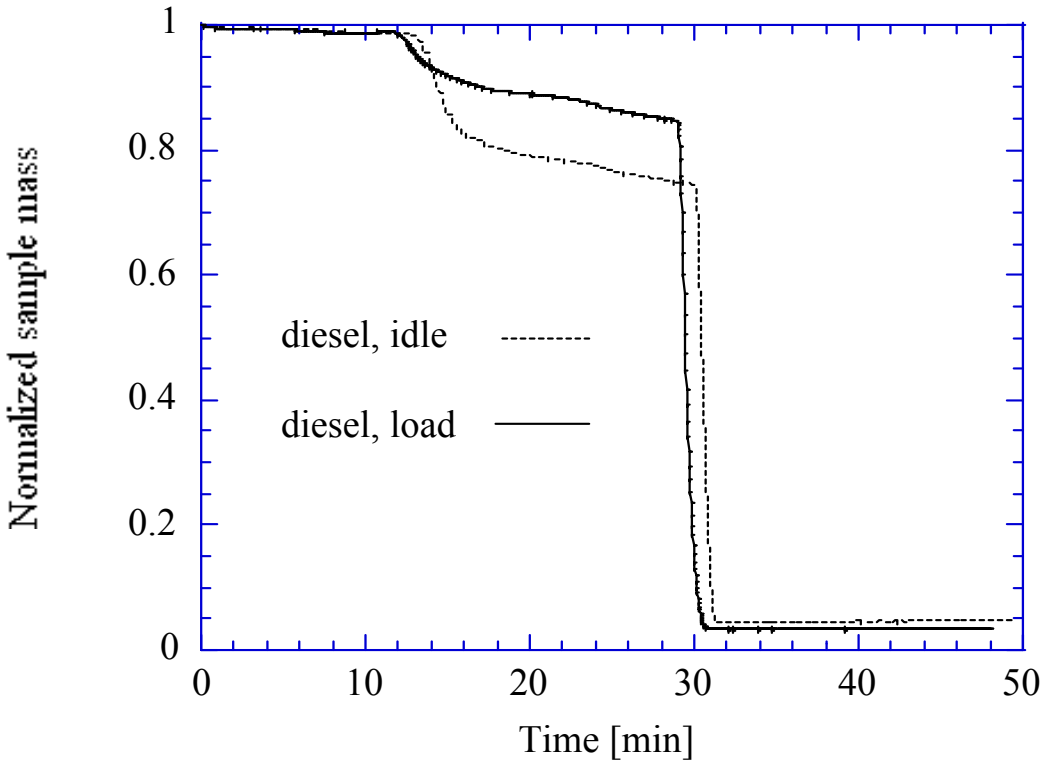


Figure 18: Typical TGA data for idle/load diesel soot samples.

Table 3: Summary of TGA results.

| Sample name | Condition | Moisture | Volatile | Residue |
|---|---|---|---|---|
| 1-7 | idle | 1.757 | 23.78 | 4.699 |
| 8-16 | load | 1.145 | 14.36 | 3.490 |
| 20-25 | idle, 4.2% ethanol + 1.3% DEC | 1.917 | 56.19 | 4.733 |
| 26-33 | load, 4.2% ethanol + 1.3% DEC | 1.375 | 16.75 | 2.910 |
| 17-19 | idle, 5% DEC | 2.488 | 61.80 | 4.614 |
| 34-36 | load, 5% DEC | 1.025 | 14.09 | 2.138 |

**Summary**

The principal results obtained for the structural properties of the suite of diesel PM samples investigated in the current study are briefly summarized below.

1. X-ray diffraction (XRD) established a graphitic crystallite width parameter that correlated well with the graphite conductance factor established by Pugmire and co-workers [7]. An aromaticity factor for diesel PM was established from the intensity of aliphatic sidebands in the XRD patterns.
2. Scanning x-ray transmission microspectroscopy (STXM) was able to identify carbon rich in C=C or C-H bonds with a resolution of ~50 nm. The former were associated primarily with graphitic soot and the latter with unburned diesel fuel or lubricating oil.

3. Carbon x-ray absorption near edge spectra (XANES) exhibited a more graphitic signal from diesel PM produced when the diesel engine was running under load than under idle conditions. The difference was enhanced by the addition of oxygenates to the diesel fuel.
4. SAXS results reveal the existence of a threefold size distribution and were used to determine the fractal dimensions of the primary particles and larger aggregates. SAXS also established that the load soot primary particles were smaller than idle soot primary particles.
5. It was shown that a number of different experimental techniques (TEM, TGA, LS) provide results that are consistent those obtained by conventional and synchrotron x-ray analytical techniques on diesel soots produced under engine idle or load conditions, using regular or oxygenated fuels.

**References:**


1. B.C. Dunn, C. Guenneau, S.A. Hilton, J. Panke, E.M. Eyring, J. Dworzanski, H.L.C. Meuzelaar, J.Z. Hu, M.S. Solum, and R.J. Pugmire, *Energy & Fuels*, **16** (2002) 177-181.
2. A. Braun, M. Bärtsch, B. Schnyder, R. Kötz, O. Haas, A. Wokaun, *Carbon* 40 (2002) 375-382.
3. A. Braun, M. Bärtsch, B. Schnyder, R. Kötz, O. Haas, H.-G. Haubold, G. Goerigk, *J.Non-Cryst.Sol*. 260 (1999) 1-14.
4. R.E. Franklin, *Acta Crystallogr*. 4 (1951) 253.
5. V.A. Drits, C. Tchoubar, X-ray Diffraction by Disordered Lamellar Structures, Springer Verlag, 1990.
6. L. Lu, V. Sahajwalla, C. Kong, D. Harris, *Carbon* 39 (2001) 1821-1833.
7. Y.J. Jiang, M.S. Solum, R.J. Pugmire, and D.M. Grant, H.H. Schobert, and P.J. Papanno, *ACS Fuel Chemistry Division Preprints*, **47(2)** (2002) 629-631.
8. Artur Braun, etc., "Studies of Diesel PM with X-ray Spectro-Microscopy", submitted to *Envir. Sci. & Technology*.
9. T. Warwick, H. Ade, A.P. Hitchcock, H. Padmore, E.G. Rightor, B.P. Tonner, *J. Elec. Spec. Rel. Phen.* **84**, 85 (1997).
10. S.Di Stasio , *Carbon*, 39 (1) (2001) pp. 109-118.

# New Method for Measuring the Graphite Content of Soots

Yi Jin Jiang, Mark S. Solum, Ronald J. Pugmire, and David M. Grant
Department of Chemistry, University of Utah, Salt Lake City, Utah 84112

Harold H. Schobert and Peter J. Pappano
The Energy Institute, The Pennsylvania State University, University Park, PA 16802

## Introduction

The amount of graphite-like structure of soots is an important parameter for understanding the composition of these materials. The structure of graphite has been studied extensively[1-6], and is described by the delocalization of the π electrons over the carbon structure. These delocalized π electrons contribute to the conductivity of graphitic material. A recently proposed structure of coals[7] and soots consists of regions or clusters that are graphite-like in nature, linked by non-conductive chain/bridging regions. The electrical conductivity of these materials will therefore depend on the extent of these graphitic regions. Therefore, by measuring the electrical conductivity of these samples it is possible to estimate the amount of graphitic materials present.

The direct measurement of electrical conductivity is a classical method[8] in which a pair of electrodes is placed across the sample. However, due to the low resistivity ($1.5\times10^{-3}$ ohm-cm),[9] the resistance of the electrical contact between the electrodes and the sample could seriously affect the measurement results, especially when the sample is a powder. In addition, the heterogeneity of the samples and the presence of nonconductive regions make it difficult to measure the electrical conductivity of the sample in this manner. In order to solve such problems, the method of measuring the quality factor (Q value) of a radio frequency (RF) coil at high frequency has been employed.[10,11]

A Q meter is used to measure the Q value of a RF coil which is defined by

$$Q = 2\pi fL/R \qquad (1)$$

where f is the applied frequency, R is the resistance of the coil at this frequency, and L is the inductance of the coil. When a sample is placed inside the coil, any conduction electrons in the sample will be driven into motion by the electric field induced by the high frequency magnetic field inside the coil according to the Faraday Law[12].

$$\nabla\times E = -\partial B/\partial t. \qquad (2)$$

The interaction of moving electrons with the graphite lattice leads to an energy loss. This energy loss inside a coil results in a decrease in the Q value of the coil and therefore a resultant increase in resistance. The ΔQ between an empty and a sample filled coil is directly proportional to ΔR. Since ΔR is a measure of the delocalized electron content, it is also a reflection of the graphitic carbon content of the sample.

Experimentally, the correlation between ΔQ and the graphitic carbon content can be obtained by performing the measurement on a series of standard samples where pure graphite is diluted with silica gel of known composition. The graphitic carbons content in the unknown sample, i.e., the coal or soot, can then be estimated by determining ΔQ on a sample of known mass.

**The Principle of the Measurement**

The Q value of an RF coil is measured with a Q meter, a classical electrical instrument.[13] Let $Q_o$ be the value of the empty coil. The value of $Q_o$ decreases to $Q_i$ when a sample that contains conductive material is placed inside the coil, but the inductance L remains essentially the same (less than 1% change). The energy loss due to the moving conduction electrons interacting with the graphite lattice causes an increase in the resistance from R to R+ΔR with a corresponding decrease in the quality factor from $Q_o$ to $Q_i$ and

$$Q_i = 2\pi fL/(R+\Delta R) \quad (3)$$

Equation 3 can be rewritten as

$$Q_i=2\pi fL/R(1+\Delta R/R)=Q_o/(1+\Delta R/R) \quad (4)$$

For the coil used in this study at f = 100 MHz, $Q_o$ = 258, L = 0.145μH and the calculated value of R is 0.353Ω. Substituting these data into equation 4 gives

$$Q_i=258/(1+\Delta R/0.353\Omega)=258/(1+\Delta R2.83\Omega^{-1}) \quad (5)$$

A plot $Q_i$ vs ΔR results in a hyperbolic curve with a vertical asymptote at ΔR = –0.353Ω. Inverting both sides of equation 5 yields the linear relationship

$$1/Q_i=(1+\Delta R2.83\Omega^{-1})/258=0.00388+\Delta R0.011\Omega^{-1} \quad (6)$$

Recognizing that ΔR is much less than 1Ω a Taylor series expansion ($1/(1+x) \cong 1-x$) yields equation 7.

$$Q_i = 258(1-\Delta R2.83\Omega^{-1}) \quad (7)$$

As mentioned earlier ΔR is proportional to the G, the quantity of graphite (mg) in this limited volume of sample. Therefore, G can be represented by

$$G=K\Delta R \quad (8)$$

By obtaining a series of $Q_i$ and ΔR values from a set of samples with known graphite concentration the coefficient K can be obtained and a linear relationship between $Q_i$ and G can be written as

$$Q_i =258[1-(G/K)2.83\Omega^{-1}] \quad (9)$$

which can be rearranged to

$$G= -1.37\times10^{-3}Q_iK\Omega +0.353K\Omega \quad (10)$$

The practical form of equation 10 will be discussed in the next section.

**Experimental Details**

A Q meter (Type 170A, Boonton Radio Corporation U. S. A.) used for measuring the Q value of a RF coil. The operating frequency used is 100MHz for reasons of convenience, coil size and Q measurement sensitivity. A five-turn solenoid coil of inside diameter 0.83 cm, and length 1.40 cm, wound from 16-swg copper wire was used for the experiments. The inductance of this solenoid coil is 0.145μH and at 100MHz the Q value is 258.

Each sample was placed in a zirconia solid-state rotor (Chemagnetics, Inc.). In each measurement a constant volume of sample (0.33 $cm^3$ ) was used which filled to solenoid. A set of standard samples was prepared by mixing pure graphite powder (Aldrich Catalogue NO: 28286-3) with silica gel (Aldrich Catalogue NO: 28859-4). The value of $Q_i$ is silica gel independent. The standard and test samples occupied the same volume. Care was taken to place the sample in the sample holder such that the entire sample was within the coil for the Q measurement. The mass of each sample was also recorded.

The measurements of the unpaired electron concentration in each sample were made on a Bruker ESR spectrometer. Experimental details of the measurement will be discussed in a subsequent paper. All NMR measurements were obtained on a Chemagnetics CMX-100 spectrometer using a PENCIL rotor spinning system under conditions described previously.[14] All experiments were carried out at room temperature.

**Results and Discussion**

Table 1 contains the $Q_i$ values associated with the standard samples of varying graphite content. The least squares fit of the data is:

$$G\ (mg) = -0.69917Q_i + 182.30 \qquad (11)$$

This is the form of equation (10) and is used to calculate the graphite content of test samples. The results of applying this calibration equation to several diesel soots and other samples are shown in Table 2. While more work remains to be done, it appears that this is a simple and accurate method of determining the amount of graphitic in diesel soot.

The C-13 MAS spectra of four of the samples examined in this study are shown in Figure 1. The spectra of two anthracites and the anthracene soot residue were obtained using the CP technique. The diesel soot spectrum was taken with the single pulse technique due to a depletion of protons in the sample which renders the CP technique ineffective. These four samples have quite different percentages of the graphitic carbon. The graphite-factors for the four samples are: 0.014, 0.148, 0.48 and 0.61 for Summit, LCNN, the 1400 K anthracene soot residue, and diesel soot #4, respectively. One can see that there is a great variation of line widths among the four samples that, to some degree, follows the graphite factor. The increased line width is due to anisotropy of the magnetic susceptibility of regions of graphene layering that is not totally removed under MAS conditions.[16,17] The Summit sample has the appearance of a normal diamagnetic sample with a very small graphite factor and no unusual line broadening. While the line width (FWHM) of the LCNN is essentially the same as that of the Summit, some line broadening appearing as Lorentzian are evident in the LCNN sample. The anthracene soot residue has even broader wings and the broadening of the main resonance is approximately 40% than that of the LCCN. The diesel engine soot has an extremely broad resonance which is also noted in samples so deficient in proton content that the CP experiment is not effective.[14]

**Conclusion**

A rather simple method seems to be useful for correlating sample conductivity with the presence of graphene layering in graphitic carbon structures in anthracitic coals and numerous soot samples. The technique reported is useful for estimating the amount graphite like structures in amorphous carbonaceous samples. It has been demonstrated that the number of unpaired electrons, per se, may not be a reliable parameter for estimating either sample conductivity or the extent of graphitization of soot samples. By utilizing a radio frequency coil one can induce a high frequency electric field in the sample and thus avoid any physical contact with the sample. This technique renders the experimental results free from any of the classical problems associated with electrical contact at the surface. The data indicate that the concentration of free radicals in the sample is not a reliable indication of either the conductivity of the sample or the amount of graphitic carbon present. High resolution TEM data indicate that different levels of

ordered structures exist in many of the samples that we have examined and an analysis of the relationship between structure and conductivity will be attempted.

Table 1. The $Q_i$ value associated the samples with different graphite content.

| Sample | Sample Weight (mg) | Graphite Content (mg) | Graphite (%) | $Q_i$ Value[a] |
|---|---|---|---|---|
| 1 | 181.9 | 60.3 | 33.2 | 182.4 |
| 2 | 185.2 | 36.5 | 19.7 | 199.2 |
| 3 | 167.3 | 24.2 | 14.5 | 222.0 |
| 4 | 177.6 | 17.2 | 9.68 | 242.2 |
| 5 | 182.7 | 8.6 | 4.7 | 248.2 |
| 6 | 193.2 | 5.8 | 3.0 | 252.0 |
| 7 | 193.0 | 4.2 | 2.2 | 254.4 |

a) The frequency of the measurement was 100MHZ; at this frequency the Q value of the empty coil is 258.

Table 2. The measured graphite-factor and unpaired electron spin concentration of some soot samples.

| Sample | Sample Weight (mg) | Graphite Factor | $Q_i$ Value[a] | Spin Concentration ($10^{19}$ spins/g) |
|---|---|---|---|---|
| Anthracene 1400 K Soot Residue | 163 | 0.48 | 148.8 | 11.00 |
| Diesel Soot Residue[b] | 192 | 0.43 | 143.0 | 0.87 |
| Ethylene Soot Residue[b] | 150 | 0.48 | 157.0 | 3.78 |
| NIST DPM 1650 Residue[b] | 180 | 0.34 | 172.0 | 1.11 |
| Diesel Soot #1 | 174 | 0.47 | 141.0 | 3.99 |
| Diesel Soot #3 | 177 | 0.28 | 150.0 | 3.60 |
| Diesel Soot #4 | 186 | 0.61 | 123.0 | 3.82 |
| Diesel Soot #5 | 186 | 0.61 | 124.0 | 3.00 |

a) The frequency of the measurement was 100MHz; at this frequency the Q value of the empty coil is 258.
Residue is the insoluble part after 24 hrs extraction with dichloromethane in a Soxhlet extraction system.

**References**


1. Mantell, C.L., Carbon and Graphite Handbook, 1968, pp. 6-43.
2. Wallace, P.R., Phys. Rev., 1947, 71, 622.
3. Schobert, H.H., The Chemistry of Hydrocarbon Fuels, 1990, pp. 293-295.
4. Mcclure, J.W., Phys. Rev., 1956, 104, 666.
5. Wagoner, G., Phys. Rev. 1960, 118, 647.
6. Singer, L.S., Wagoner, G., Proc. Fifth Carbon Conf, 1963, pp. 65-71.
7. Celzard, A., Mareche, J. F., Payot, F.,Begin, D., Furdin, G., Carbon, 2000, 38, 1207.
8. Terman, F. E., Radio Engineer's Handbook, 1943, pp. 26-47.

9. Tyler, W. W., Wilson Jr., A. C., Phys. Rev. 1953, 89, 870.
10. Terman, F. E., Radio Engineer's Handbook, 1943, pp. 74-83.
11. Jiang, Y. J., J. Magn. Reson., 2000, 142, 386.
12. Hayt Jr, W. H., Engineering Electromagnetics, 1981, pp. 346-353.
13. Terman, F. E., Radio Engineer's Handbook, 1943, p. 916.
14. Solum, M. S., Sarofim, A. F., Pugmire, R. J., Fletcher, T. H., Zhang, H., Energy & Fuels, 2001, 15, 961.
15. Orendt, A. M., Facelli, J. C., Bai, S., Rai, A., Gossett, M., Scott, L., Boerio-Goates, J., Pugmire, R. J., Grant, D. M., J. Phys. Chem. A, 2000, 104, 149.
16. Kume, K., Hiroyama, Y., *Solid State Commun*., **1988**, 65, 617.
17. Freitas, J. C. C., Emmerich, F. G., Cernicchiaro, G. R. C., Sampaio, L.C.; Bonagamba, T. J., *Solid State NMR*, **2001**, 20, 61.

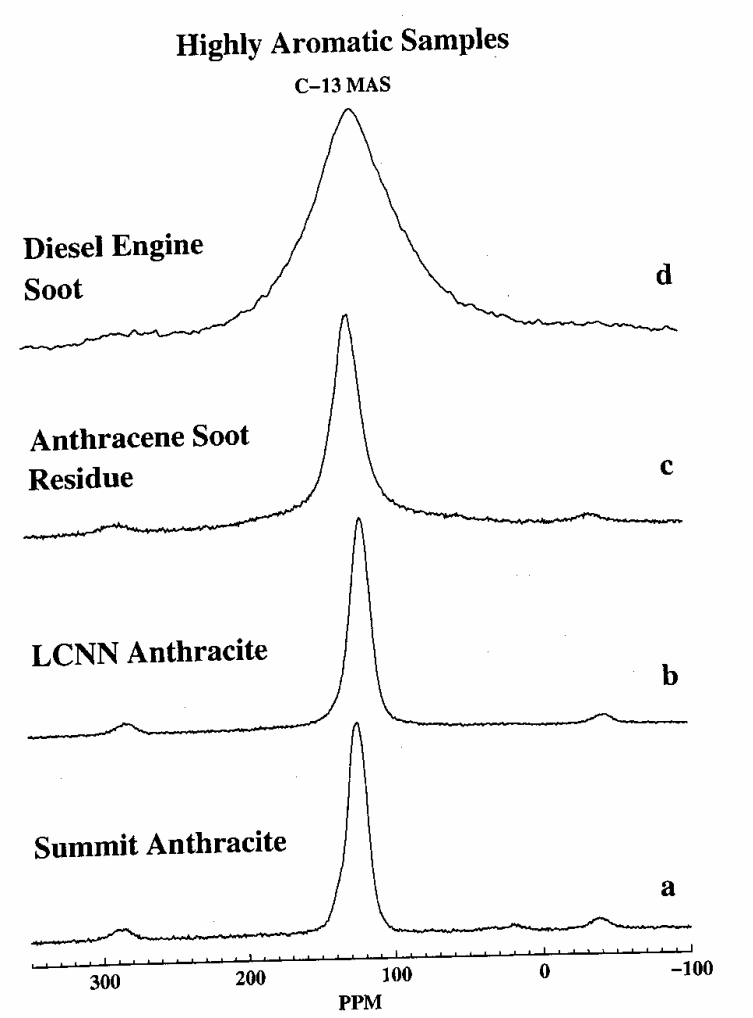


**Figure 1.** Carbon-13 MAS spectra of four of the samples. The spectra in a, b, c were taken with the CP technique all with a 1 s pulse delay. a) 3 ms contact time b) 10 ms contact time, c) 10 ms contact time d) spectrum taken with the single pulse method and using a 10 s pulse delay.

# TEM studies of ultrafine PM from diesel and jet engine exhausts

Naresh Shah, Yuanzhi Chen, and Gerald P. Huffman
University of Kentucky, Consortium for Fossil Fuel Science and Department of Chemical & Materials Engineering, 107 Whalen Building, 533 S. Limestone St., Lexington, KY 40506

## Introduction

There is considerable concern over the possible health effects of ultrafine PM, typically defined as PM <0.1μm in mean diameter. Although such PM constitutes a relatively small percentage of the overall mass of PM2.5, it accounts for a large percentage of the number of airborne PM2.5 particles, is easily inhalable into human airways, and presents a large surface area and very fine particle diameter to interact with and penetrate cell walls.

In the current study, transmission electron microscopy (TEM) has been used to investigate ultrafine carbonaceous PM derived from diesel and jet engine exhausts.

## Experimental Procedure

Microscope:

The principal instrument used was a JEOL 2010F high resolution TEM. This microscope has a field emission gun, windowless EDX spectrometer, high angle dark field detector, peltier cooled 2048x2048 CCD camera for imaging, and a separate peltier cooled CCD camera for parallel EELS spectroscopy.

Sample Preparation:

Sample preparation for TEM observation is usually trivial but vitally important. We have used several sample preparation techniques. For large powder samples (>200 mg), a TEM grid is carefully immersed in the dry powder and twisted around. The grid is removed from the powder sample, tapped a few times to dislodge large, loose, agglomerates and observed in the TEM.

For smaller quantities of loose powder (a few mg), the powder is suspended in about 5 mL of acetone and ultra-sonicated for several hours. A few drops of the suspension are placed on the TEM grid and observed in the TEM. This technique consistently provides excellent TEM samples with a uniform distribution of particulates of controllable surface density. Though this has been the most widely used technique for sample preparation, it has an inherent problem that acetone soluble components can be leached out, altering the chemistry of the sample.

In-situ TEM sample preparation by collecting the sample directly on the grid is usually more difficult but yields the highest quality pristine samples. A TEM grid has to be able to withstand the physical conditions (temperature, flow, ambient cleanliness) of the sample collection point to collect samples in this manner.

## Results and Discussion

*Diesel PM:*

Six samples of diesel PM were prepared in a two-cylinder diesel engine test facility at the University of Utah combustion laboratory. As discussed in other sections of this report, the

samples were prepared from three different diesel fuels with the engine running under idle and load conditions. Although several other techniques were able to discern significant differences in graphitic content versus unburned diesel fuel and lube oil content for different fuels and running conditions, we were unable to detect clear differences between the various samples using TEM. This is undoubtedly because of the nature of the technique, which is capable of examining only a limited number of particles in detail and is not readily adaptable to discerning "whole sample" properties unless the sample is quite uniform in nature. Nevertheless, the high-resolution TEM (HRTEM) results provide considerable insight into the nature of the "graphitic" structure of the soot and the fractural nature of diesel PM.

The TEM samples were prepared by dry and acetone suspension methods. Typical TEM images at several magnifications are shown in Figures 1-3. Relatively low magnification images indicate soot particle agglomerates in which the primary diesel PM globules (20 to 50 nm in size) are contained in chain-like structures (Figure 1)

Due to the "kinks" in the structure, these soot particles have a tendency to physically interlock with each other to produce larger agglomerates. This physical interlocking is strong enough to survive sonication in acetone for over an hour. These structures are three-dimensional even at the nanometer scale. Since TEM can "see through" the particles, the images do not show this third dimension information, except that they become little less transparent when stacked over each other.

At higher magnifications, TEM reveals the internal structure of these primary diesel PM globules (Figure 2). Specifically, the globules show contrast due to graphene layers oriented such that the planes are parallel to the electron beam. Typically these graphene layers are contained in stacks of up to ~10 (002) planes with linear dimensions ~5-20 nm. These stacked graphene layers are not completely parallel and are predominantly curved, forming onion-like structures. The interplanar distance between the graphene layers is not fixed and varies from approximately 0.33 to 0.5 nm (the 002 spacing of graphite is 0.337 nm). There are number of "onions" in a single globule of a diesel soot particle varies from about 1 to 10, with some onions only 2-3 graphene layers thick.

*Jet engine PM emissions:*
PM samples from a jet engine exhaust were collected at the T-80 test combustion facilities of the Wright Patterson Air Force Research Laboratory in collaboration with Edwin Corporan and Bill Harrison of the AFRL and Matthew DeWitt of the University of Dayton Research Institute of the University of Dayton. PM samples were directly collected on TEM grids using a heated smoke trail probe. Samples were collected during test runs using standard JP8 jet fuel with and without the addition of 10 volume percent of Norpar, a high purity Fischer-Tropsch additive, at both idle and cruise conditions. Both SiO substrate and holey C substrate TEM grids were used for PM collection. Holey C substrate grids showed the presence of individual fine PM particles uniformly dispersed over the entire area as well as some large aggregates of PM sparsely sprinkled over the grid. However, PM deposition on the SiO substrate appeared to have been strongly affected by the local airflow patterns. Total quantity of deposited PM was much smaller and there were no large aggregates of PM. Consequently, very little time was spent in analyzing the samples collected on SiO grids.

The holey C substrate showed many particles attached to the C substrate and hanging over the holes. These particles appeared to be growing out of the C substrate as there was no clear demarcation where the substrate ended and particles began. Some of the features appeared to be developed by condensation of the vapor phase to semi-liquid/solid phase right on the substrate.

TEM analyses of the jet PM samples with and without the Norpar additive did not reveal any major differences in the PM morphology and microstructure, even though the Norpar additives to the jet fuel caused significant reductions in PM emissions. However, there was a definite difference between PM samples collected under idle and under cruise conditions. The idle condition samples were more heterogeneous with larger amounts of non-carbonaceous matter than the cruise condition samples. The morphology of the fine PM in cruise samples showed structure rather similar to the structure of diesel PM, that is, chain-like structures of globules 20-100 nm in mean diameter (Figure 4). The morphology of the PM aggregates obtained under idle conditions showed larger agglomerated particles with knobby rough surfaces and almost no chain like growth (Figure 5).

It is also worth noting that the jet PM contains significant amounts of several inorganic elements. Results obtained by XRF analysis conducted by Prof. Dave Robertson are shown in the table below. Typical STEM x-ray maps of a PM particle containing Fe-rich metallic inclusions are shown in Figure 6.

XRF results of selected elements for jet PM (ng/cm^2)

| Sample Name | P | S | Ca | Fe | Co | Ni | Zn | Ga | Ba | Pb |
|---|---|---|---|---|---|---|---|---|---|---|
| Average of 3 Blanks | 0 | 0 | 5193 | 227 | 12 | 5.5 | 38.1 | 0 | 1213 | 74 |
| Filter 34 JP8 @idle | 773 | 731 | 5995 | 555 | 48 | 53 | 143 | 6.7 | 1940 | 65 |
| Filter 40 JP8 @cruise | 939 | 112 | 6022 | 377 | 0 | 24 | 80.8 | 0 | 1600 | 60 |
| Filter 42 JP8+Norpar @idle | 362 | 63 | 5875 | 344 | 19 | 7.4 | 125 | 4.5 | 1930 | 81 |
| Filter 45 JP8+Norpar @cruise | 377 | 95 | 6354 | 405 | 6.7 | 22 | 131 | 5.9 | 1840 | 72 |

A major problems in TEM analyses of the jet PM samples was the electron beam damage to the sample. Apparently, the jet PM sample contained enough volatile organic material to heat up, volatilize, interact with the beam and re-deposit back on the sample to create unusual and misleading artifacts. This phenomenon usually got more severe with higher energy density of the beam at higher magnifications. Typical structures formed are shown in Figure 7. Because of this unusual problem, we could not analyze the samples at high enough magnifications to detect any graphene layers or onion structures. Drying the sample overnight under an infrared lamp (~60-80 C) overnight did not alleviate this problem. We will attempt solvent extraction to alleviate this problem in the near future.

**Summary and Conclusions**

High resolution TEM provides significant insight into the structure of carbonaceous PM emitted from diesel engines. Two significant observations should be emphasized.

1. Diesel PM exhibits a distinctive microstructure that consists primarily of three dimensional chain-like structures of 20-100 nm primary PM globules.
2. High magnification, high resolution TEM reveals that the primary globules consist of onion-like structures made up of graphene layers. Typically 3-10 graphene layers make up the "onion rings", with the layer spacing decreasing from approximately 4.5 to 3.4 nm as the number of layers increases.

TEM has also been used to examine PM derived from a jet engine. The jet PM samples were collected in collaboration with Edwin Corporan and William Harrison of the Air Force Research Laboratory (AFRL) at the Wright Patterson Air Force Base and Matthew DeWitt of the University of Dayton Research Institute. The preliminary results are as follows.

1. With the jet engine running under cruise conditions, chain-like structures of 20-100 nm primary PM globules very similar to the diesel PM are observed. Under idle conditions, however, larger more equant agglomerates are observed.
2. Attempts to observe graphitic structures at higher magnification were unsuccessful, due to the growth of unusual fibrous carbon structures. Such structures could arise from the volatilization and re-deposition of unburned fuel and lube oil.

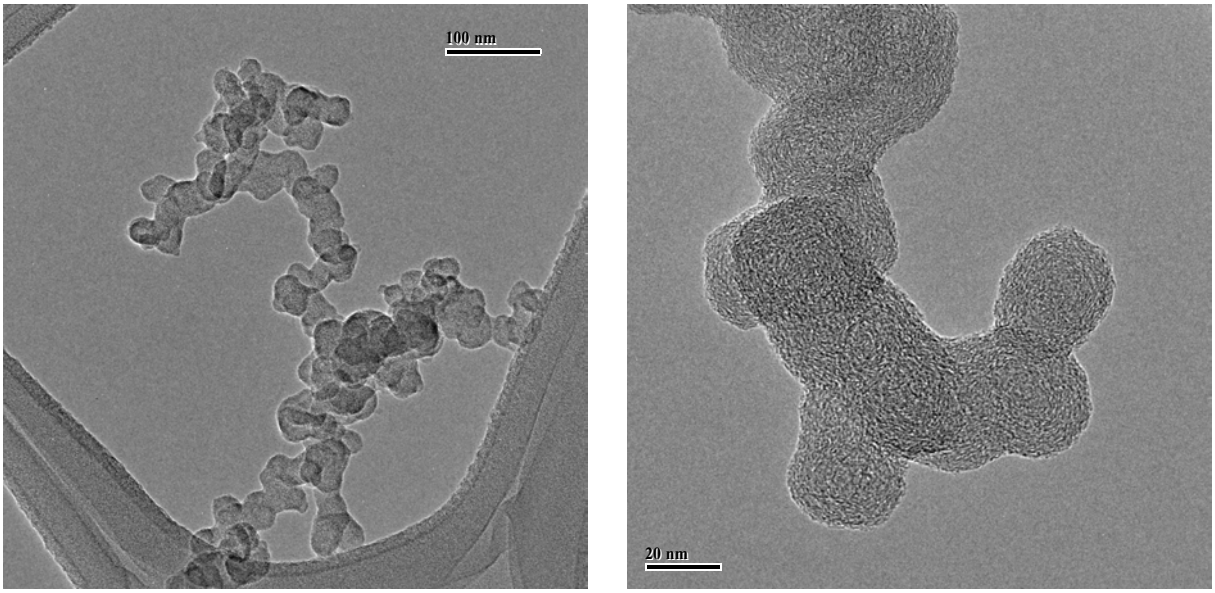


Figure 1. Chain-like agglomerates of primary diesel PM particulates.

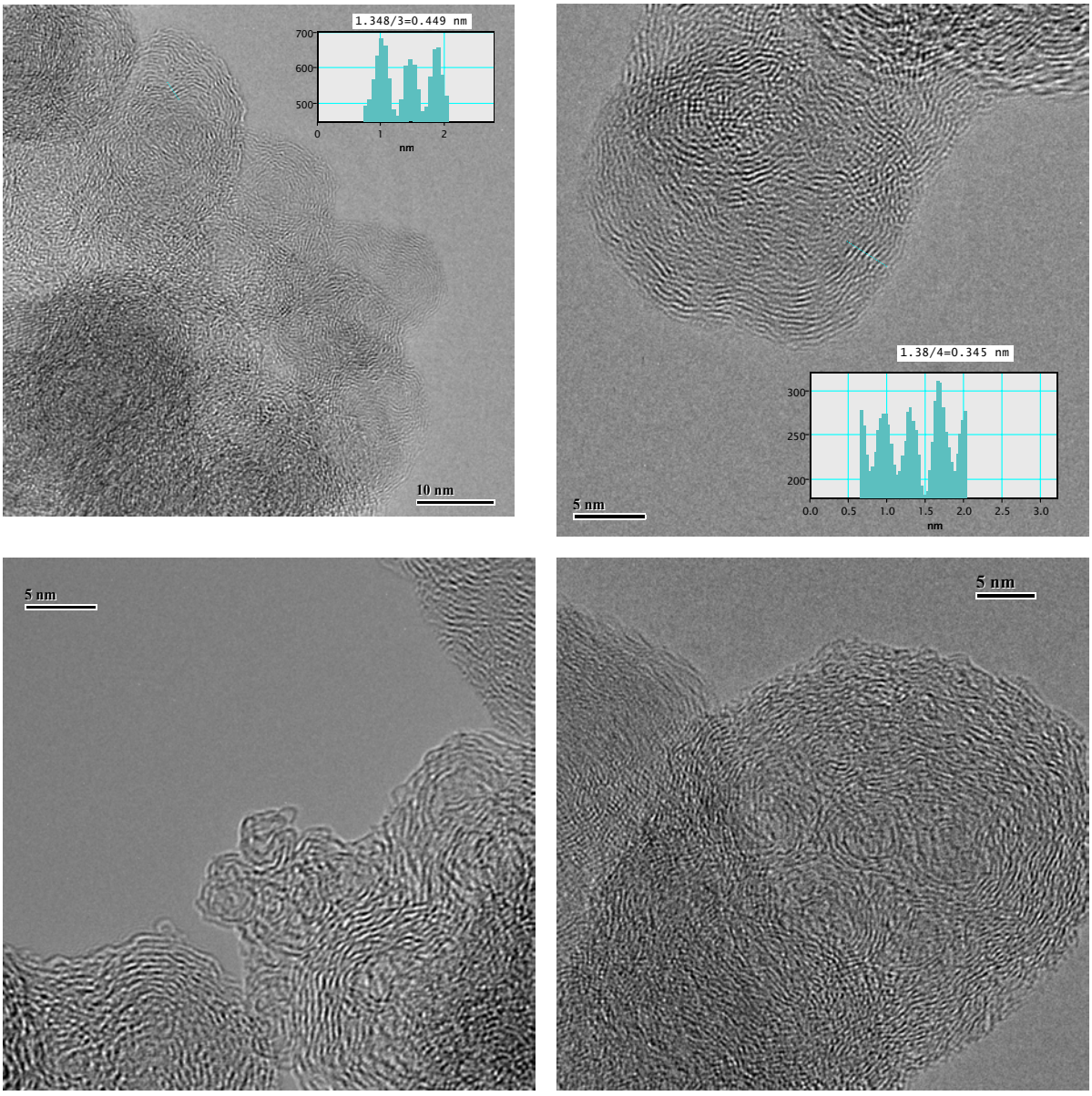


Figure 2. HRTEM micrographs showing the nature of the nanoscale graphitic regions in diesel particulates. The onion-like graphene layer structures are quite distinctive.

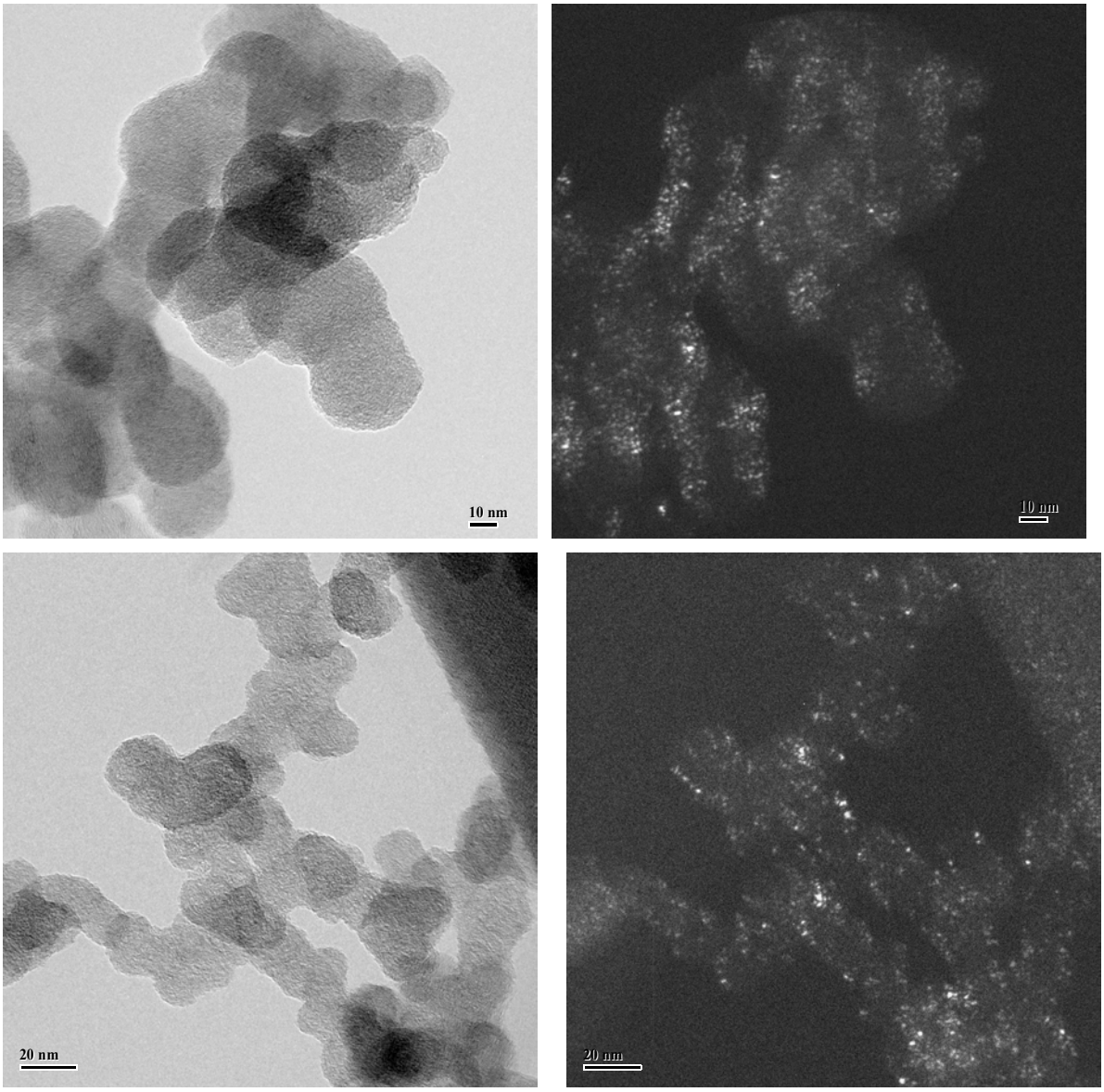


Figure 3. (0000) bright field and (0002) dark field images of soot particles containing several primary globules. Note that the bright areas in the dark field images, which are due to regions meeting the 0002 Bragg condition.

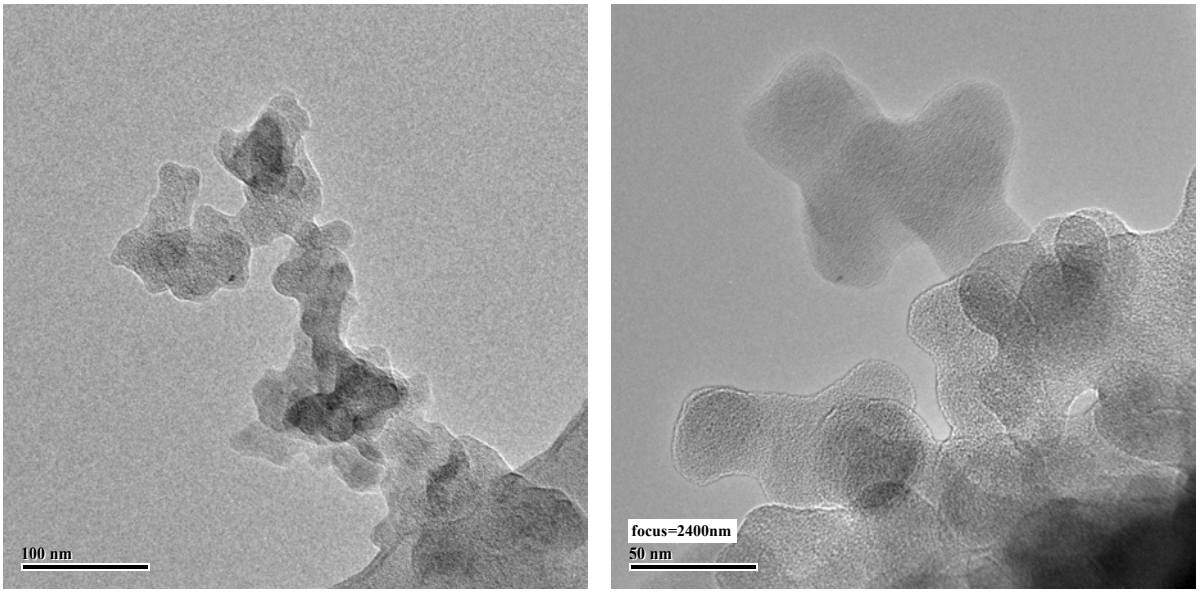


Figure 4. Chain-like structures of 20-100 nm globules observed in PM from a jet engine running under cruise conditions are similar to those observed in diesel engine PM.

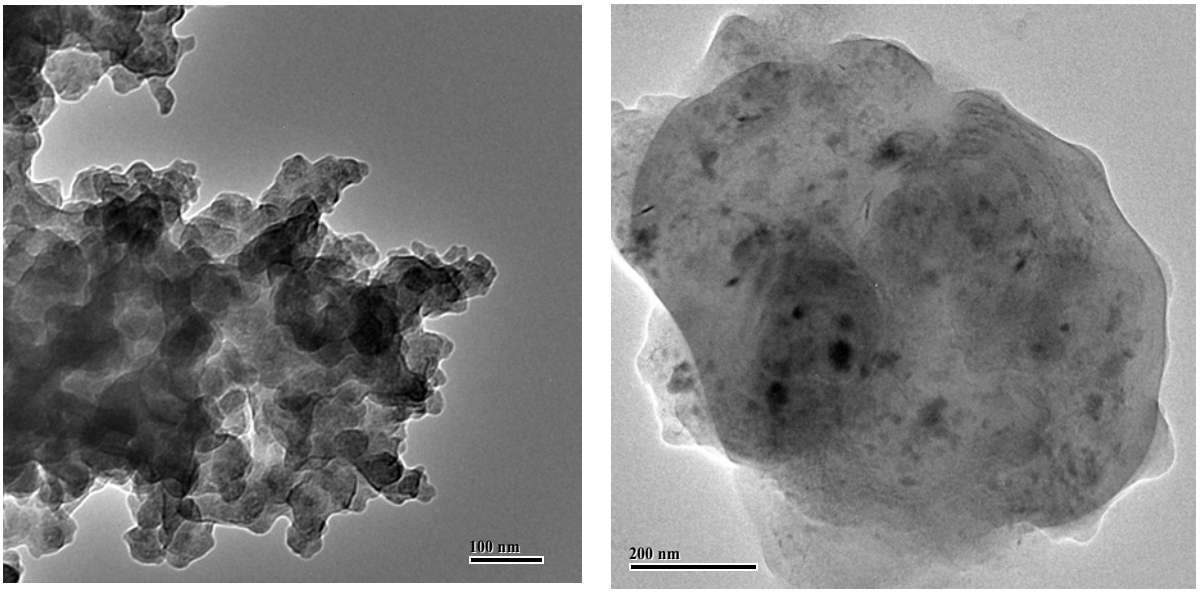


Figure 5. Jet PM collected under engine idle conditions tends to consist of larger, more condensed aggregates. Inorganic inclusions are evident in the particle on the right.

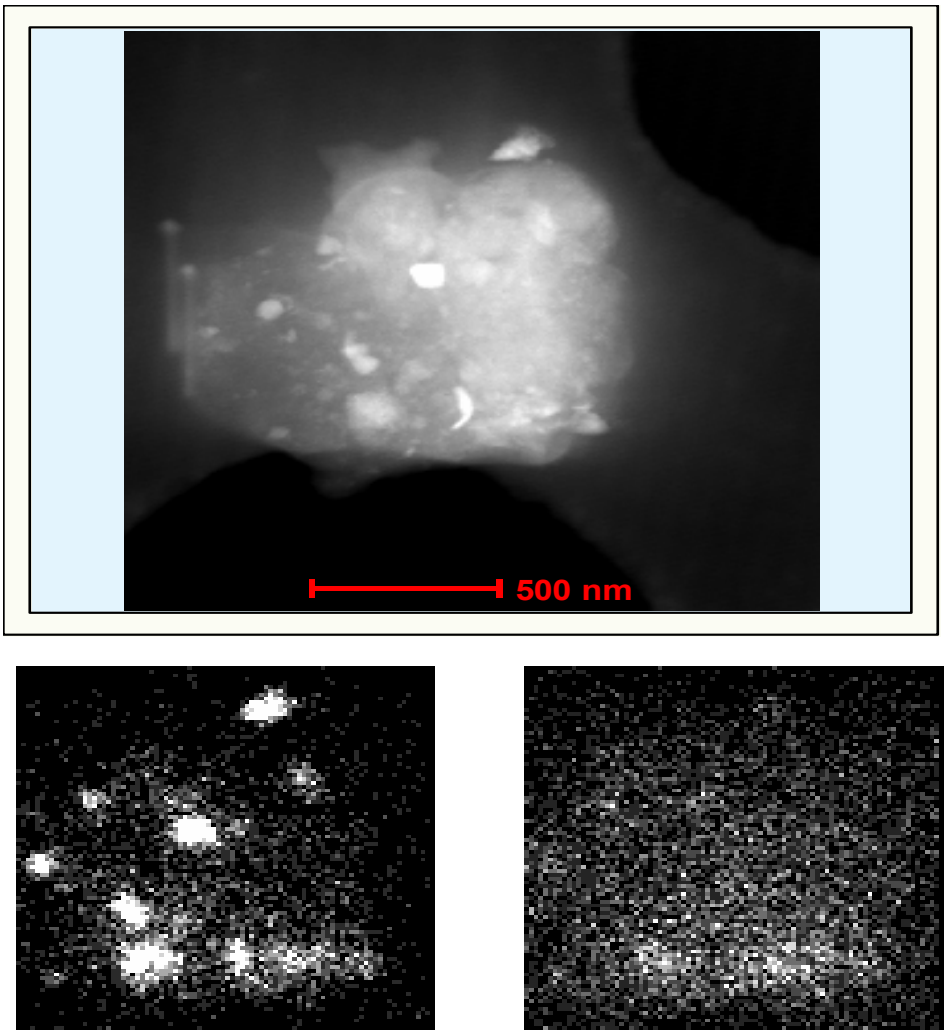


Figure 6. This stem image and Fe and O x-ray maps of a jet PM particle show that it contains nanoscale Fe-rich particles that are predominantly metallic.

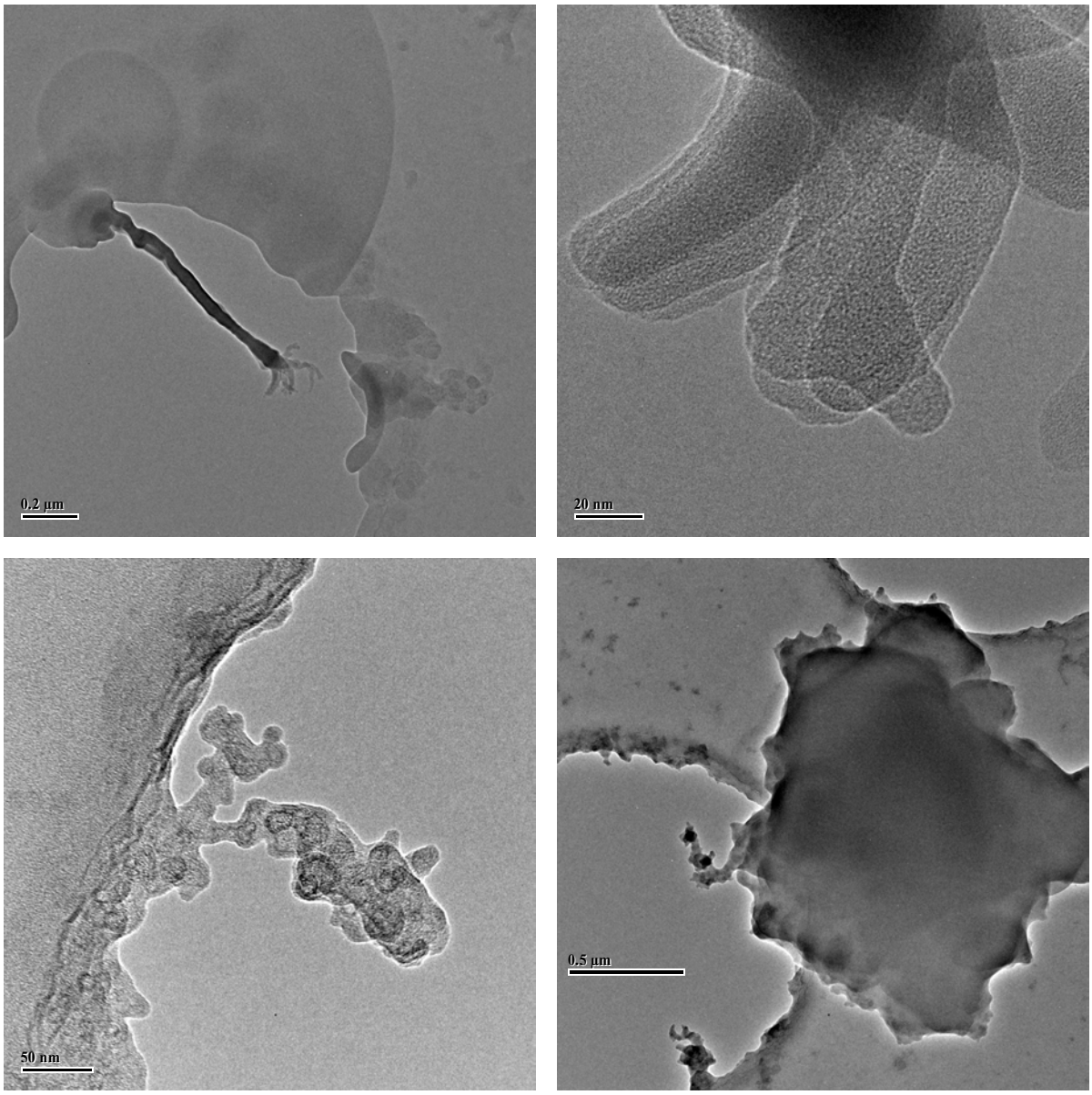


Figure 7. TEM micrographs illustrating unusual fibrous carbon structures produced when attempting to investigate the jet PM under high resolution, high magnification conditions. (TOP). Linear soot agglomerate (like diesel soot) showing secondary deposition.

# Gas Chromatography/Mass Spectrometry and Multivariate Data Analysis of Organic Combustion Signatures in Ambient Particulate Matter

Henk Meuzelaar, Neil Arnold, SueAnne Sheya and JoAnn Lighty

Research activities during the past year have focused on: (1) deconvolution and identification of organic combustion signatures in complex urban PM samples; and (2) generation, collection and characterization of diesel engine soot samples under well-defined operating conditions.

## 1. Combustion Signatures in Ambient PM Samples

Thermal Desorption (TD) GC/MS profiles from 24-hr ambient PM samples, collected on quartz fiber (QF) filters at 11 different receptor sites within the Paso del Norte airshed along the US/Mexico border, were examined for organic combustion signatures using exploratory factor analysis techniques.

The Paso del Norte airshed encompasses the sprawling megacity of Juarez (pop. ~ 1,800,000) and the city of El Paso (pop. ~ 200,000) separated only by the Rio Grande River and accompanying border clearance zone. Due to marked contrasts in culture, economic development, industrial practices and environmental regulations, the large metropolitan area formed by these nearly contiguous cities is home to a highly complex assortment of ambient PM sources. Combustion-type PM sources range from a broad array of mobile sources and industrial furnaces to open kilns, ovens, piles, drums and pits burning all manner of biomass and waste products. In view of this extreme complexity, compilation of a comprehensive inventory of organic PM emission sources, particularly on the Juarez side, is virtually impossible. Therefore, we used detailed speciation of organic PM components in spatially distributed receptor samples by TD- GC/MS in combination with exploratory Factor Analysis in order to numerically extract prominent organic combustion signatures while trying to reference these to known geographical concentrations of certain types of combustion sources. As reported by Sheya [1], this approach has enabled us to recognize specific biomass combustion sources, including fireplaces and brick kilns, as well as urban dust sources and mobile sources.

Figure 1A reveals a spontaneous demarcation between factor analysis scores produced by TD-GC/MS profiles of PM-associated organics in 11 receptor samples obtained on different sides of the US/Mexico border. The corresponding factor loading plot in fig. 1b demonstrates this demarcation to be primarily due to higher relative concentrations of polynuclear aromatic hydrocarbons (e.g. associated with brick kilns and other soot-forming combustion processes) plus animal fatty acids (primarily associated with cooking) on the Mexican side of the border and of fossil terpenoids (associated with incomplete combustion of petroleum-derived fuels) plus alcohols and ketones (e.g., associated with automotive catalytic converters) on the US side. The chemical process associations used here are largely based on the pioneering work of Cass et al. [2]. The results of rapid, exploratory source attribution studies such as this allows one to zoom in on key PM-associated compound suites representative of certain classes of combustion sources, thereby reducing the problem of myriads of different individual combustion sources in the Paso del Norte air basin to more manageable proportions. Furthermore, this approach

provides an important shortcut to population exposure risk studies, such as demonstrated by Mejia et al [3].

Notwithstanding the current emphasis on PM2.5 or PM1.0, conventional PM10 samples remain the logical choice for many broad-based scientific studies. Ambient particulate matter classifications such as "PM10", "PM2.5" and "PM1.0" represent operational concepts whose primary relevance lies in a hypothetical mechanistic relationship, or empirically observed correlation, with possible health end effects. Use of these classifications outside their narrow operational boundaries, e.g., in order to try and answer fundamental scientific questions about PM formation and distribution mechanisms, is likely to result in artificially skewed measurement data. Moreover, exclusion of organic chemical combustion signatures associated with larger ambient particles, e.g., in the 3 - 7 micron range, violates two fundamental principles of multivariate statistical analysis, namely: (a) to strive towards a multivariate normal distribution of measurement data; and (b) to avoid a-priori data exclusions, whenever practical. Fortuitously, inclusion of a broader range of particle sizes does not at all preclude the possibility of investigating the potential relationships between particle size and particle composition. As long as the intrinsic dimensionality of the measurement data space is large enough to accommodate the major sources of variance associated with particle size it may prove possible to numerically extract the various signatures involved. In fact, as demonstrated by Windig et al [4] numerical deconvolution of spectroscopic signatures in complex organic matter is often possible, even in the absence of known instrumental separation methods.

## 2. Collection of Well-defined Diesel Soot Samples

PM source modeling calculations, based on emission inventories in combination with known emission factor and PM dispersion/deposition behavior assumptions, indicate that in urban air sheds where diesel engines constitute more than a few percent of all mobile sources, diesel soot tends to become the dominant source of ambient carbonaceous PM, particularly in the fine particulate matter range [5]. Thus far, there appear to be no reliable analytical methods to distinguish individual diesel soot particles from other soot producing sources. Nonetheless, the work of Cass et al. [2] on has produced sufficiently characteristic combustion signatures for PM-associated organic compounds to enable source apportionment which distinguishes between diesel and gasoline engines as well as between automotive engines with or without catalytic converters. Since recent reports suggest that: (a) ambient soot-type PM may have a disproportionately large negative effect on morbidity and mortality [6]; and (b) atmospheric soot-type PM could have a marked effect on global warming and cooling [7], it would seem to be quite important to develop a more rational chemical classification of diesel soot components than achievable by the current, archaic "organic carbon" vs. “black carbon" classification techniques. As argued in a recent editorial [8], similar procedure-dependent operational concepts such as "fixed carbon" in coal science or "humic acid" in soil science have only served to delay the introduction of more rigorous analytical methodologies and chemical classifications in these research communities. Moreover, terms such as "organic carbon", "black carbon", or "inorganic carbon" are in direct conflict with accepted scientific definitions of the terms "organic", "black" and "inorganic", respectively. In view of the above-described crucially important role of soot-type PM in environmental health studies as well as in physico-chemical atmospheric models a better founded scientific description and classification of carbon structures and forms in ambient particulate matter is urgently needed.

C13 NMR is one of the most powerful methods for characterizing highly condensed carbonaceous materials. Moreover, the empirical pyrolytic method currently used to determine the amount of "organic carbon" and "black carbon" in ambient PM samples neither meets reaction control criteria for modern "analytical pyrolysis" methods, nor uses advanced analytical techniques to determine the nature and concentration of the volatile compounds evolved, e.g., such as described by Dworzanski et al. for char and soot-type materials [9] by means of TG/MS methods. However, in order to use both TG- and NMR-based analytical methods, it is desirable to collect several grams of diesel soot under sufficiently well-defined reaction conditions to enable a meaningful comparison of carbonaceous structures and compositions. To this end a small diesel engine test bed was developed, as described in previous reports [10]. However, preliminary analysis of the PM samples obtained by TD-GC/MS (Dr. Meuzelaar & co-workers), C13NMR (Dr. Pugmire & co-workers) and XRF (Dr. Robertson & co-workers) techniques suggested that conventional hi-vol QF filter sampling, using well-defined filter flows, produces unacceptably large variations in the composition of PM collected on the QF filters because of filter temperature fluctuations caused by differences in diesel engine load and rpm.

This has prompted a complete redesign of the PM and VOC sampling train in collaboration with Dr. Sarofim and his associates David Wagner and Kerry Kelly. This redesign was completed in October 2002. Presently, a series of engine tests is being carried out which aims to produce gram quantities of diesel engine soot samples from well-characterized diesel fuels, fuel blends and additives under well-defined engine operating conditions. These samples will be made available to Dr. Pugmire's group for C13 NMR analysis and will further be investigated by conventional "organic carbon vs. black carbon" test procedures as well as the more advanced analytical pyrolysis methods discussed previously. Also, in close collaboration with Dr. Sarofim & associates we will be attempting to determine the effect of variations in engine exhaust temperature and residence time on soot composition. The results of the various analytical methodologies will be integrated and compared by means of canonical correlation methods for multisource analytical data, such as reported by Meuzelaar et al. [11].

**References**


1. Sheya, S.N. "Development of Thermal Desorption-Gas Chromatography/Mass Spectrometry as a Rapid Method for Ambient Particulate Characterization," Ph.D. Thesis, University of Utah, December 2002.
2. Rogge, W.F.; Hildemann, L.M.; Mazurek, M.A.; Cass, G.R. "Sources of Fine Organic Aerosol. 2. Noncatalyst and Catalyst-Equipped Automobiles and Heavy-Duty Diesel Trucks," Environ. Sci. Technol., 1993, 27(4) 836-651.
3. Mejia-Valazquez, G. "GIS-based Criteria Pollutant Dispersion Modeling, Source Apportionment and Risk Assessment," to be presented at the 96th Annual AWMA Meeting, San Diego, CA, 2003.
4. Windig, W.; Meuzelaar, H.L.C. "Numerical Extraction of Components from Mixture Spectra by Multivariate Data Analysis," in: Computer-Enhanced Analytical Spectroscopy, H.L.C. Meuzelaar and T.L. Isenhour, Plenum Publishing, 1987, Vol. 1, 67-102.
5. Kinney, P.L.; Aggarwal, M.; Northridge, M.E.; Janssen, N.A.H.; Shepard, P. "Airborne Concentrations of PM2.5 and Diesel Exhaust Particles on Harlem Sidewalks: A Community-Based Pilot Study," Environ. Health Perspect, 2000, 108, 213-218.

6. Peters, A.; Docker, D.W.; Muller, J.E.; Mittleman, M.A.; “Increased Particulate Air Pollution and the Triggering of Myocardial Infarction,” Circulation, 2001, 103, 2810-2815.
7. Menon, S.; Hansen, J.; Nazarenko, L.; and Luo, Y. “Climate Effects of Black Carbon Aerosols in China and India Surabi Menon,” Science, 2002, 297, 2250-2253.
8. Meuzelaar, H.L.C. “Organic Carbon?,” Field Anal. Chem. Technol., 2000, 4(2-3), 71-72.
9. Dworzanski, J.P.; Meuzelaar, H.L.C.; “Pyrolysis Mass Spectrometry, Methods,” in: The Encyclopedia of Spectroscopy and Spectrometry, Mass Spectrometry, John Lindon, George Tanter and John Holmes, Academic Press Ltd., London, 1999, 1906-1919.
10. Sarofim. A.F.; Pugmire, R.J.; Meuzelaar, H.L.C.; Kelly, K. “Investigation of Organic and Inorganic PM2.5 by NMR, TD/GC/MS and Laboratory Combustion Experiments,” Annual Report, Molecular Structure and Microstructure of PM2.5 Derived from Stationary and Mobile Fossil Fuel Sources, NSF Award #0089133, 2001.
11. Meuzelaar, H.L.C.; Statheropoulos, M.; Huai, H.; Yun, Y. “Canonical Correlation Analysis of Multisource Fossil Fuel Data,” in; Computer-Enhanced Analytical Spectroscopy, Peter A. Jurs, Plenum Publishers, 1992, Vol. 111, 185-213.

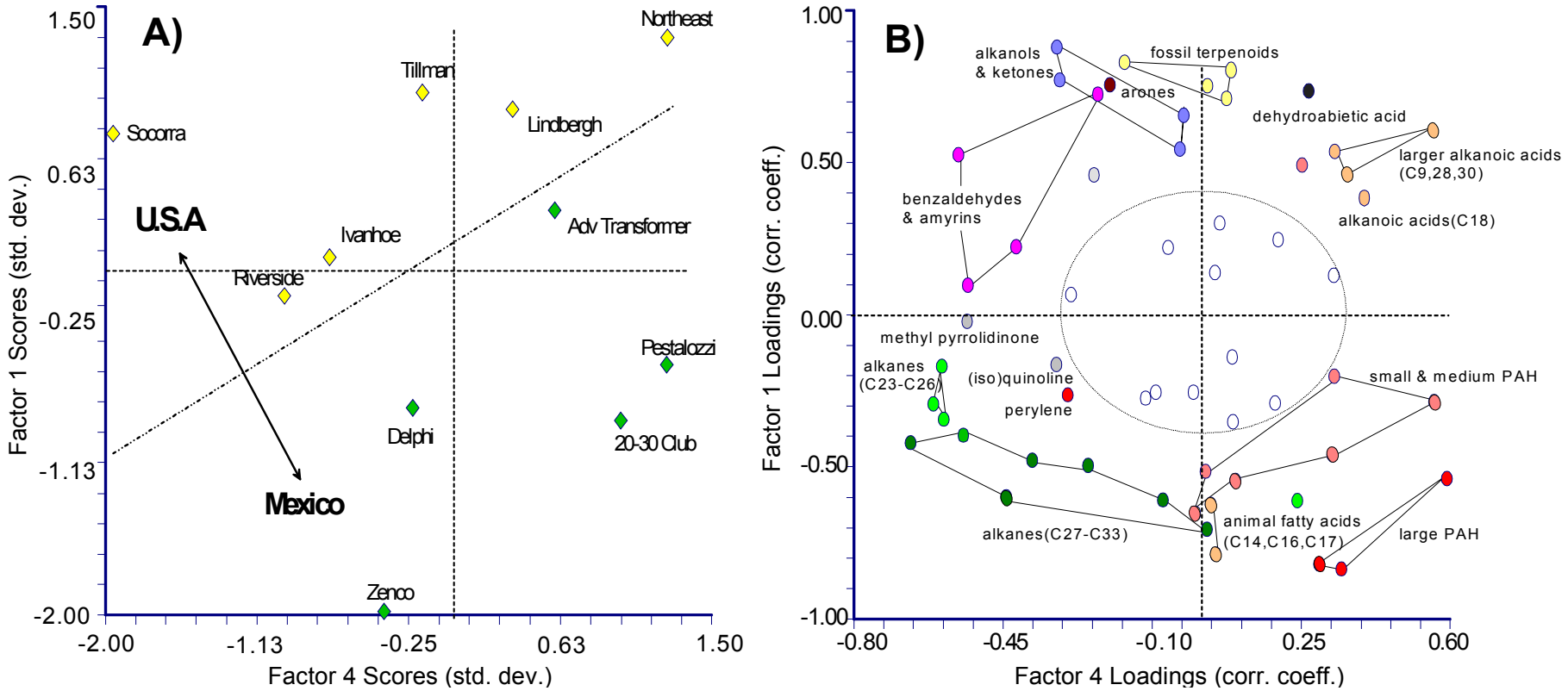


Figure 1. Factor 1 versus factor 4 scores A) and loadings B) for TD-GC/MS profiles of PM10 receptor samples from 11 Paso del Norte sites. The US sites can be separated from the five Mexican sites in these plots which represent 27% of the total variance.

# Upgrades to the Small Diesel Engine Test Facility

A.F. Sarofim and J.S. Lighty
University of Utah

## Generation of Well-Defined Diesel Soot Samples

Because diesel PM is such an important contributor to fine PM concentrations in the atmosphere and diesel PM composition can vary dramatically with fuel and engine condition, the investigators have been upgrading their diesel engine test facility to provide more consistent and reproducible conditions. The upgrades focused on improving engine control, temperature sensing, air-flow monitoring, and fuel consumption. With the upgrades, an operator can monitor and record a number of parameters, such as brake-specific fuel consumption and horsepower (Figure 1).

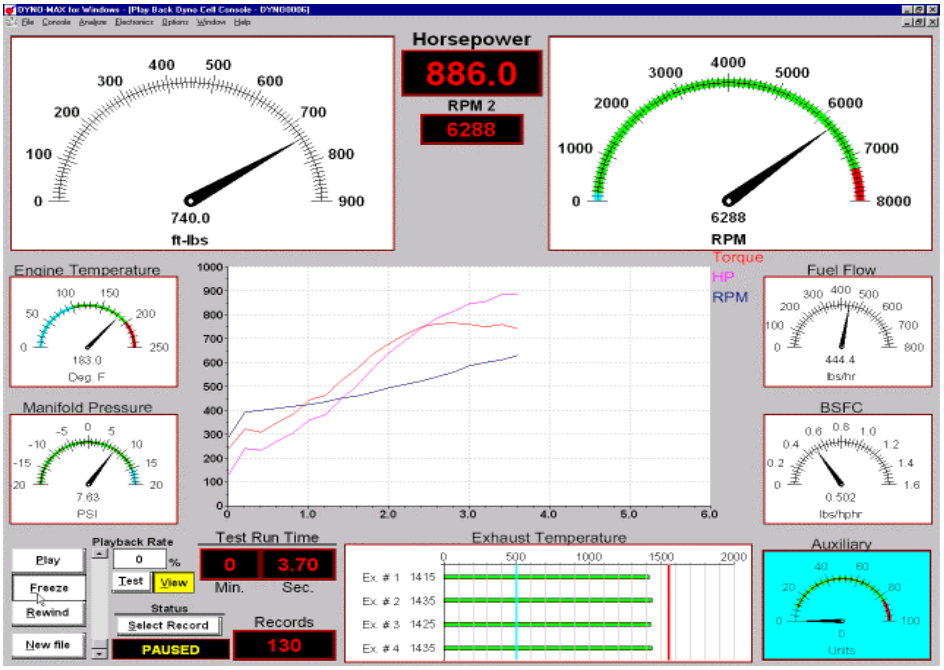


Figure 1. Example of the parameters that are now monitored in the engine test facility.

The two-cylinder, 482 cc Kubota diesel engine was upgraded with improved sensing and control elements to monitor and control engine conditions. Specifically, an auto throttle servo and an auto load servo valve improved engine control. Both provide feedback to a software system that controls engine rpm and engine load, as provided by a water-brake, direct-shaft mounted dynamometer. A data channel expansion unit was installed to automate the throttle and load control. This enables the operator to view and adjust engine speed and load, and also accommodates preprogrammed transient cycles.

In order to ensure reproducible test conditions, the engine was also upgraded with a number of sensors. Engine oil and coolant temperatures are monitored with thermistors; intake, exhaust manifold, and critical sampling points are monitored for temperatures with thermocouples. In

addition, incorporating a cold-junction compensator enhanced the accuracy of the temperature measurements.

Air flow meter turbine units were installed to measure exhaust and intake rates. The exhaust can now be quantified by adjusting the exhaust gas density in the interface software or by initial calibration using the Kubota engine manufacturer's performance data. The intake air now passes a series of high surface area HEPA filters prior to the intake air flow meter turbine. Using the HEPA-filtered intake can help determine the effect of PM in the intake on the formation of PM in the exhaust.

Fuel consumption is now automatically measured with a low-volume flow sensor that reports fuel consumption to the software interface. For very low fuel consumption rates, a digital laboratory bench scale with real-time updating can be used. This requires that an external fuel tank be placed on the scale, and the scale is equipped with RS-232 output, which reports mass to a computer.

**Diesel Engine Experimental Plan**

With completion of the engine upgrades, the investigators have developed a set of experiments to determine the effect on PM of engine operation conditions and fuel composition. The current test matrix involves varying engine load, cetane number, composition (fixed cetane number), and composition (variable cetane number). Currently, it comprises forty different tests, and it may be revised as the tests progress. Each set of tests will be performed at three conditions: 1200 rpm (idle), 1600 rpm with 10 ft-lb torque, and 2500 rpm with 10 ft-lb torque.

# XAFS Spectroscopic Characterization of Particulate Matter from Combustion of Residual Oil and Other Petroleum Sources

Frank E. Huggins[1], Sidharta Pattanaik[1], Devadas Panjala[1], Gerald P. Huffman[1], J. David Robertson[2], and Joseph Kyger[2]
[1]University of Kentucky, [2]University of Missouri

## A. Introduction.

The work described herein continues the studies initiated in the first year of the program. In this work we are using mainly spectroscopic techniques, such as XAFS and iron Mössbauer spectroscopies, to obtain an understanding of *how* various key elements occur in complex aerosol materials known collectively as particulate matter, (PM). These spectroscopic methods, with their ability to focus on a specific element and return information about the local structure and bonding, are excellent speciation methods for elements in fine aerosol materials. As described last year, we are examining PM samples from both stationary and mobile major primary combustion sources, as well as the fine ambient PM less than 2.5 um in size ($PM_{2.5}$) (secondary PM) collected in regulation federal reference method (FRM) $PM_{2.5}$ air sampling devices.

Our overall objective in this work is to obtain information on the speciation of various elements in PM and assess the information for application to understanding health effects and for source apportionment purposes. The principal findings of our previous research on residual oil fly-ash PM samples, diesel exhaust PM samples, and ambient PM filters are listed below:

- Demonstration that sulfur in primary $PM_{2.5}$ from three major fossil-fuel combustion processes (residual oil combustion, coal combustion and diesel engine combustion) can exist in a variety of minor forms in addition to sulfate.
- The presence of thiophenic sulfur appears related to the amount of unburnt carbon in the primary PM sample.
- Other minor sulfur forms may be diagnostic for a specific combustion process. For example, the presence of sulfite in PM may be indicative of combustion of western US coals and the presence of bisulfate may be indicative of diesel-derived PM.
- Most metals are present in ROFA-derived and diesel-derived PM as sulfates; however, iron is an exception and may exist largely as oxide or oxyhydroxide forms.
- Coarse ROFA PM ($PM_{2.5+}$) appears to contain metal sulfides of Ni, Fe and Cu, but such sulfides are largely absent from fine ROFA PM ($PM_{2.5}$). However, their presence may be related to the lean combustion conditions under which the residual oil was combusted.
- A certain fraction of nickel in ROFA $PM_{2.5+}$ samples was found as nickel subsulfide, a reputed carcinogenic compound of nickel. Again, this may be largely due to the conditions under which the residual oil was combusted.
- Sulfur in PM samples from diesel exhaust is more dispersed and/or diluted in such samples from engines under load than at idle.
- XAFS experiments can be performed with reasonable success on Teflon filters used in FRM ambient air monitoring devices, as long as the sample is collected over a four-day or longer period.
- Sulfur in ambient $PM_{2.5}$ samples appears to exist almost entirely as sulfate.

- Zinc in ambient $PM_{2.5}$ exists as fully hydrated zinc sulfate ($ZnSO_4.7H_2O$); in contrast, anhydrous or only partially hydrated zinc sulfates may be present in ROFA and diesel-derived $PM_{2.5}$.

Based on such findings, one of the main goals for the present year was to combine XAFS spectroscopy and leaching behavior for improved speciation investigation of ROFA and coal PM. This has been the main thrust of the work in the present year and has resulted in improved understanding of the speciation of a number of key elements, especially in ROFA PM. In addition, we have initiated studies on the speciation of elements in PM from jet fuel combustion and continued investigations on diesel PM and ambient PM.

**B. XAFS spectroscopy and leaching behavior for improved element speciation in primary PM samples.**

Three ROFA samples, all consisting of both $PM_{2.5}$ and $PM_{2.5+}$ fractions, were selected for leaching. The $PM_{2.5}$ and $PM_{2.5+}$ fractions of the Baseline #5 (BL5) ROFA were subjected to leaching by pentane, water, and 1N HCl acid. The leachings were done for 15 minutes each at room temperature and repeated five times for each solution. The leachings were not done sequentially, but in batch mode. The leachate solutions were collected and saved for analysis, while the residues from the leachings were subjected to XAFS and other analyses. The coarse and fine fractions of two other ROFA samples, high-sulfur #6 (HS6) and low-sulfur #6 (LS6), were exposed to aqueous leaching in the course of analysis by ion chromatography (IC). The residues of the IC extractions of these four fractions were also examined by XAFS spectroscopy. The results are summarized below.

B1. XAFS of leached ROFA PM samples.

*(i) Sulfur:* Sulfur XAFS investigation was conducted on all leached ROFA PM samples and the results were quite consistent from one ROFA PM sample to the next. A suite of sulfur spectra for the BL5 ROFA samples are shown in Figures 1 and 2 for the leached fine $PM_{2.5}$ and coarse $PM_{2.5+}$ fractions, respectively.

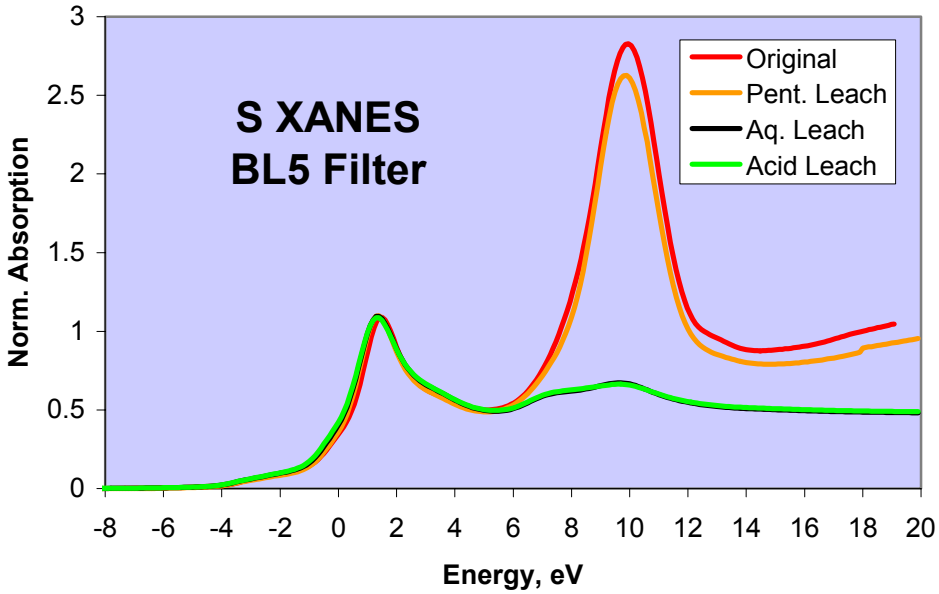


Figure 1: Sulfur XANES spectra of the $PM_{2.5}$ fraction of BL5 ROFA PM subjected to batch leachings in pentane, water, and IN HCl. Spectra are normalized to the same peak-height for the thiophene absorption at approximately 1.3 eV above the zero-point of energy for the sulfur XANES, which is taken by definition as occurring at 2472 eV.

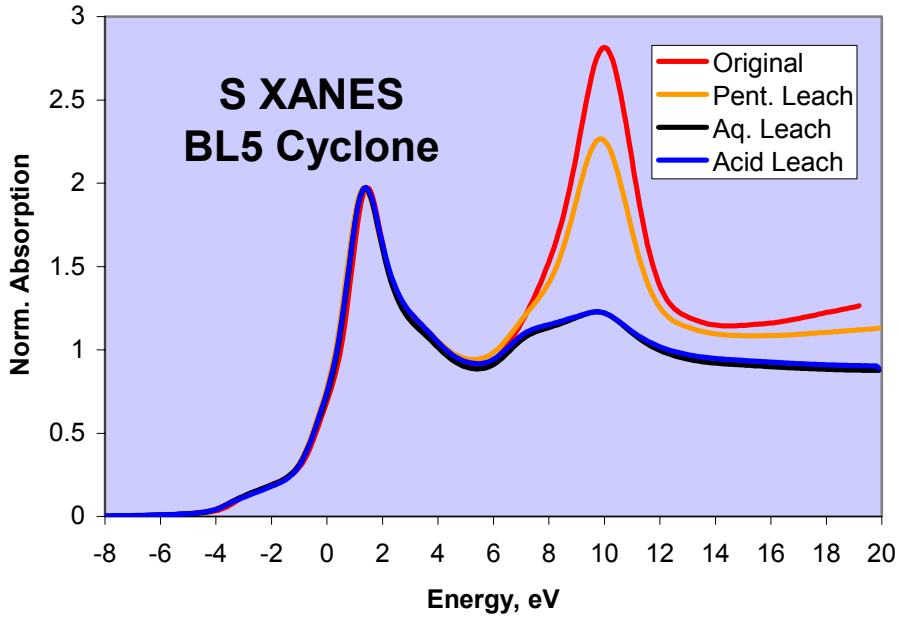


Figure 2: Sulfur XANES spectra of the $PM_{2.5+}$ fraction of BL5 ROFA PM subjected to batch leachings in pentane, water, and 1N HCl. Spectra are normalized to the same peak-height for the thiophene absorption at approximately 1.3 eV above the zero-point of energy for the sulfur XANES, which is taken by definition as occurring at 2472 eV.

The spectra of the leached ROFA PM samples show clearly that the pentane leaching has little effect on the forms of sulfur in the PM samples. However, the aqueous and acid leachings have virtually identical effects on the sulfur spectra and show that most of the sulfate sulfur can be removed from ROFA PM by either treatment. Furthermore, none of the three solutions has any effect on the reduced sulfur forms in the ROFA PM. It would appear that the elemental sulfur, thiophenic sulfur, and inorganic sulfide sulfur are largely unaffected by any of the leaching solutions attempted.

Although they were only subjected to aqueous leaching, the sulfur XANES spectra of the HS6 and LS6 leached residues show virtually identical results to those for the corresponding spectra of BL5 fractions. Almost all of the sulfate sulfur was removed by aqueous leaching, but the reduced sulfur forms were unaffected by the aqueous treatment. Hence, the behavior of all six fractions of ROFA PM subjected to aqueous leaching was identical.

The sulfur XANES spectra of the leached ROFA samples have been subjected to the calibrated least-squares fitting, described elsewhere [1,2], in order to quantify the different forms of sulfur in the leached samples. The results of this procedure are shown in Table 1 and 2 respectively for the BL5 ROFA PM and the HS6 and LS6 ROFA PM, respectively. The least-squares fitted data for the original sample, published elsewhere [3], is also shown for comparison purposes.

Table 1: Results from least-squares fitting of sulfur XANES spectra of original and leached BL5 ROFA PM residues.

| BL5 ROFA $PM_{2.5}$ | Orig. | Pent. | Aq. | Acid |
|---|---|---|---|---|
| Pyrrhotite | 11 | 15 | 26 | 24 |
| Elemental | 5 | 5 | 10 | 11 |
| Thiophene | 24 | 29 | 60 | 63 |
| Other | 5 | 8 | 0 | 0 |
| Sulfate | 55 | 44 | 4 | 3 |

| BL5 ROFA $PM_{2.5+}$ | Orig. | Pent. | Aq. | Acid |
|---|---|---|---|---|
| Pyrrhotite | 19 | 20 | 33 | 32 |
| Elemental | 8 | 7 | 8 | 7 |
| Thiophene | 37 | 44 | 57 | 58 |
| Other | 4 | 3 | 0 | 0 |
| Sulfate | 32 | 26 | 3 | 3 |

It can be seen from these two tables that the %S as sulfate has decreased dramatically as a result of aqueous leaching and that there has been a corresponding increase in the reduced forms of sulfur in the samples. However, there does remain some sulfur as sulfate, particularly in the HS6 and LS6 samples. Due to differences in leaching procedure, it is likely that that the aqueous leaching has not been so thorough in the case of these two samples compared to that for the BL5 samples. Alternatively, it could mean that there exist some insoluble sulfates in these samples that are more abundant in the HS6 and LS6 ROFA ash. Calcium sulfates have been reported to be present in ROFA PM samples [3]. These and other alkaline earth sulfates (e.g. $SrSO_4$, $BaSO_4$) are known to be only sparingly soluble in aqueous solutions.

Table 2: Results from least-squares fitting of sulfur XANES spectra of original and leached HS6 and LS6 ROFA PM residues.

| HS6 ROFA | Filter, $PM_{2.5}$ | | Cycl., $PM_{2.5+}$ | |
|---|---|---|---|---|
| | Orig. | Aq. | Orig | Aq |
| Pyrrhotite | 11 | 28 | 26 | 38 |
| Elemental | 5 | 9 | 9 | 11 |
| Thiophene | 29 | 46 | 39 | 40 |
| Other | 1 | 7 | 0 | 6 |
| Sulfate | 54 | 11 | 26 | 6 |

| LS6 ROFA | Filter, $PM_{2.5}$ | | Cycl., $PM_{2.5+}$ | |
|---|---|---|---|---|
| | Orig. | Aq. | Orig | Aq |
| Pyrrhotite | 0 | 0 | 0 | 0 |
| Elemental | 0 | 6 | 6 | 7 |
| Thiophene | 14 | 75 | 34 | 66 |
| Other | 2 | 3 | 2 | 9 |
| Sulfate | 84 | 17 | 58 | 19 |

For the BL5 samples, we have estimated the relative change in sulfur contents brought about by the leaching. This is estimated from the thiophene sulfur contents, assuming no loss of thiophene in any leaching solution. The data are presented in Figure 3. These trends should be compared to the corresponding data shown in Table 4 measured by MS-ICP by Joe Kyger and Dave Robertson at the U. Missouri. There is very good agreement for the trends exhibited by the $PM_{2.5}$ (filter) samples, but the agreement is less good for the $PM_{2.5+}$ (cyclone) samples and may indicate that there is a sampling problem for the $PM_{2.5+}$ samples.

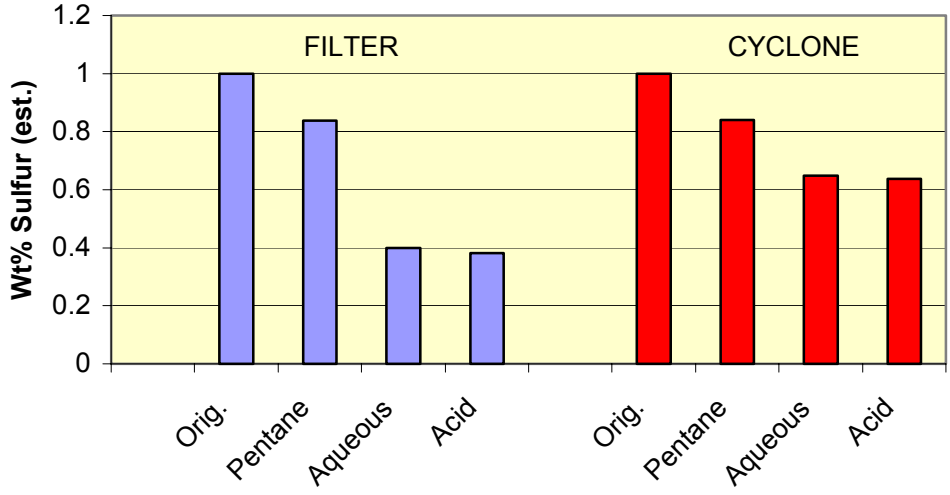


Figure 3: Estimated change in relative sulfur contents for BL5 ROFA samples as calculated from the sulfur XANES data for thiophene, assuming no loss of thiophenic sulfur in the leaching procedures.

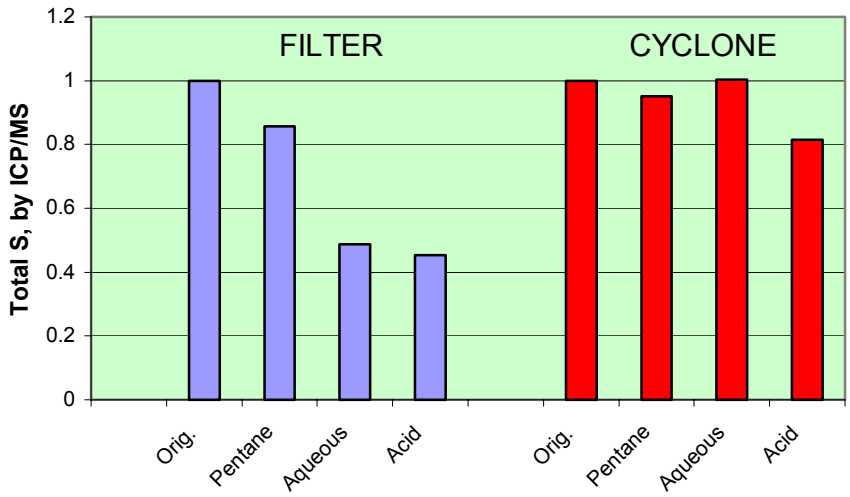


Figure 4: Relative sulfur contents measured for leached BL5 PM samples by ICP/MS. Data courtesy of J. Kyger and J. D. Robertson, U. Missouri.

*(ii) Nickel:* Nickel is typically the second most abundant metallic element in ROFA PM, after vanadium. In earlier work, based largely on Ni K-edge XAFS spectroscopy, we have identified the presence of nickel sulfate and nickel ferrite in fly-ash and PM samples from commercial power plants burning residual oil [4,5]. Nickel sulfide was generally absent or negligibly small in the samples from the commercial plants. However, a nickel sulfide thought to be the subsulfide $Ni_3S_2$ was revealed in preliminary leaching and XAFS investigations of the ROFA PM samples. This result has now been confirmed by XAFS examination of Ni in the leaching residues from the ROFA samples in more recent work that is presented here. Figures 5 and 6 show the Ni XANES spectra and Ni EXAFS/RSFs for the LS6 ROFA $PM_{2.5}$ and $PM_{2.5+}$ samples before and after aqueous leaching. It is clear that the residue phases for the two size fractions are quite different from each other. In fact, by comparison with Ni standards [4,5], they can be identified as nickel ferrite ($NiFe_2O_4$) and nickel sulfide, respectively, in the $PM_{2.5}$ and $PM_{2.5+}$ fractions. The HS6 ROFA samples do not show evidence for the significant presence of nickel ferrite, but a nickel sulfide phase is clearly present in the leached $PM_{2.5+}$ fraction.

The Ni XANES data for the BL5 leached ROFA samples are shown in Figures 7 and 8 for the $PM_{2.5}$ and $PM_{2.5+}$ fractions. Again, as was noted for sulfur, the pentane leaching appears to have relatively little effect on the spectra and Ni speciation. However, the aqueous and acid leachings do bring about major changes in the Ni speciation. For the BL5 $PM_{2.5+}$ fraction, the aqueous and acid leaching clearly reveal a nickel sulfide, while the nickel ferrite is somewhat revealed by the leachings, although not to the same extent as in the LS6 $PM_{2.5}$ sample.

To quantify the nickel speciation, we resorted to least-squares fitting of the nickel XANES spectra. In previous attempts of this nature [6], we had limited the least-squares fitting to only two compounds: Ni sulfate and Ni ferrite in $PM_{2.5}$ samples or Ni sulfate and Ni sulfide in $PM_{2.5+}$ samples. However, it is naïve to expect that such a clean and clear difference in Ni speciation between $PM_{2.5}$ and $PM_{2.5+}$ samples actually exists. For this reason, then we attempted to

simulate all the Ni XANES spectra using a linear least-squares fitting procedure based on all three nickel compounds that we knew to be present in these materials.

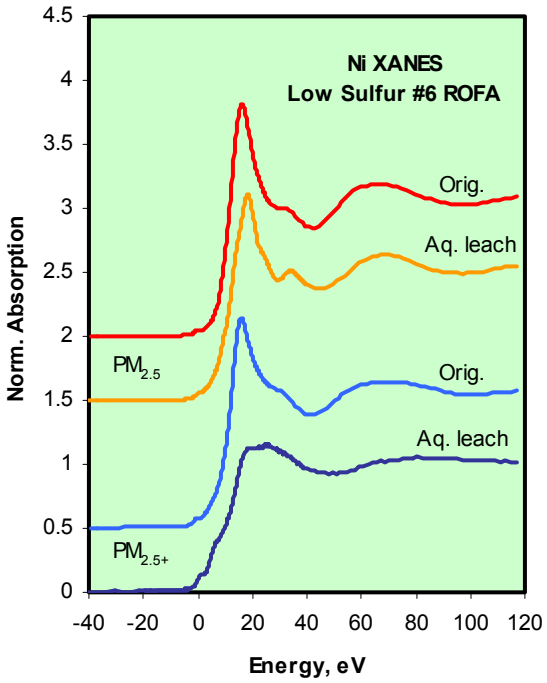


Figure 5: Ni XANES spectra for LS6 ROFA PM samples before and after aqueous leaching.

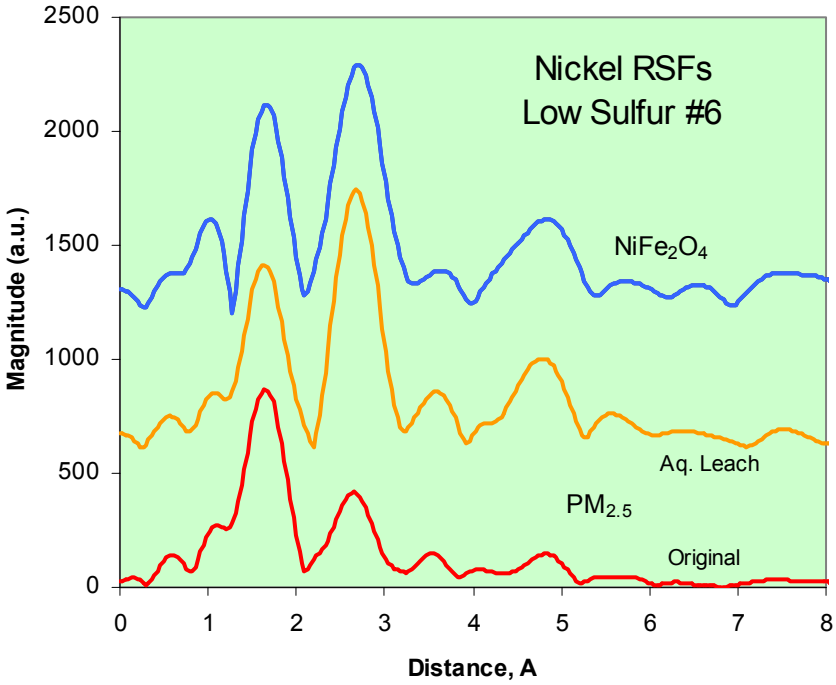


Figure 6: RSFs for Ni in LS6 ROFA $PM_{2.5}$ sample before and after aqueous leaching. Also shown for comparison purposes is the RSF for nickel ferrite, $NiFe_2O_4$.

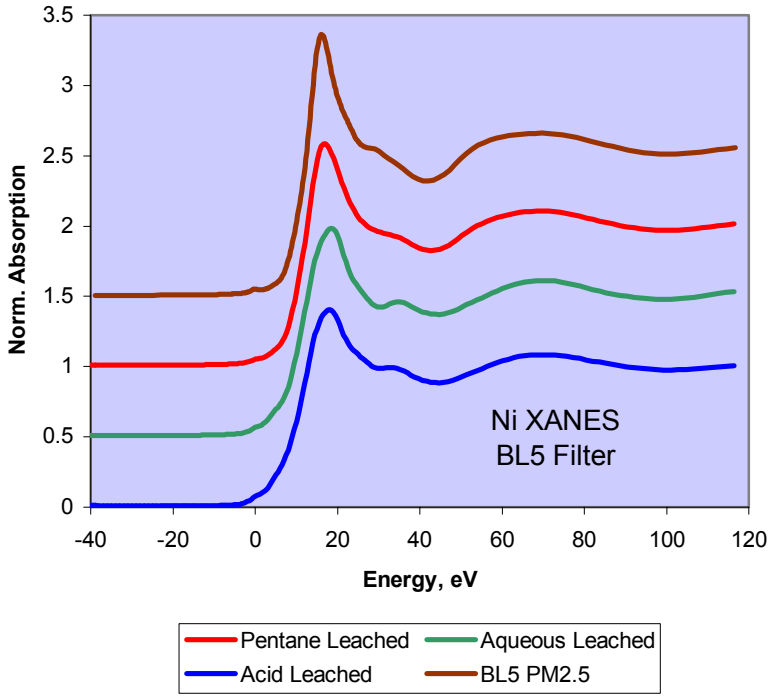


Figure 7: Ni XANES spectra for leached samples of BL5 $PM_{2.5}$.

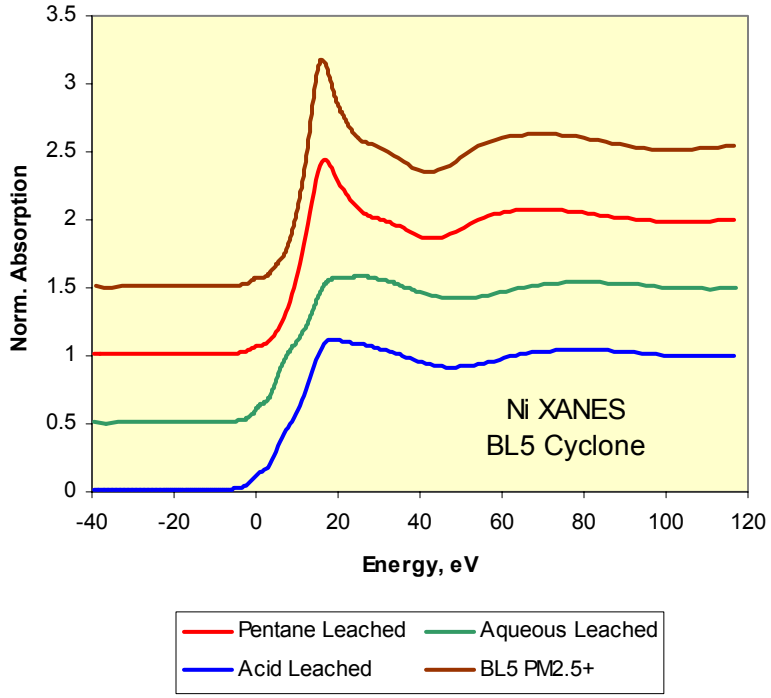


Figure 8: Ni XANES spectra for leached samples pf BL5 $PM_{2.5+}$.

An example of the least-squares fitting of a Ni XANES spectrum from the aqueous leached BL5 $PM_{2.5}$ sample is shown in Figure 9. Data from the least-squares fitting on the nickel speciation for all ROFA samples, both original and leached, are summarized in Table 3.

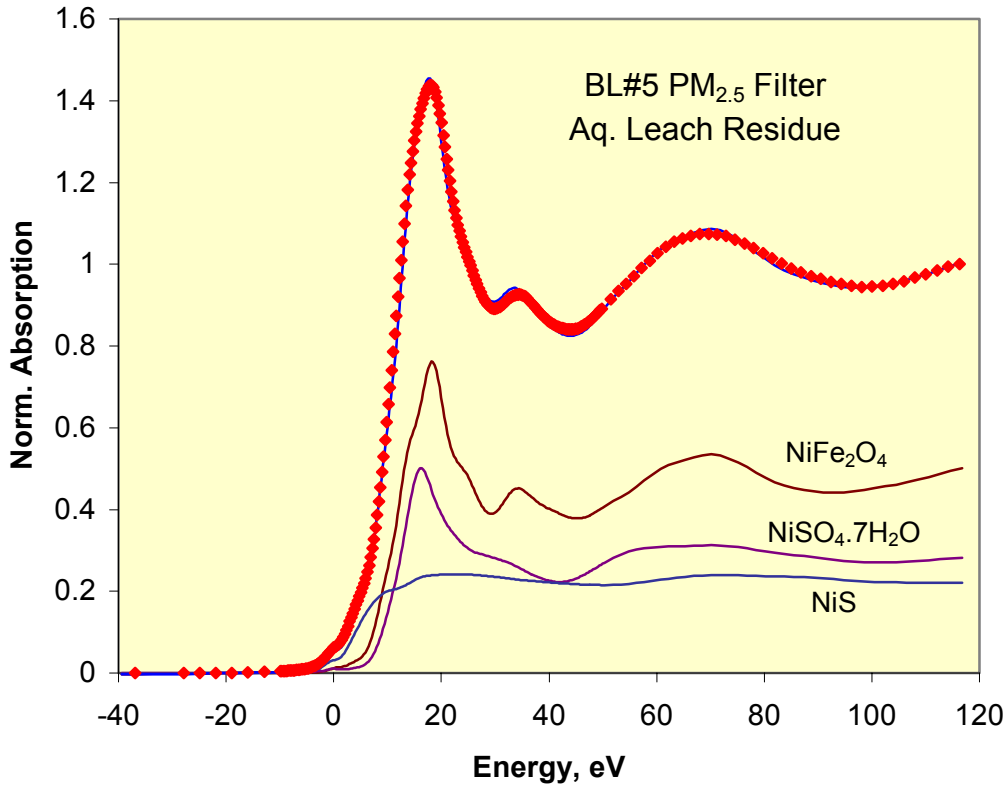


Figure 9: An example of a least-squares fit Ni XANES spectrum using the three major Ni-bearing components identified in ROFA PM samples. The three components are shown at the relative heights of their contribution to the XANES spectrum (q.v. Table 3)

The data shown in Table 3 indicate that, as expected, all three Ni compounds are indeed present in both coarse and fine PM fractions of the ROFA samples. However, it is also clear that there is a tendency for the Ni sulfide to be found in greater proportions in the coarse $PM_{2.5+}$ fractions than in the corresponding fine $PM_{2.5}$ fractions. Conversely, there is relatively little nickel ferrite present in the coarse fraction; indeed, for all $PM_{2.5+}$ samples, no Ni ferrite was observed to be significant relative to a detection limit estimated to be no more than 5% of the Ni. For this Ni phase, it can be argued that it is indeed restricted to the fine $PM_{2.5}$ fractions. For the one sample prepared in a refractory furnace (BL6R), the nickel speciation is predominantly nickel sulfate with a very minor contribution from Ni ferrite. We note also that whereas nickel sulfate is entirely removed from the $PM_{2.5+}$ samples by aqueous leaching, nickel sulfate remains significant in a number of $PM_{2.5}$ samples even after aqueous and acid leaching. Why nickel sulfate should be completely dissolved from coarse PM and not from fine PM would appear to be quite unlikely. It may therefore imply that what we are interpreting as nickel sulfate in the aqueous and acid leached $PM_{2.5}$ samples may in fact be an unidentified insoluble Ni form. Furthermore, it is possible that the Ni ferrite is extremely small sized (nano-particles) and may also be substituted by other elements so that the standard $NiFe_2O_4$ spectrum is not a very good match for that in the $PM_{2.5}$ samples. However, there does not appear to have been reported an XAFS study of nano-$NiFe_2O_4$, although there have been a number of Mössbauer studies of this material in nano form.[7-9].

Table 3: Summary of results from least-squares fitting of Ni XANES Spectra of original and leached ROFA PM samples .

| Sample | %Ni as sulfate | %Ni as sulfide | %Ni as ferrite |
|---|---|---|---|
| LS#6 Filter | 69 | 7 | 24 |
| LS#6 Filter aq. Leach | -- | 13 | 87 |
| LS#6 Cyclone | 75 | 25 | -- |
| LS#6 Cyclone aq. Leach | <5 | >95 | <5 |
| MS#6 Filter | 87 | 5 | 8 |
| MS#6 Cyclone | 81 | 19 | -- |
| HS#6 Filter | 89 | 5 | 6 |
| HS#6 Filter aq. Leach | 40 | 42 | 18 |
| HS#6 Cyclone | 71 | 25 | 4 |
| HS#6 Cyclone aq. Leach | <5 | >95 | <5 |
| BL#5 Filter | 90 | <5 | 10 |
| BL#5 Filter Pent. Leach | 67 | 9 | 24 |
| BL#5 Filter aq. Leach | 29 | 23 | 48 |
| BL#5 Filter acid Leach | 30 | 34 | 36 |
| BL#5 Cyclone | 82 | 18 | -- |
| BL#5 Cyclone Pent. Leach | 66 | 34 | -- |
| BL#5 Cyclone aq. Leach | <5 | >95 | <5 |
| BL#5 Cyclone acid Leach | <5 | >95 | <5 |
| BL#6 Refractory Furnace | 93 | -- | 7 |

Interestingly, when we do compare the iron Mössbauer data for the BL5 ROFA $PM_{2.5}$ sample (presented in last year's report) with that for small-particle $NiFe_2O_4$, there is a very strong resemblance to the spectra published by Ma et al. [7] and Sui et al. [8] for nano-$NiFe_2O_4$, nominally of an average particle size of about 12 nm.

Additional information on the possible particle size of Ni species in ROFA PM may be forthcoming from anomalous small-angle X-ray scattering (ASAXS). In 2002, we made some measurements by ASAXS at the Ni K-edge at the BESSERC SAXS facility at the Advanced Photon Source (APS), Argonne National Laboratory, on the leached ROFA PM BL5 and HS6 samples. The preliminary analysis of the data for the BL5 PM samples is summarized in Table 4. The first observation one makes from these data would appear at first sight to be counter-intuitive: the average particle size determined for the nickel species in the coarser $PM_{2.5+}$ leaching residues is significantly smaller than that determined for the finer $PM_{2.5}$ leaching residues fractions. As part of an attempt to rationalize these results, we should recall that nickel in the residual oil is largely present as individual Ni atoms in porphyrin groups or other organically bound species. One must also recall that the Ni content of the $PM_{2.5+}$ fraction is much less than that of the $PM_{2.5}$ fraction and, furthermore, that the LOI for the $PM_{2.5+}$ fraction is

higher than that for the $PM_{2.5}$ fraction, indicating that the Ni in the $PM_{2.5}$ fraction has experienced somewhat more complete combustion. It may therefore be advanced that the agglomeration of Ni species for the $PM_{2.5}$ fraction has progressed more than it has for the Ni in the $PM_{2.5+}$ fraction because of just those two reasons.

Table 4: Preliminary results on Ni species size from ASAXS measurements.

| *Leaching Residue* | *ROFA Filter, $PM_{2.5}$* | | *ROFA Cyclone, $PM_{2.5+}$* | |
|---|---|---|---|---|
| | *$<R_{ave}>$ in nm* | *Width, σ, in nm* | *$<R_{ave}>$ in nm* | *Width, σ, in nm* |
| *Pentane* | *10.0 ± 0.6* | *4.6* | *6.8 ± 1.2* | *3.9* |
| *Aqueous* | *8.2 ± 0.2* | *3.3* | *5.7 ± 2.0* | *5.1* |
| *Acid (1N HCl)* | *9.6 ± 0.5* | *4.9* | *6.1 ± 0.2* | *3.5* |

Further development of this method will be attempted because the preliminary analysis of the ASAXS data does not take into account the fact that the speciation changes from residue to residue. Whether or not this has a large influence on the derived Ni species size remains to be evaluated.

*(iii) Vanadium:* A similar approach to that developed above for Ni has been taken for the analysis of vanadium in the ROFA PM samples. From the V XANES spectra obtained from leached ROFA PM samples, we identify three main vanadium species present in most of the samples: vanadyl sulfate, $VOSO_4.xH_2O$, vanadium oxide, tentatively identified as small-particle $VO_2$, and a vanadium sulfide. These components are best shown in the V XANES spectra presented in Figures 10 and 11.

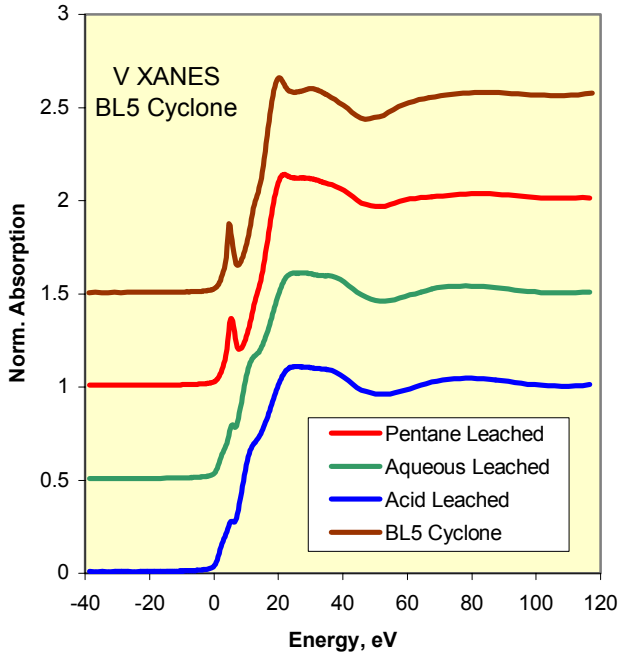


Figure 10: Vanadium XANES of original and leached BL5 $PM_{2.5+}$ ROFA.

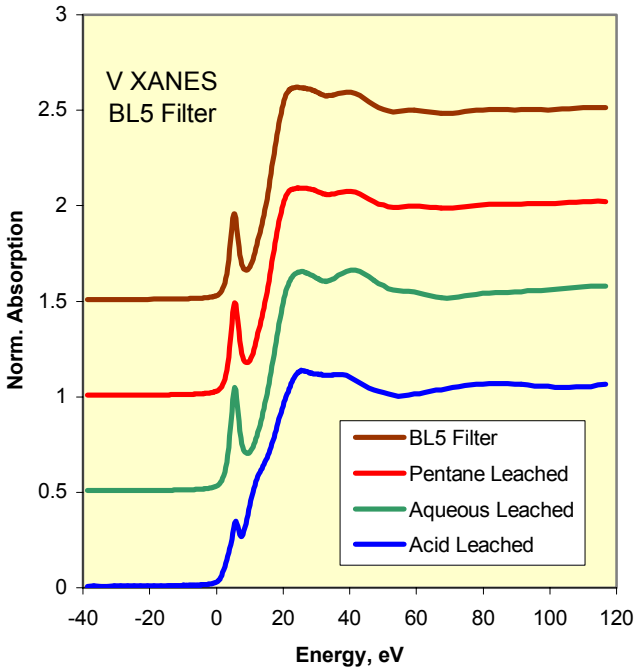


Figure 11: Vanadium XANES of original and leached BL5 $PM_{2.5}$ ROFA.

A clear distinction can be seen between the original spectra for the $PM_{2.5+}$ and $PM_{2.5}$ fractions of the BL5 PM. Based on the spectral profile, the V form dominant in the $PM_{2.5+}$ fraction is vanadyl sulfate, whereas the dominant form in the $PM_{2.5}$ fraction is believed to be $VO_2$. The former spectrum, which also dominates the spectra of both the original LS6 PM fractions (Figure 12), is closely similar to that we have measured for $VOSO_4.xH_2O$ and that reported by Frank and Hodgson [10], but differs somewhat from that reported by Wong et al. [11]. For both acid leached BL5 PM fractions, a quite different spectrum is observed; a similar spectrum is seen for the aqueous leached $PM_{2.5+}$ fraction, but not for the aqueous leached $PM_{2.5}$ fraction. Instead, the latter spectrum resembles that of $VO_2$, although the match is not exact as the XANES peaks for ROFA PM appear broadened in comparison for those of $VO_2$. We suspect that small particle-size effects may explain the difference. The remaining vanadium form, best exemplified by the spectrum of acid-leached BL5 $PM_{2.5+}$ residue, has the shape and character of a vanadium sulfide. However, it is clearly different from that of $V_2S_3$ reported by Wong et al. [11] and a positive identification of this sulfide has not yet been made.

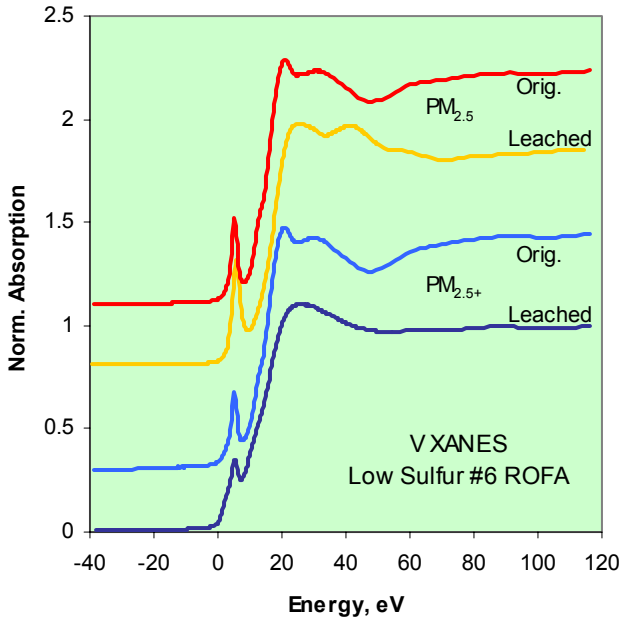


Figure 12: V XANES spectra for the original and aqueous leached LS6 PM fractions.

Despite the uncertainty of the interpretations of the spectra, however, it is clear that the vanadium XANES spectra of the ROFA PM consist mainly of the three spectral components represented by vanadyl sulfate, the vanadium oxide and vanadium sulfide. Rather than using the standard but less representative spectra for $VO_2$ and $V_2S_3$, we chose to use the spectrum shown in Figure 10 for the acid-leached BL5 $PM_{2.5+}$ sample for the vanadium sulfide component and the spectrum shown in Figure 12 for the aqueous leached LS6 $PM_{2.5}$ sample for the vanadium oxide component. We recognize that the latter spectrum may include a minor contribution from vanadium sulfide in addition to the dominant $VO_2$ species, but it is unlikely that the sulfide component represents more than 10% of the vanadium in this particular residue sample.

Using these three components, the V XANES spectra of all the ROFA PM samples, original and leached, were then least-squares fit to determine the percentages of vanadium present as vanadyl sulfate, vanadium oxide ($VO_2$) and vanadium sulfide ($V_xS_y$). The results of the least-squares fitting are summarized in Table 5. Except for the original and aqueous leached HS6 $PM_{2.5}$ samples, all the spectra could be reasonably well fit using the three components described above. For the HS6 $PM_{2.5}$ samples, it would appear that an additional vanadium species must be present, although the vanadium oxide is clearly a major component. For these spectra, we note that the pre-edge peak is larger than that in $VO_2$ and the absorption edge appears to be shifted to slightly higher energy; such differences are suggestive of the presence of V in the pentavalent oxidation state, probably in the form of a vanadate. SEM data suggests the possible presence of other vanadium containing phases for the HS6 $PM_{2.5}$ sample, including phases of composition Ca-V-S and Na-V-P. Possibly significant amounts of the vanadate anion ($VO_4^{3-}$) can substitute for $SO_4^{2-}$ or $PO_4^{3-}$ anions in sulfate or phosphate phases.

Table 5: Results of least-squares fitting of vanadium XANES spectra of original and leached ROFA PM samples.

| Sample | %V as sulfate | %V as oxide | %V as sulfide |
|---|---|---|---|
| LS#6 Filter | 70 | 28 | 2 |
| LS#6 Filter aq. Leach | -- | 100 | -- |
| LS#6 Cyclone | 82 | -- | 18 |
| LS#6 Cyclone aq. Leach | -- | 50 | 50 |
| MS#6 Filter | 78 | 11 | 11 |
| MS#6 Cyclone | 82 | -- | 18 |
| HS#6 Filter | ** | >50** | ** |
| HS#6 Filter aq. Leach | ** | >80** | ** |
| HS#6 Cyclone | 20 | 67 | 13 |
| HS#6 Cyclone aq. Leach | | 60 | 40 |
| BL#5 Filter (1999) | 27 | 73 | -- |
| BL#5 Filter (2002) | 0 | 100 | 0 |
| BL#5 Filter Pent. Leach | -- | 95 | 5 |
| BL#5 Filter aq. Leach | -- | 90 | 10 |
| BL#5 Filter acid Leach | -- | 39 | 61 |
| BL#5 Cyclone (1999) | 72 | -- | 28 |
| BL#5 Cyclone Pent. Leach | 33 | 34 | 33 |
| BL#5 Cyclone aq. Leach | -- | 10 | 90 |
| BL#5 Cyclone acid Leach | 0 | 0 | 100 |
| BL#6 Refractory Furnace | 100 | 0 | 0 |

** Inadequately fit by the three phases included in fitting scheme. Presence of an additional compound (a vanadate?) is suspected (see text).

Another observation relates to the spectra of the original sample of BL5 $PM_{2.5}$, measured three years apart. As indicated in Table 5 and in Figure 13, these spectra are quite different. The data suggest that the vanadyl sulfate present initially has hydrolyzed into vanadium oxide during storage. A similar mechanism would also explain the difference in vanadium speciation between the original BL5 $PM_{2.5+}$ sample and the pentane–leached sample measured three years later. Note also that vanadium oxide is only observed for those $PM_{2.5+}$ samples subjected to leaching in 2002. None of the spectra of the original $PM_{2.5+}$ samples measured in 1999 indicate the presence of significant vanadium oxide. All of these observations can be explained by the conversion of vanadyl sulfate into vanadium oxide during the course of the three years. Note that vanadium oxide *is* observed for the original $PM_{2.5}$ samples and that no vanadyl sulfate is observed for any leached $PM_{2.5}$ sample measured in 2002. These observations suggest that the conversion of vanadyl sulfate to oxide was already well underway when the original samples were first measured in 1999. These observations are also consistent with the difference in particle size between the $PM_{2.5}$ and $PM_{2.5+}$ samples (the smaller particle-size $PM_{2.5}$ samples would be expected to hydrolyze more rapidly than the coarser $PM_{2.5+}$ samples).

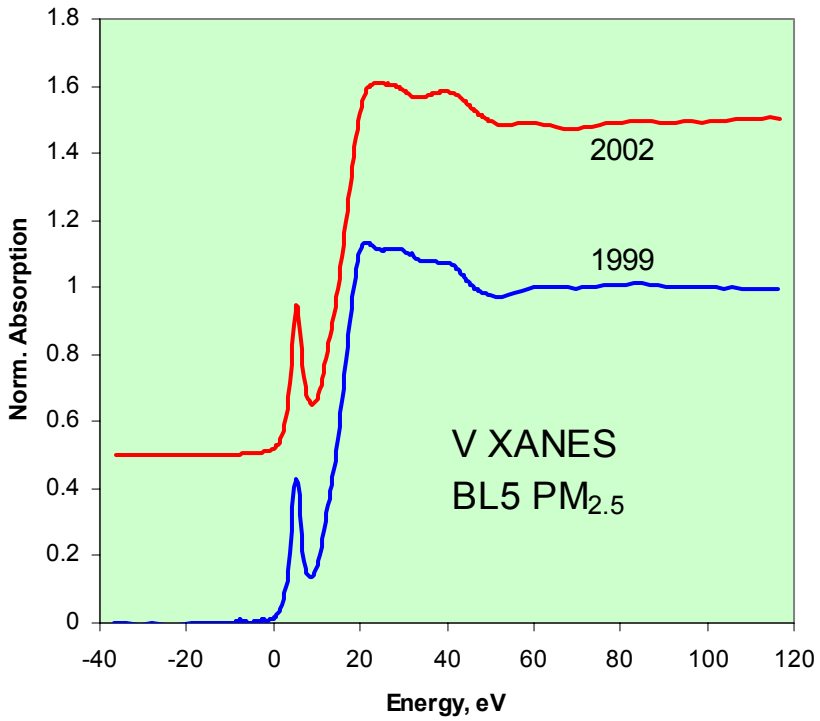


Figure 13: Comparison of V XANES spectra for BL5 ROFA $PM_{2.5}$ taken 3 years apart.

*(iv) Iron:* Leaching data for iron in HS6 PM, LS6 PM, and BL5 $PM_{2.5}$ ROFA samples are shown in Figures 14, 15 and 16, respectively. In comparison to nickel and vanadium, there is much less change in the overall spectrum as a result of leaching and this is also seen in analytical data for the leached samples also. Much smaller fractions of iron are removed by the different leaching solutions than is observed for Ni or V. Our initial conjecture [3,6] that iron was present largely in the form of a ferric sulfate appears to be incorrect; rather, as already discussed for Ni, significant fractions of the iron appear to be present in the form of Ni ferrite, $NiFe_2O_4$, particularly in the fine $PM_{2.5}$ fractions. Typically in analyses of ROFA PM, it is found that the Fe content is significantly less than that of Ni, and therefore, even though only a small fraction of the Ni may be present as Ni ferrite, significant amounts of the iron may be accounted for by this phase given the 1:2 atomic ratio of Ni:Fe in the ferrite phase and the lower content of iron in the ROFA PM. In this regard, we have also already noted that the Mössbauer spectrum of Fe in the BL5 $PM_{2.5}$ sample is closely similar to that exhibited by nano-particles of nickel ferrite.

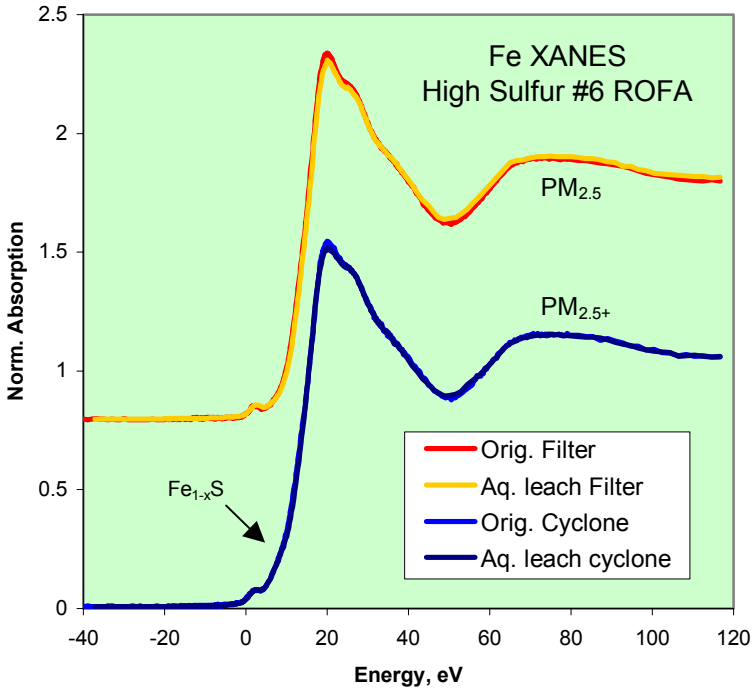


Figure 14: Fe XANES spectra of HS6 PM samples. Note the close similarity of the spectral traces for the original PM samples and those of the corresponding aqueous leached samples.

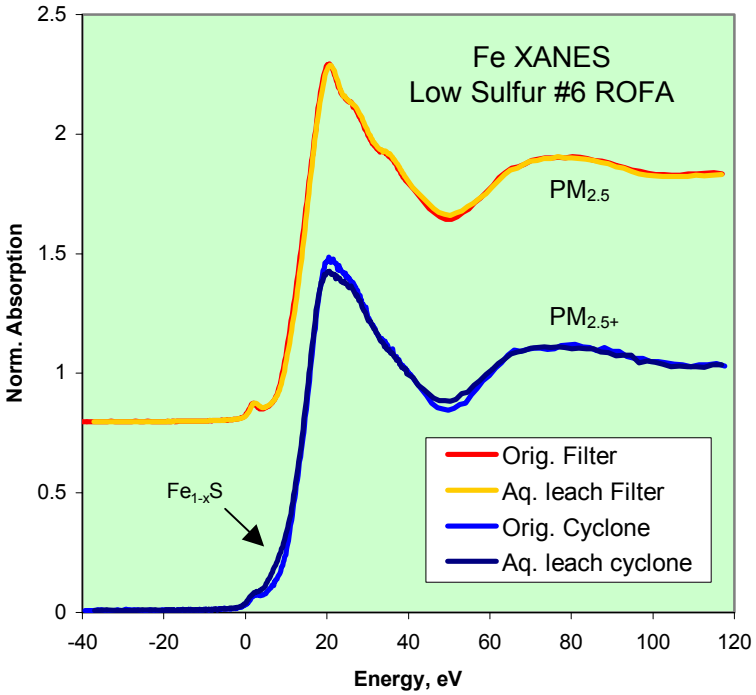


Figure 15: Fe XANES spectra of LS6 PM samples. Note the close similarity of the spectral traces for the original PM samples and those of the corresponding aqueous leached samples.

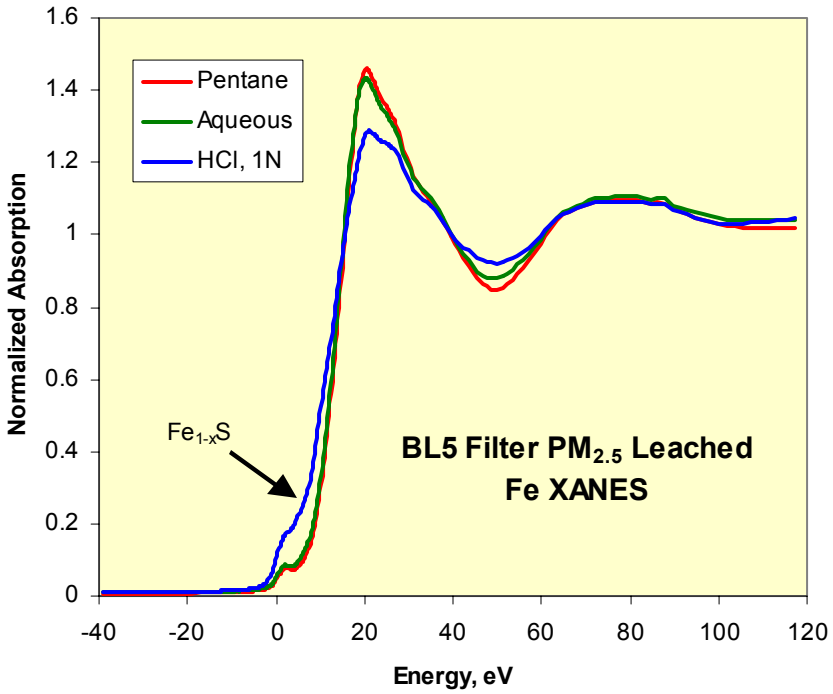


Figure 16: Fe XANES spectra of leached BL5 $PM_{2.5}$ residues. Note the close similarity of the spectral trace for the pentane-leached residue and that of the aqueous leached residue.

It is clear from Figures 14-16 that aqueous leaching has virtually no effect on the iron speciation and this observation confirms that there is no readily soluble iron sulfate phase present in the PM. The Mössbauer data reported previously indicate that the presence of ferrous iron in ROFA PM samples is negligible. Hence, we need be concerned only with ferric iron phases. However, there are numerous different ferric-bearing sulfates of varying solubilities known to form in nature [12]. A significant number (~15) of these sulfates only involve ferric iron, sulfate anions ($SO_4^{2-}$), hydroxyl ions ($OH^-$), and waters of hydration and can be represented by the general formula: $(Fe^{3+})_x(SO_4^{2-})_y(OH^-)_z.nH_2O$; however, the majority of these are reasonably soluble in water and nearly all ferric sulfates are soluble in dilute HCl. Hence, the likelihood of significant iron sulfate being in these samples appears to be low.

The Mössbauer spectrum of BL5 $PM_{2.5+}$ indicates the presence of magnetite and possibly hematite, rather than Ni ferrite, in this sample; however, the data are not of high quality because of their low iron content. Further Mössbauer spectra will be attempted on the leached fractions of these samples to try and resolve further these issues of the iron speciation.

Iron-bearing sulfide is clearly present in the BL5 PM samples; its presence is revealed by acid leaching. Comparison of the $PM_{2.5}$ and $PM_{2.5+}$ iron XANES spectra also shows a low-energy shoulder in the $PM_{2.5+}$ fractions that arises from iron sulfide.

In summary, the iron speciation in ROFA PM samples appears to consist of largely iron oxide and sulfide phases. Much of the iron in $PM_{2.5}$ fractions can be accounted for by its occurrence in the spinel phase, nickel ferrite, whereas other iron oxides, magnetite and possibly hematite are

more prevalent in $PM_{2.5+}$ samples. Iron sulfide appears to be a minor component of $PM_{2.5+}$ fractions and probably is also present in most $PM_{2.5}$ fractions as well, in similar fashion to what we have seen for V and Ni sulfides.

*(v) Other Elements*: Both zinc and copper in ROFA PM have also been examined by leaching and XAFS technique. Representative spectra are shown in Figures 17 and 18.

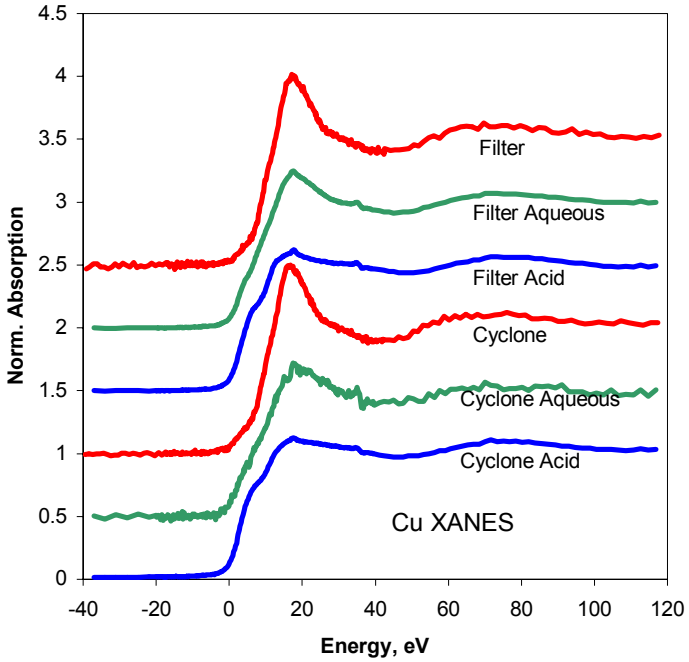


Figure 17: Cu XANES spectra of residues of leached BL5 ROFA PM fractions.

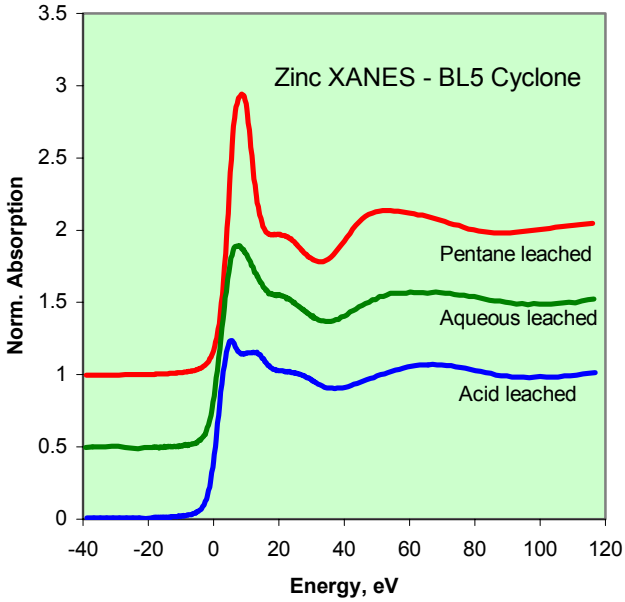


Figure 18: Zn XANES spectra of residues of leached BL5 ROFA $PM_{2.5+}$ fractions.

Both elements exhibit similar behavior to that seen for other elements. Copper sulfate and zinc sulfate dominate the spectra of the original samples and these divalent sulfates are removed by aqueous and more completely by acid leaching. In the case of copper, copper sulfide is revealed as the dominant insoluble copper phase in both BL5 acid-leached $PM_{2.5}$ and $PM_{2.5+}$ fractions, whereas zinc sulfide (ZnS) is revealed in the acid-leached BL5 $PM_{2.5+}$ residue and the aqueous-leached HS6 $PM_{2.5+}$ residue. Zinc ferrite ($ZnFe_2O_4$) for the BL5 acid-leached $PM_{2.5}$ residue and zinc oxide (ZnO) for the LS6 aqueous-leached $PM_{2.5}$ residue were identified.

The XANES spectra of both Cu and Zn in aqueous-leached residues of most ROFA PM samples appear to exhibit mixed assemblages of the sulfate and other phases. For example, the spectra of the aqueous-leached residues shown for Cu in Figure 17 and for Zn in Figure 18 appear to be a mixture of the sulfate and sulfide. Least-squares fitting of the XANES spectra is planned for these elements.

Previous work reported in last year's report showed that the arsenic concentration of the LS6 samples was significantly higher than the other samples investigated. Hence, the aqueous leached residues of these samples were investigated at the As K-edge. As XANES spectra are shown in Figure 19 for the two original LS6 PM samples and the LS6 aqueous leached $PM_{2.5}$ residue. The corresponding LS6 $PM_{2.5+}$ residue exhibited virtually no spectrum at all.

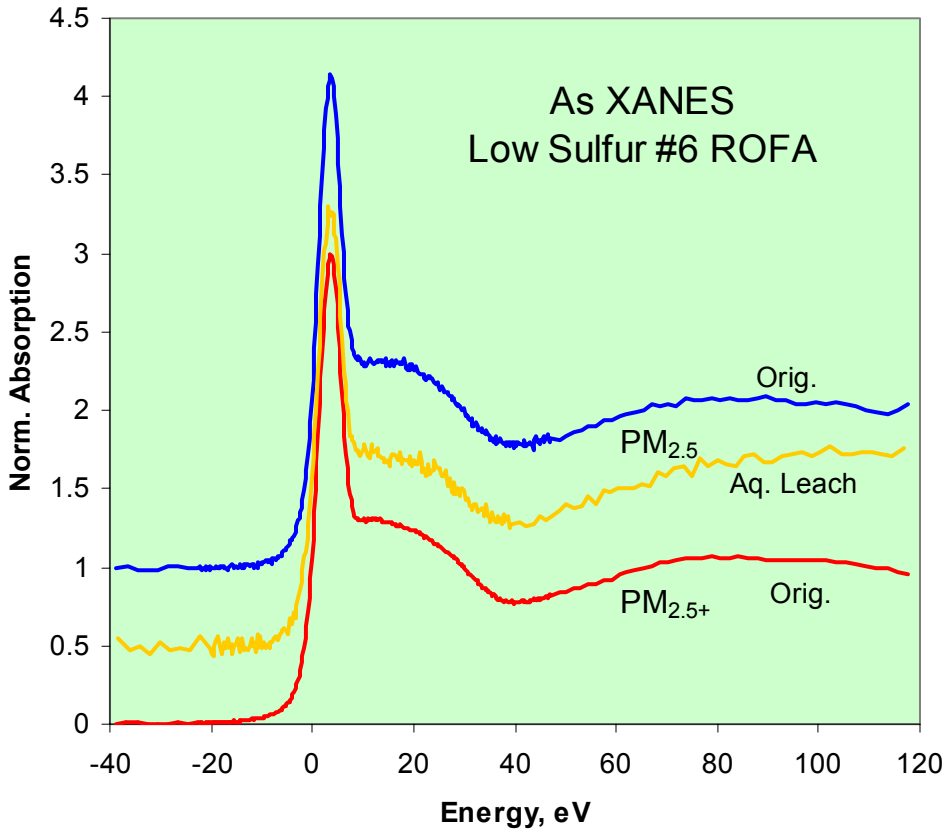


Figure 19. As XANES spectra of the aqueous leached residue the LS6 PM samples.

The BL5 samples subjected to aqueous and acid leaching showed similar results to As in LS6 ROFA PM. The BL5 $PM_{2.5+}$ leached residues showed quite weak As XANES spectra, especially the acid leached sample, whereas the BL5 $PM_{2.5}$ leached residues exhibited a strong spectrum for the aqueous leached $PM_{2.5}$, but virtually no spectrum for the acid leached $PM_{2.5}$. This suggests that the $PM_{2.5}$ samples contain two different arsenates; one that is soluble in $H_2O$; the other not but which is soluble in HCl acid. In contrast, the $PM_{2.5+}$ samples contain just the arsenate that is soluble in $H_2O$.

*(vi) Conclusions on metal speciation in ROFA PM*: Although some minor details remain to be resolved, it is clear that most metals in ROFA PM are present as some combination of sulfate, oxide, and sulfide species. The major exception is iron, which does not appear to form sulfates significantly, but rather occurs virtually entirely as ferric spinels and/or other ferric oxides and iron sulfide. Sulfide phases tend to be more prevalent for most metals in the coarser $PM_{2.5+}$ fractions, whereas oxide phases are more prevalent in the smaller particle size $PM_{2.5}$ fractions. Cu (and perhaps also Pb) is an exception in that there is little evidence for oxide phases in either size fraction and Cu sulfide is abundant in both size fractions. There is some evidence, from Mössbauer spectroscopy, to suggest that the oxide phases, particularly the Ni ferrite, are exceedingly fine in particle size (~ 10 nm). However, preliminary data from ASAXS measurements at the Ni K absorption edge indicate that <u>all</u> nickel phases are exceedingly small (<10 nm) and more so for the coarser $PM_{2.5+}$ fraction.

Although this XAFS investigation of leached residues appears to resolve many of the questions regarding the speciation of sulfur and major metals in ROFA PM, there are a number of loose ends that remain to be examined and resolved. These include:

- XAFS investigation of nanocrystalline oxides, such as $NiFe_2O_4$ or $VO_2$, not only to complement other studies performed on these materials, but to establish also what information about nanocrystalline materials might be obtained from XAFS spectroscopy that can be applicable to the major questions surrounding PM.

- The ASAXS investigation needs to be repeated (i) on other ROFA samples and (ii) with other elements (e.g. V) to see if the preliminary conclusions reached herein for Ni are also found in other situations. In addition, more fundamental studies need to be done to establish exactly what the parameters derived from the fitting of the ASAXS data mean.

- Why does iron not exhibit the formation of sulfates? How does the nickel ferrite form?

- Why do oxides occur predominantly in the $PM_{2.5}$ fractions and much less so in the $PM_{2.5+}$ fractions? Conversely, why are sulfides more prevalent in the $PM_{2.5+}$ fraction?

Such investigations would be valuable for understanding the formation, structure and speciation of PM samples,

**C. PM from Jet test engines at Wright-Patterson AFB**

Four samples of particulate matter were collected from jet engines at Wright-Patterson Air Force Base on silica filters and returned to Kentucky for XAFS survey. To date, only sulfur and iron XAFS studies have been attempted on these samples, except for one sample that was also subjected to Cr XAFS spectroscopy. The sulfur XANES data (Figure 20) reveal that almost all of the sulfur is present as sulfate in all four samples; however, some minor amounts of thiophene and sulfoxide appear also to be present, especially for sample Jet PM 34, which exhibited the S XANES spectrum with the best signal/noise ratio. However, even taken together, these minor forms of sulfur do not amount to more than 10% of the overall sulfur in the sample.

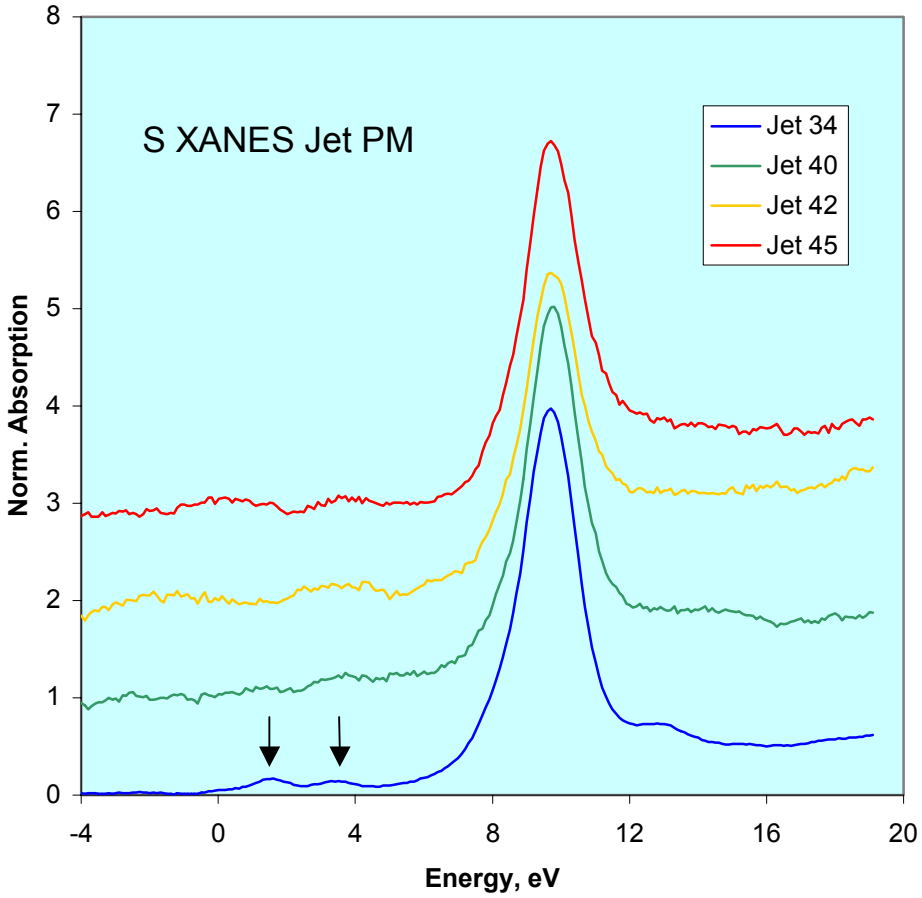


Figure20: S XANES spectra of PM from jet engines collected on a silica filter. The peaks at 10 eV arise from sulfate sulfur; minor peaks indicated at about 1.3 and 3.2 eV in lowest spectrum arise from thiophene and sulfoxide forms, respectively.

The iron XANES spectra are shown in Figure 21. The corresponding EXAFS data were a little too weak to give consistent RSFs and are not reported. The Fe XANES spectra are all very similar, although there is some very minor variation noted for the pre-edge peak and there is a variation in signal/noise ratio reflecting a variation in iron content. The shape of the pre-edge peak and the overall spectrum are indicative of Fe(III), largely in four-coordination. The single

Cr XANES spectrum obtained for sample Jet PM 34 was very noisy. However, the Cr XANES profile is indicative of Cr(III) sulfate, when compared with our database of Cr standards [16]. Additional elements (e.g. zinc) will be examined in the near future.

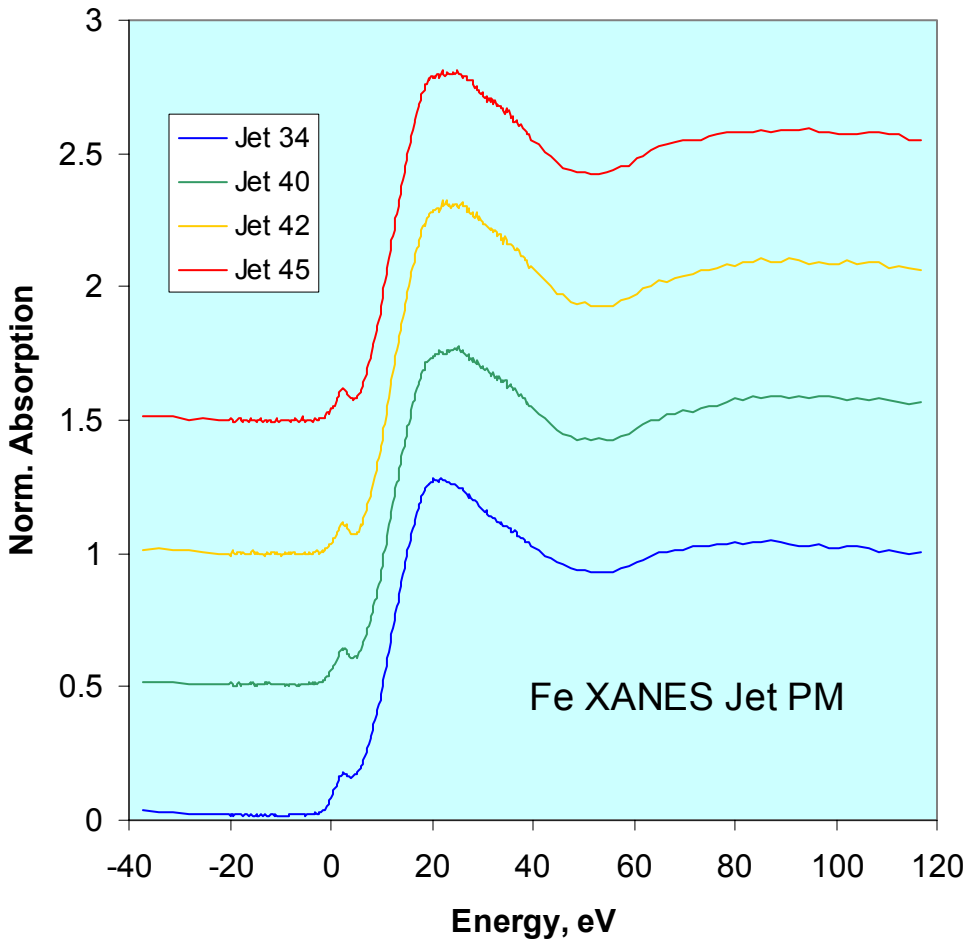


Figure 21. Iron XANES spectra of Jet PM samples from Wright-Patterson AFB.

**D. Ambient filter samples.**

Relatively little work was done on characterizing elements by XAFS spectroscopy in ambient PM samples during the current year. However, an exception was the work done on two ambient PM samples collected in the Houston area as part of the Houston, Texas, regional PM study. Two ambient PM samples were collected each for four days during November, 2001, and returned to us for analysis in January 2002. One of these samples was examined by XAFS spectroscopy at the following edges: S, V, Cr, Fe, Ni, Zn and As edges. The signal/noise ratio varied greatly for these elements with Fe, Zn and S being strong, Ni and Cr intermediate and V and As being weak. Both Cr and Fe indicated the presence of significant metallic forms; such forms were evident in the RSFs as well as the XANES spectra of these elements. The remainder of the elements were by and large non-metallic in form; Ni and Zn in the form of sulfates, V as $V_2O_4$, As as arsenate, and S as sulfate(Figure 22).

.

.

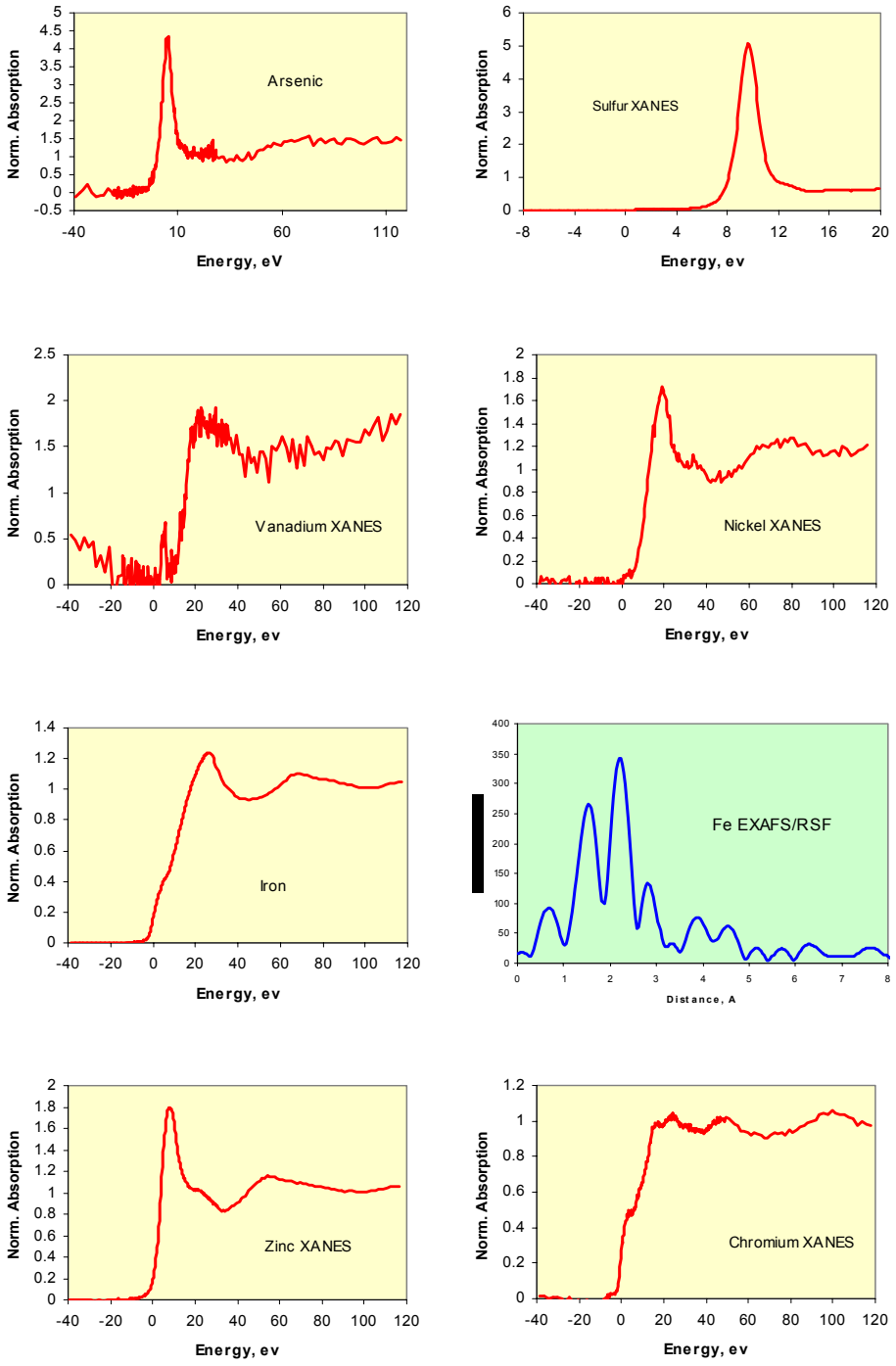


Figure 22: XANES spectra of arsenic, sulfur, vanadium, nickel, iron, zinc and chromium in the ambient filter sample, HRM-3, collected as part of the Houston Regional PM study. Also shown is the Fe EXAFS/RSF plot for iron, proving that the iron is mostly present as metallic iron.

A comparative study was also conducted on a filter sample collected in Lexington for four days. However, only four elements were examined: S, Cr, Ni and Zn. These are shown in Figure 23.

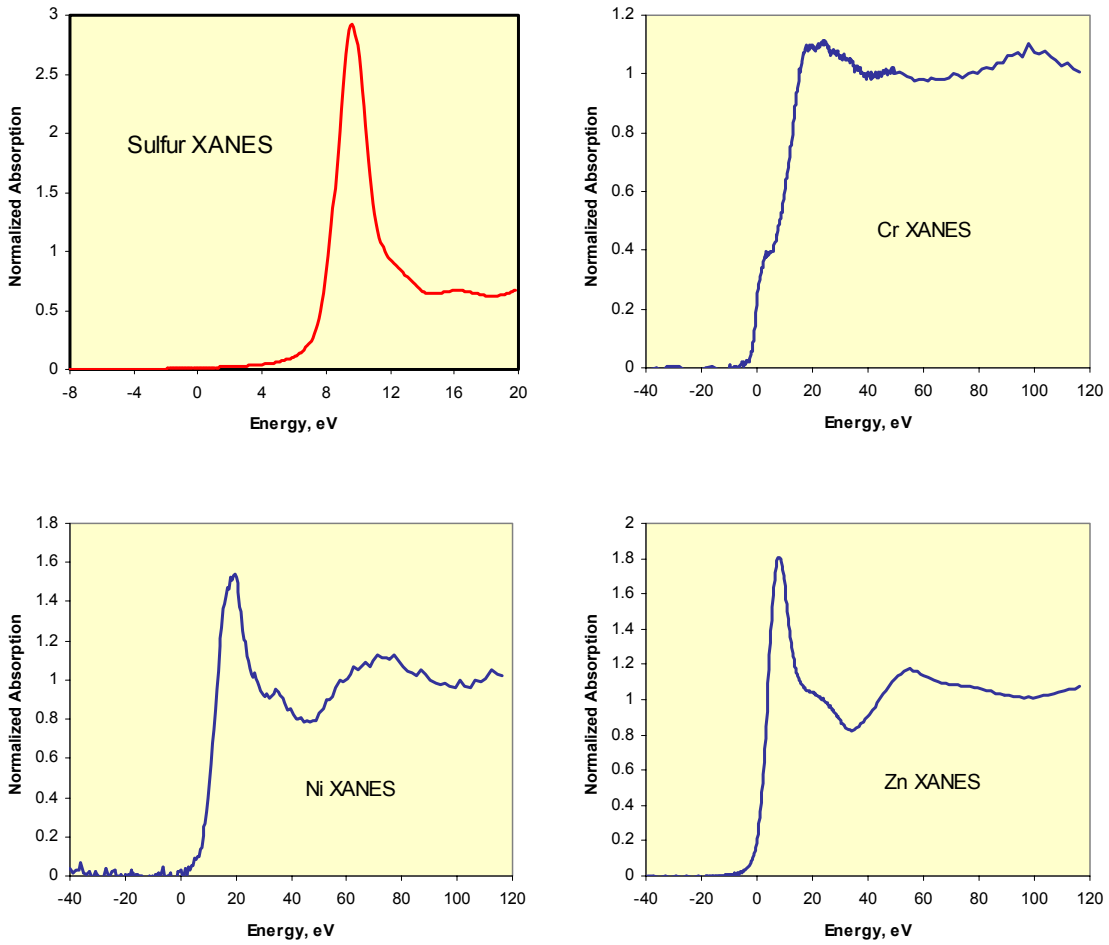


Figure 23: XANES spectra of sulfur, chromium, nickel and zinc in the ambient filter sample, LEX-58, collected in Lexington, KY.

In comparison to the data for the Houston sample, the XANES data exhibited for S, Ni and Zn in the Lexington sample are surprisingly similar and suggest that they are present predominantly as sulfates. Chromium in the Lexington filter is partly metallic; the fraction of metallic chromium is less than that present in the Houston sample.

**Conclusions**

Significant progress has been made in metal speciation of fine particulate matter from petroleum combustion sources. The combination of leaching using aqueous or acid solutions with XAFS spectroscopy has revealed a wealth of information about minor phases present in ROFA PM samples. Such studies have significantly augmented our earlier studies based solely on XAFS examination of the original bulk material. Some conclusions are listed below for the different types of materials investigated.

It has shown quite conclusively that sulfates are the dominant form of occurrence of most metals in ROFA PM and that most metals exhibit minor sulfide and oxide occurrences. The major

exceptions to this overall scheme are (i) iron, which appears not to form significant sulfates; and (ii) base metals such as lead and copper, which appear not to form oxides. The sulfide occurrences constitute a higher fraction of the metal in the coarse PM fractions compared to fine PM fractions. In contrast, oxide phases tend to be found only in the finest PM < 2.5 um fractions. We suspect that these differences relate to the combustion process and that the oxide is formed as burn-out goes closer to completion, whereas sulfide is preserved in coarser particulate.

An examination of PM from engines burning jet fuel has been initiated. So far only sulfur and Fe have been examined in such materials. Sulfur is present almost exclusively as sulfate, but some very minor organosulfur compounds (thiophene, sulfoxide) have also been identified.

Ambient $PM_{2.5}$ collected on Teflon filters continue to be examined by XAFS spectroscopy. In recent months, we have compared and contrasted the speciation of sulfur and a number of metals collected on $PM_{2.5}$ filters in Houston, TX, and in Lexington, KY. Despite significant differences in the industrial natures of the two cities, some of the metals occur in very similar forms in the two locations. Most interesting was the observation of both iron and chromium present in metallic forms in these two locations.

A manuscript has been prepared describing the results of the combined XAFS and leaching approaches for elucidation of the forms of elements in ROFA PM and submitted for publication [15]. In addition, we will continue to pursue some new directions. Plans have been made to examine other ROFA PM samples by means of ASAXS measurements at not only the Ni K-edge but also the V K-edge to supplement the study briefly described herein on Ni in the BL5 ROFA samples.

**References**


1. G. P. Huffman, S. Mitra, F. E. Huggins, and N. Shah, Quantitative analysis of all major forms of sulfur in coal by X-ray absorption fine structure spectroscopy. **Energy & Fuels**, 5, 574-581, (1991).
2. M. M. Taghiei, F. E. Huggins, N. Shah, and G. P. Huffman, In situ X-ray absorption fine structure (XAFS) spectroscopy investigation of sulfur functional groups during pyrolysis and oxidation. **Energy & Fuels**, 6, 293-300, (1992).
3. G. P. Huffman, F. E. Huggins, N. Shah, R. Huggins, W. P. Linak, C. A. Miller, R. J. Pugmire, H. L. C. Meuzelaar, M. S. Seehra, and A. Manivannan, Characterization of fine particulate matter produced by combustion of residual fuel oil, **J. Air Waste Management Assoc. (Special issue on PM2000: Particulate Matter and Health)**, 50, 1106-1114, (2000).
4. K. C. Galbreath, D. L. Toman, C. J. Zygarlicke, F. E. Huggins, G. P. Huffman, and J. L. Wong, Nickel speciation of residual oil fly-ash and ambient particulate matter using X-ray absorption spectroscopy, **J. Air Waste Management Assoc.**, 50, 1876-1886, (2000).
5. F. E. Huggins, G. P. Huffman, K. C. Galbreath, D. L. Toman, and J. L. Wong, Speciation of nickel in residual fly-ash by XAFS spectroscopy, **Preprints, ACS Div. Fuel Chem.,** 45(2), 388-392, (2000).
6. S. Pattanaik, F. E. Huggins, G. P. Huffman, W. P. Linak, and C. A. Miller, XAFS Spectroscopy Analysis of Metals and Sulfur in Fine PM from the Combustion of Residual Oil, **ACS Fuel Chem. Div. Preprints,** 46(2), 626-7, (2001).

7. Y. G. Ma, M. Z. Jin, M. L. Lui, G. Chen, Y. Sui, Y. Tian, G. J. Zhang, and Y. Q. Jia, Effect of high pressure on Mössbauer spectra of $NiFe_2O_4$ ultrafine particles with different grain sizes, **Mat. Chem. Phys.** 65, 79-84, (2000).
8. Y. Sui, W-H. Su, F-L. Zheng, and D-P. Xu, Investigation on interface atomic state in compacted $NiFe_2O_4$ nanocrystalline by Mössbauer spectroscopy, **Mat. Sci. Engineer**. A286, 115-118, (2000).
9. M. Rajendran, A. K. Bhattacharya, D. Das, S. N. Chintalapudi, and C. K. Majumdar, Magneric properties of nanocrystalline $NiFe_2O_4$ powders prepared by an aqueous oxidative precipitation process, **Mod. Phys. B.**, 15, 305-312, (2001).
10. P. Frank and K. O. Hodgson, Defining chemical species in complex environments using K-edge X-ray absorption spectroscopy: Vanadium in intact blood cells and Henze solution from the tunicate Acsidia ceratodes, **Inorg. Chem**. 39, 6018-6027, (2000).
11. J. Wong, F. W. Lytle, R. P. Messmer, and D. H. Maylotte, K-edge absorption spectra of selected vanadium compounds, **Phys. Rev. B.,** 30, 5596-5610, (1984).
12. C. Palache, H. Berman, and C. Frondel, **Dana's System of Mineralogy,** Volume 1, J. Wiley and Sons, ($7^{th}$ Edition), New York, 1944.
13. F. E. Huggins, G. P. Huffman, and J. D. Robertson, Speciation of elements in NIST particulate matter SRMs 1648 and 1650, **J. Haz. Mat.**, 74, 1-23, (2000).
14. S. C. B. Myneni, X-ray and vibrational spectroscopy of sulfate in earth materials. Chapter 2 in: **Sulfate Minerals** (C. N. Alpers, J. L. Jambor and D. K. Nordstrom. Eds.), **Rev. Mineral. Geochem.**, Vol. 40, Mineral. Soc. Amer., Washington DC, pp. 113-172, (2000).
15. Frank E. Huggins, Gerald P. Huffman, William P. Linak, C. Andrew Miller, "Quantifying Hazardous Species in Particulate Matter Derived from Fossil-Fuel Combustion", submitted to *Environmental Science & Technology*.

# Evaluation of support materials for CCSEM analysis of carbonaceous particles in PM samples

Yuanzhi Chen and Gerald P. Huffman
University of Kentucky

Although CCSEM has had great success in the analysis of inorganic particles, a problem is encountered when attempting to analyze particulate samples for which carbon is a significant constituent. This is obviously the case for airborne particulates, since ambient $PM_{2.5}$ typically contains 20-50% of carbonaceous material. In urban areas, diesel emissions are the major component of carbonaceous PM. The difficulty is in distinguishing the carbon x-ray signal from the particles from that emitted by the supporting substrate or from contaminants in the SEM sample chamber. In this study, we examined standard spherical glass particles on several substrates to determine the seriousness of this problem and how it could be eliminated.

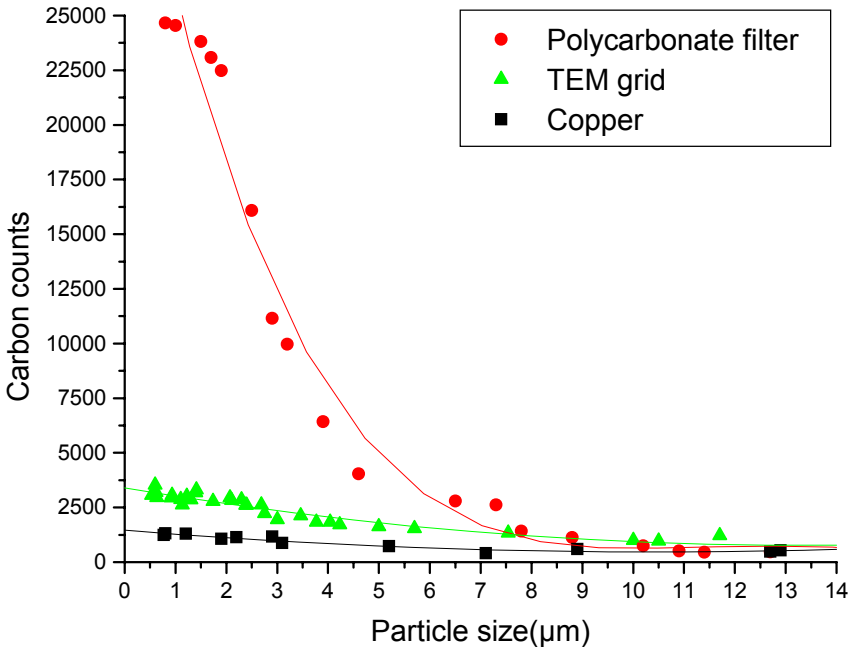


Figure 1. Carbon signal as a function of particle size.

Energy dispersive x-ray (EDX) analysis of K-411 spherical glass particles (Si, Mg, Ca, Fe and O) with different diameters was carried out with the electron beam in the spot mode at an electron energy of 20 keV with an x-ray take-off angle of 35 degrees using several support materials. These included a polycarbonate filter, which is the standard support material used in CCSEM analysis of inorganic particles, a TEM grid, and a polished copper foil.

Carbon signals (total counts) obtained in a 60 sec counting time for these three supports are shown as a function of particle size in Figure 1. The polycarbonate filter shows very strong carbon signals in the small particle size range because it is a relatively thick filter and the electron beam excites carbon x-rays from a region several μm in diameter. The TEM, on the other hand, shows much lower carbon signals because the thickness of carbon film on the grid is in the nanometer range (~20 nm). This was noted previously by Laskin and Cowin in their SEM/EDX study of laboratory-generated aerosols [1]. This indicates that TEM grids can be used as supports for SEM analysis of sub-micron carbonaceous particles. The copper foil substrate shows even weaker carbon signals, which probably arise from chamber contaminants (e.g., hydrocarbons from pump oil). For larger particles (>7μm), the difference in the carbon signal is small for all three supports.

The data in Figure 2 were obtained from small (~0.2-0.4 μm) flyash particles derived from the combustion of a Wyodak subbituminous coal. Figure 2 (a) shows that there is basically no count difference between the polycarbonate filter background and carbonaceous particles. However, inorganic particles are readily distinguished, even though the carbon background counts from the filter are still dominant. Consequently, polycarbonate filters should be used for CCSEM analysis of submicron particles only if they are predominantly inorganic and the carbon background count can be ignored.

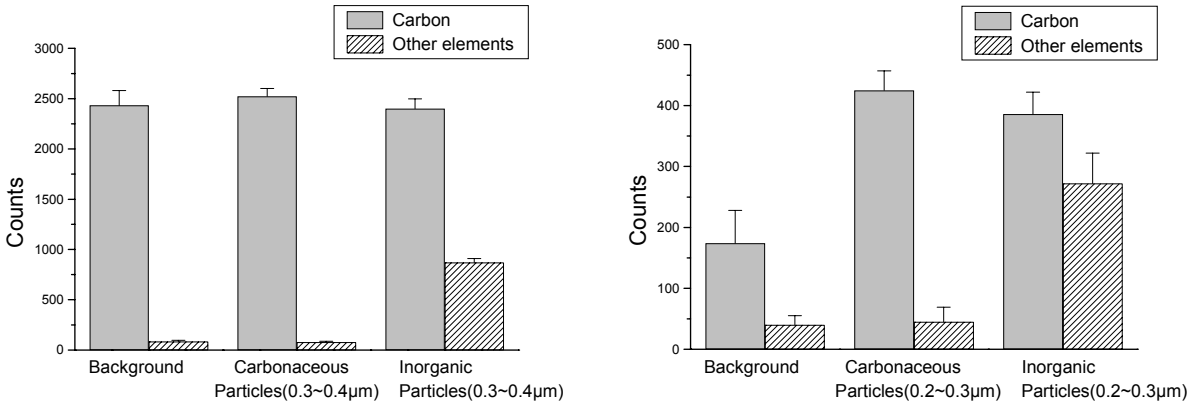


Polycarbonate filter TEM grid

Figure 2. Comparisons of count differences among background, sub-micro carbonaceous and inorganic particles on different support materials.

Figure 2(b) shows the difference between carbon and non-carbon counts among background, carbonaceous, and inorganic particles on TEM grids, which indicates that submicron carbonaceous particles ( ~0.2-0.3μm) can be distinguished from both inorganic particles of similar size and the carbon film background. TEM grids therefore appear promising as supports for CCSEM analysis of $PM_{2.5}$ that contains a substantial amount of carbonaceous material. The use of metallic foils, such as copper or beryllium [2], as supports should also be further explored.

***References:***

1. A. Laskin and J.P. Cowin, *Analytical Chemistry*, **73** (2001) 1023-1029.
2. G.P. Huffman, N. Shah, F.E. Huggins, G.S. Casuccio, and W.J. Mershon, *American Chemical Society, Division of Fuel Chemistry Preprints* **36(3)**, 1155-1163 (1991).

# Elemental and Isotopic Analysis of $PM_{2.5}$

J. David Robertson, Department of Chemistry University of Missouri, Columbia, MO

One of the primary goals of this program is to increase our understanding of the sources and chemistry of fine air particulate from stationary and mobile fossil fuel combustion sources. Key to this effort is the development of additional source signature variables that can be used to identify source emissions. For example, most source-receptor models assign the sulfate observed in ambient particulate to sulfur dioxide produced by coal combustion or emitted from vehicle exhaust. This model may, however, be overestimating the contribution of fossil fuel to the sulfate component of ambient particulate. Another example is the need for marker compounds for assigning particulate to gasoline vehicle emissions. Since lead was removed from gasoline, there has not been an adequate elemental signature for gasoline vehicle emissions and researchers have had to rely upon challenging and lengthy organic compound analysis. And finally, given the large contribution of carbonaceous material to fine air particulate, it is critical that markers be developed for understanding the sources of organic and elemental carbon in $PM_{2.5}$. Previous studies have relied on organic marker compounds or ratios as indicators for petrogenic or biogenic sources. For example ratios of anthracene and flouranthene are useful for indicating combustion of biological material while the ratio of alkyl PAH's to the parent PAH can indicate fossil fuel combustion. Many of the organic markers used in these studies have, however, multiple sources. Because the identification of reliable marker compounds is critical to our understanding the source and chemistry of $PM_{2.5}$:

We have developed a method for determining sulfur isotope ratios and are now investigating the possibility of combining isotope ratio data with trace-element and mode-of-occurrence data to determine what fraction of the sulfate in $PM_{2.5}$ originates from coal combustion versus, for example, combustion of petroleum-based fuels for transportation.

We have developed analytical methods for measuring the platinum group elements in fine air particulate samples and are working with Environment Canada to investigate how this source signature varies from in-use light duty gasoline motor vehicles.

We have initiated collaboration with the Center for Accelerator Mass Spectrometry to investigate the use of $^{14}C$ as a marker to distinguish between petrogenic and biogenic sources of carbon in $PM_{2.5}$.

**Sulfur Isotope Ratios in $PM_{2.5}$**

Most source-receptor models assign the sulfate observed in ambient particulate to sulfur dioxide produced by coal combustion or emitted from vehicle exhaust. This model may, however, be overestimating the contribution of fossil fuel to the sulfate component of ambient particulate. Hitchcock and Black used sulfur isotope-ratio measurements to identify the source of atmospheric sulfur oxides near Wallops Island, Virginia [1]. In this anoxic marsh environment there was no evidence of the presence of transported pollutant sulfate even though the sampled air masses had passed over very large sources of anthropogenic sulfur and contained a number of metal pollutants associated with combustion. While one would not expect to see large biogenic

contributions to the sulfate in an urban environment, we are investigating the possibility of combining isotope ratio data with trace-element and mode-of-occurrence data to determine what fraction of the sulfate in PM2.5 originates from coal combustion versus, for example, combustion of fossil fuels for transportation.

The most important cause for sulfur isotope fractionation in nature is the reduction of sulfate ions by anaerobic bacteria. The extent of fractionation is variable and depends on temperature, the sulfate reservoir, the bacterial metabolic rate, and on the $H_2S$ expulsion rate. Fractionation also occurs during isotope exchange reactions due to the different rates at which sulfur-oxygen bonds are broken. While the $\delta^{34}S_{CDT}$ values of petroleum span a wide range from 0.8 to +32 ppt [2], the sulfur isotopic composition of a given pool is constant and pools in the same reservoir rock within a sedimentary basin have similar $\delta^{34}S$ values. Likewise, the isotopic composition of sulfur in coal varies widely from $\delta^{34}S$ of +24 to 0.30 ppt.

Natural sources of sulfur in the atmosphere include volcanic gases, sulfur compounds released by sulfate-reducing bacteria, sulfate particles from sea spray, and sulfur compounds released by plants. Anthropogenic sources of sulfur include combustion of coal and fuel oil, petroleum refining, mineral processing, and automobile and truck exhaust. Clearly, one must know the isotope composition of both natural and anthropogenic sources to develop an accurate source apportionment model and many studies have been carried out in Europe, the Arctic, and America to trace sulfate in the atmosphere and in precipitation by using sulfur isotope ratios [3].
Given that inductively coupled plasma mass spectrometry (ICP-MS) is an acceptable method routinely used for the determination of inorganic compounds in ambient air [4], we have developed a method of simultaneously determining the sulfur isotope ratio and inorganic components in a PM2.5 sample. The measurements are performed with a VG Axiom high-resolution magnetic sector ICP-MS that is fitted with an alumina injector, HF-resistant microbore PFA nebulizer, and Teflon cyclonic spray chamber. The microbore nebulizer uses a sample flow rate of only 100 μL/min. In order to resolve 32S and 34S from isobaric interferences, the isotope ratio measurements are made at a mass resolution of 4000. In contrast to many isotope ratio measurements, we are using a single collector. A single run consists of 4 mass sweeps over the 32S and 34S peaks with 30 points per peak and a dwell time of 20 ms per point. An isotope ratio measurement is the average of 5 repetitions of 10 runs per sample. Each sample measurement is blanketed by a secondary sulfur standard.

Thus far, we have investigated $PM_{2.5}$ from two coal and two fuel oil samples. These were digested using a Milestone Laboratory Systems Ethos Plus sealed vessel microwave digestion system in which 50 mg samples were digested in a 13 ml 8:2:3 high purity reverse aqua regia-HF-H2O2 solution. The digested samples were transferred, filtered, and diluted with high purity 2% nitric to a final sulfur concentration of 400 ppb before analysis.

Relative standard deviation values for $^{32}S/^{34}S$ of 0.2 to 0.5 % RSD are typical after discarding, at most, one run of the data by selectively removing those values that lie outside 1 standard deviation of the mean. A precision of 0.2 % RSD will result in an error of 3 ppt on $\delta^{34}S$ values. While this error is larger than that obtained with a multi-collector thermal ionization mass spectrometry measurement, it is small enough to allow us to distinguish among the wide range of sulfur isotope ratios that one expects from different coal and petroleum sources (+32 to 0.30 ppt).

The sulfur isotope ratio values for the fine particulate matter and fuels from the combustion of two oils and two coals are presented in Table 1. In contrast to our preliminary work first reported during method development, there does not appear to be any fractionation of sulfur isotopes during the combustion/particulate collection of these materials. There also does not appear to be any sulfur fractionation among the different forms of sulfur in Baseline 5 Oil.

**Table 1.** $\delta^{34}S$ Values Obtained by HR-ICP-MS

| Sample | Fuel | Cyclone | Filter |
|---|---|---|---|
| High Sulfur No. 6 Oil | 9.6 | 10.2 | |
| Baseline 5 Oil | | 10.7 | 9.2 |
| Baseline 5 Pentane Residue | | 10.8 | 10.3 |
| Baseline 5 Acid Residue | | 9.5 | 8.3 |
| Western Kentucky Coal | 8.7 | 6.3 | 8.5 |
| Montana | -5.7 | -3.2 | -2.9 |

**Platinum Group Elements in $PM_{2.5}$ from In-Use Gasoline Motor Vehicles**

Recently we began collaboration with Lisa Graham of Environment Canada to investigate the occurrence of the platinum group elements (PGEs) found in the fine air particulate from in-use light duty gasoline motor vehicles. This project is an extension of a Natural Resources Canada Program of energy Research and Development (PERD) project entitled "Determination of the concentration, composition and sources of airborne carbonaceous particles in Canada." The four main components of the original PERD project was (1) Detailed chemical and size distribution measurements to develop complete emissions profiles for the fine particulate matter emitted from current Canadian motor vehicles; (2) Obtaining a complete chemical account of the total PM2.5 mass in ambient air by determining the contribution of carbonaceous particles and their main chemical species and classes; (3) Determining what percentage of the carbonaceous particles are from anthropogenic versus natural sources, what percentage of the anthropogenic particles are from transportation and of these what percentage are of secondary and primary origin; and (4) Developing and testing a comprehensive model capable of predicting the mass concentration of particle phase carbon in conjunction with inorganics and other relevant chemical and dynamic processes.

In the PERD study, seventy-five in-use light duty gasoline fuelled passenger cars and trucks were tested on a chassis dynamometer over two repeats of the Hot-505 cycle. For each test, gaseous emissions of CO, CO2, NOX and THC were measured. Dilute exhaust concentrations were also recorded second by second over each test. Over the two repeats, samples were collected for determining PM2.5 mass emission rate, as well as emissions of SO2, NH3, organic acids, organic and inorganic ions, trace metals, organic and inorganic carbon and emissions of a range of organic compounds (alkanes, alkylcyclohexanes, petroleum biomarkers, PAH and PASH). Samples of the engine lubrication oil were collected from each of the test vehicles to aid in correlating emissions composition with lube oil composition. The vehicles selected for testing were chosen to represent the top 70% of the on-road vehicle fleet in British Columbia. Both vehicles passing their AirCare inspection and vehicles failing the inspection were tested in proportion to their presence in the fleet. The vehicles tested ranged in model years from 1978 to 1998. Of these, 50 were light duty passenger cars and 20 were light duty trucks.

Since lead was removed from gasoline, there has not been an adequate elemental signature for gasoline vehicle emissions and researchers have had to rely upon challenging and lengthy organic compound analysis. As a result of our collaboration with Dr. Graham, we have developed analytical methods for measuring the platinum group elements in fine air particulate samples and are working with Environment Canada to investigate how this source signature varies from in-use light duty gasoline motor vehicles. While all 75 vehicles in the PERD study will be investigated, the results for the first 24, oldest vehicles, are given in Table 2 below. The samples were prepared by sealed-vessel acid microwave digestion. Optima grade hydrochloric acid (HCl) (6 mL), Optima grade nitric acid (2 mL), and TraceMetal grade hydrofluoric acid (HF) (1 mL) were added to samples. The samples were sealed and digested at 180 C using a mixture of HCl, $HNO_3$ and HF. After digestion, the samples were cooled to room temperature and the vessels were fitted into an evaporation apparatus and the samples evaporated to near dryness under slight vacuum in the microwave oven. Hydrochloric acid (2 mL) was then added to each sample and the sample re-evaporated. This step was repeated twice more in order to eliminate all HF from the samples. The sample residues were then re-dissolved in 0.24 M HCl, and this solution transferred to pre-weighed polypropylene test tubes with rinsing. The recovery for the PGEs, from three separate preparations, ranged from 82 – 107%.

While only 24 samples have been analyzed to date, a strong correlation is observed between Rh and Pt in the fine particulate (Figure 1). Likewise, a good correlation is observed between the amount of Pd and Pt (Figure 2) when the limited number of samples is divided into those vehicles designed for the Canadian standard (Figure 3) and those vehicles designed for the U.S. 49 state standard (Figure 4). Given that Zereini *et al.* have recently demonstrated that PGE particles from automotive catalytic converters, particularly those bound to fine particulate matter, are capable of being airborne and transported [5], these preliminary results indicate that these three PGEs may serve as a strong elemental signature for gasoline vehicle particulate emissions with the improved sensitivities of the high-resolution inductively coupled plasma mass spectrometer. The only other significant source of Pt, Pd, and Rh emissions to the biosphere is the noble metal industry [6].

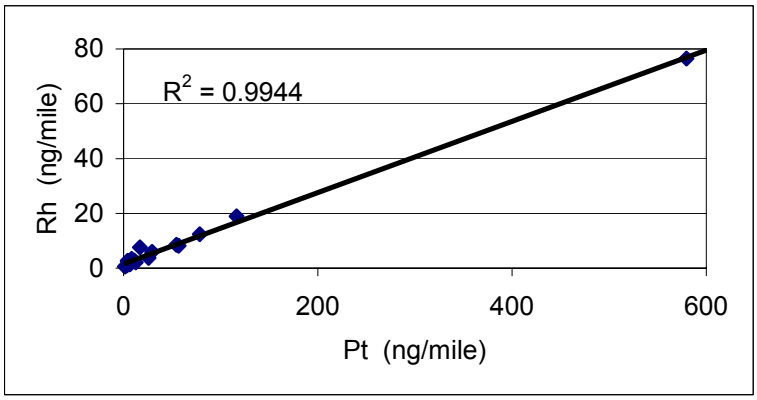


Figure 1. Rh and Pt emissions from Gasoline Vehicles

Table 2. Platinum Group Elements in PM2.5 from Gasoline Motor Vehicles

| Year | Make | Model | Category | PM2.5 mg/mile | Rh ng/mile | Pd ng/mile | Pt ng/mile |
|---|---|---|---|---|---|---|---|
| 1978 | Pontiac | Acadian | C | 9.81 | 2.49 | 1.84 | 7.14 |
| 1980 | Toyota | Tercel | C | 23.26 | 0.55 | (0.89) | 1.29 |
| 1981 | Ford | Fairmont | C | 51.23 | 8.18 | (0.21) | 56.8 |
| 1982 | Volkswagen | Jetta | C | 39.46 | 1.43 | 2.69 | 6.46 |
| 1983 | Mazda | GLC | C | 53.09 | 2.66 | 7.31 | 4.34 |
| 1984 | Oldsmobile | Cutlass | C | 18.93 | (0.045) | (0.18) | 1387 |
| 1984 | Chrysler | LeBaron | C | 16.25 | 2.53 | 1.25 | 4.20 |
| 1985 | Toyota | Tercel | C | 99.77 | 0.89 | 26.18 | 2.93 |
| 1985 | Plymouth | Horizon | C | 39.69 | 8.53 | (0.86) | 54.26 |
| 1986 | Mazda | 626 | C | 6.78 | 12.43 | 133.74 | 78.35 |
| 1986 | Plymouth | Voyager | T | 10.55 | 3.34 | 3.53 | 8.18 |
| 1987 | Toyota | Corolla | C | 3.37 | (0.05) | 11.24 | 20.68 |
| 1987 | Toyota | Tercel | C | 17.29 | (0.13) | 329.27 | 259.40 |
| 1984 | Buick | Century | C | 2.86 | (0.05) | 74.68 | 255.44 |
| 1985 | Toyota | Corolla | C | 4.04 | 6.01 | 5.47 | 29.28 |
| 1986 | Chev | Cavalier | C | 13.55 | 1.58 | 3.36 | 5.36 |
| 1987 | Nissan | Sentra | C | 11.79 | 18.91 | 30.64 | 116.25 |
| 1987 | Pontiac | Fiero | C | 14.56 | 3.75 | 8.36 | 25.82 |
| 1987 | Acura | Integra | C | 3.40 | (0.10) | (0.75) | 72.37 |
| 1988 | Honda | Accord | C | 2.18 | 1.24 | (0.70) | 4.31 |
| 1988 | Ford | Bronco | T | 2.98 | 7.58 | 7.37 | 16.83 |
| 1988 | Chevrolet | Cavalier | C | 2.64 | 2.81 | 9.57 | 10.93 |
| 1988 | Buick | Regal | C | 7.00 | 76.46 | (0.21) | 579.68 |
| 1988 | BMW | 325 | C | 9.01 | 2.13 | 1.97 | 12.43 |

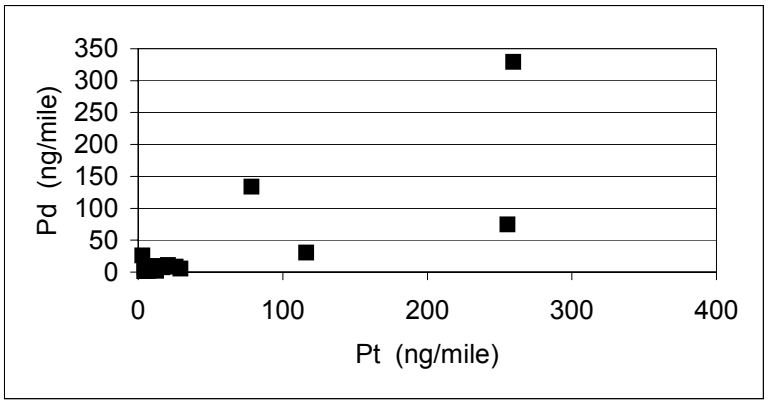


Figure 2. Pd and Pt Emissions from Gasoline Vehicles

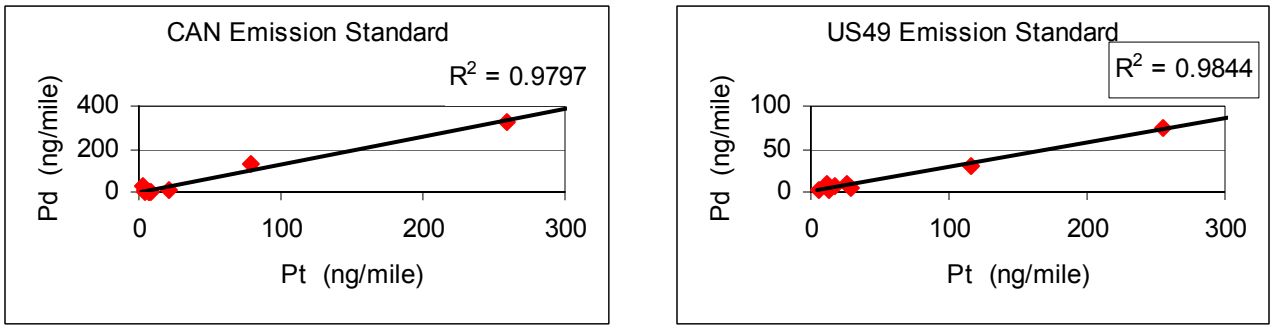


Figure 3. Correlation between Pd and Pt for a limited number of samples from samples from vehicles designed for the Canadian standard (left) and from vehicles designed for the U.S. 49 state standard (right).

**References:**


1. D.R. Hitchcock and M.S. Black, *Atmosph. Environ.*, 1984, *18,* 1.
2. G. Faure, *Principles of Isotope Geology*, 2nd Ed., Wiley & Sons: New York, 1986; pp 526-7.
3. H. Mukai *et al.*, *Environ. Sci. Technol.*, 2001, *35*, 1064 and references therein.
4. Compendium Method IO-3.5, Compendium of methods for the determination of inorganic compounds in ambient air, Center for Env. Res. Info. Office of Research and Development, U.S. EPA, Cincinnati, OH.
5. F. Zereini, *et al.*, *Environ. Scie. Technol.,* 2001, *35*, 1996.
6. F. Dirksen, F. Zereini, B. Skerstupp and H. Urban in *Emissionen von Platinmetallen – Analytik, Umwelt- und Gesundheistrelevanz.* F. Zereini and F. Alt, Eds. Springer Verlag: Berlin/Heidelberg, 1999.

# Appendix: Publications and presentations

Publications and recent presentations resulting from this research are listed below.


1. Siddhartha Pattanaik, Frank E. Huggins, Gerald P. Huffman, William P. Linak and C. Andrew Miller, "XAFS Spectroscopy Analysis of Metals and Sulfur in Fine PM from the Combustion of Residual Oil," **2001**, *ACS Fuel Chem. Div. Preprints, 46(2)*, 626-7.
2. Joseph Kyger and J. David Robertson, "Sulfur Isotope Ratios in $PM_{2.5}$." Presented at the Symposium on Ambient Fine Particulate Matter ($PM_{2.5}$): Relation to Production and Utilization of Fossil Fuels, American Chemical Society Fall Meeting, Chicago, IL, Aug. 26-30, 2001. **2001**, *ACS Fuel Chem. Div. Preprints,* ***46(2),*** 609.
3. Jerry E. Hunt, R. E. Winans, N. A. Tomczyk, and R. J. Pugmire, "Molecular Characterization of Hydrocarbons from Soots in Low Temperature Flames of Biphenyl and Illinois No.6 Coal," Symposium on Environmental challenges for Fossil Fuel Combustion: Emission Issues in fossil Fuel Utilization, 221st ACS National Meeting, San Diego, CA, April 1-5, **2001**, *Division of Fuel Chemistry Preprints,* ***46(1),*** 294-295.
4. Cluster Analysis of 13C Chemical shift Tensor Principal Values in Polycyclic Aromatic Hydrocarbons, J. C. Facelli, B. K. Nakagawa, A. M. Orendt, R. J. Pugmire, J. Phys Chem. A, **2001**, 105, 7468.
5. J. Z. Hu, M. S. Solum, C. M. V. Taylor, R. J. Pugmire, and D. M. Grant, "Structural Determination in Carbonaceous Solids Using Advanced Solid State NMR Techniques," **2001**, *Energy & Fuels,* ***15***, 14.
6. M. S. Solum, A. F. Sarofim, R. J. Pugmire, T.H. Fletcher, and H. Zhang, "$^{13}$C NMR Analysis of Soot Produced from Model Compounds and a Coal," **2001**, *Energy & Fuels*, ***15***, 961.
7. G. P. Huffman, F. E. Huggins, N. Shah, R. Huggins, W. P. Linak, C. A. Miller, R. J. Pugmire, H. L. C. Meuzelaar, M. Seehra, and A. Mannivannan, "Characterization of Fine Particulate Matter Produced by Combustion of Residual Fuel Oil," **2000**, *J. Air & Waste Management Assoc.*, ***50***, 1106-1114.
8. G. P. Huffman, F. E. Huggins, N. Shah, S. Pattanaik, H. L. C. Meuzelaar and Sun Joo Jeon, D. Smith, B. Harris, M. S. Seehra and A. Manivannan, "Structure of Primary $PM_{2.5}$ Derived from Diesel Truck Exhaust," **2000**, *ACS Div. Fuel Chem. Preprints,* ***45(3)***, 441-445.
9. Jeon, S.J.; Sheya, S.N.; Meuzelaar, H.L.C.; Lighty, J.S.; Jarman, W.M.; Kasteler, C.; Sarofim, A.F. "Receptor and Source Profiling by GC/MS Analysis of Temporally- and Spatially-resolved PM Samples," Proc. of the AWMA PM2000: Particulate Matter and Health - The Scientific Basis for Regulatory Decision-making Specialty Conference & Exhibition, Jan. 2000, Charleston, SC, 2000, 10ASP7, 26-27.
10. F.E. Huggins And G. P. Huffman, X-ray Absorption Fine Structure (XAFS) Spectroscopic Characterization of Emissions from Combustion of Fossil Fuels, invited plenary talk presented at International Conference on Materials Engineering for Resources, Akita, Japan, Oct., 2001.

12. Meuzelaar, H.L.C., Dworzanski, J.P., Arnold, N.S., McClennen, W.H. and Wager, D.J. "Advances in Field-Portable Mobile GC/MS Instrumentation" Field Anal. Chem. Technol., 2000, 4(1), 3-13.

13. Arnold, N.S., Dworzanski, J.P., Sheya, S.N., McClennen, W.H. and Meuzelaar, H.L.C. Design Considerations in Field-portable GC-Based Hyphenated Instrumentation, Field Anal. Chem. Technol., 2000, 4(5), 219-238.

14. Jeon, S.J., Sheya, S.N., Meuzelaar, H.L.C., Lighty, J.S., Jarman, W.M., Kasteler, C., Sarofim, A.F. and Simoneit, B.R.T. Exploratory Studies of PM10 Receptor and Source Profiling by GC/MS and Principal Component Analysis of Temporally and Spatially Resolved Ambient Samples, J. of Air & Waste Management Assoc., 2001, 51, 766-784.

15. Jeon, S.J., Lighty, J.S., Jarman, W.M., Kasteler, C., Sheya S.N., Meuzelaar, H.L.C. "Comparison of Thermal Desorption and Solvent Extraction GC/MS Methods for Characterization of Semi-Volatile Organic Compounds in Ambient PM10 Samples," Environ. Anal. Chem., 2002, submitted.

16. Sheya, S.N. 2002. Development of Thermal Desorption-Gas Chromatography/ Mass Spectrometry as a Rapid Method for Ambient Particulate Characterization, Ph.D. Thesis, University of Utah, December 2002.

17. Meuzelaar, H.L.C. "Thermal Sample Treatment Methods in Field Analytical Chemistry" Keynote Lecture, International Symposium on Analytical Pyrolysis of Polymers jointed with The 4th Conference on Analytical Pyrolysis in Japan**,** Nagoya, Japan, January 2002.

18. T. Shoji, F.E. Huggins, G.P. Huffman, W.P. Linak, and C.A. Miller, "XAFS Spectroscopy Analysis of Selected Elements in Fine Particulate Matter Derived from Coal Combustion", *Energy & Fuels*, **16** (2001) 325-329.

19. Y.J. Jiang, M.S. Solum, R.J. Pugmire, D.M. Grant, H.H. Schobert, and P.J. Pappano, "A new method for measuring the graphite content of anthracite coals and soots", *Energy & Fuels*, **16** (2002) 1296-1300.

20. Frank E. Huggins and Gerald P. Huffman, "X-ray Absorption Fine Structure (XAFS) Spectroscopic Characterization of Emissions from Combustion of Fossil Fuels", *Int. J. Soc. Mater. Eng. Resour.*, **10**, No. 1 (2002) 1-13.

21. R.J. Pugmire, M.S. Solum, Y.J. Jiang, A.F. Sarofim, J. Veranth, H.H. Schobert, and P.J. Pappano, "The study of soot formation by solid state NMR spectroscopy", *ACS, Fuel Chemistry Division Preprints*, **47(2)** (2002), 733-735.

22. Sheya, S.A.; Dworzanski, J.D.; Meuzelaar, H.L.C.; "Characterization of Organic Constituents in Tropospheric Aerosols by Novel, Rapid GC/MS Techniques," SCERP Monograph, 2002, (in press).

23. Jeon, S.J., Lighty, J.S., Jarman, W.M., Kasteler, C., Sheya S.N., Meuzelaar, H.L.C. "Comparison of Thermal Desorption and Solvent Extraction GC/MS Methods for Characterization of Semi-Volatile Organic Compounds in Ambient PM10 Samples," Environ. Anal. Chem., 2002, submitted.

24. Artur Braun, N. Shah, F.E. Huggins, G.P. Huffman, K. Kelley, A. Sarofim, S. Wirick, and C. Jacobsen, "Investigation of fine particulate matter from a diesel engine using scanning

transmission x-ray microspectroscopy", *ACS, Fuel Chemistry Division Preprints*, **47(2)** (2002), 627-628.

25. Y.J. Jiang, M.S. Solum, R.J. Pugmire, H.H. Schobert, and P.J. Pappano, "New method for measuring the graphite content of anthracite coals and soots", *ACS, Fuel Chemistry Division Preprints*, **47(2)** (2002), 733-735.

27. F.E. Huggins, D. Panjala, S. Pattanaik, G.P. Huffman, J.R. Kyger, J.D. Robertson, W.P. Linak, and C.A. Miller, "Combining a leaching procedure and XAFS spectroscopy for identification of sulfur and metal species in fine particulate matter from combustion sources", *ACS, Fuel Chemistry Division Preprints*, **47(2)** (2002), 681-682.

28. R.J. Pugmire, M.S. Solum, Y.J. Jiang, A.F. Sarofim, J. Veranth, H.H. Schobert, and P.J. Pappano, "The study of soot formation by solid state NMR spectroscopy", *ACS, Fuel Chemistry Division Preprints*, **47(2)** (2002), 733-735.

29. "Measurement of Fine Particulate Matter Using Electron Microscopy Techniques", Gary S. Casuccio, Steven F. Schlaegle, Traci L. Lersch, Gerald P. Huffman, Y. T. Chen, and Naresh Shah, Air Quality III conference, Sept. 9-12, 2002, Arlington, VA; to be published in a special issue of *Fuel Processing Technology*.

30. "Indirect and Direct Nickel Speciation Measurements of Urban Particulate Matter", Kevin C. Galbreath, Charlene R. Crocker, Carolyn M. Nyberg, Frank E. Huggins, Gerald P. Huffman, and Kenneth P. Larson, *Journal of Environmental Monitoring*, 5 (2003) 56N-61N.

31. "Quantifying Hazardous Species in Particulate Matter Derived from Fossil-Fuel Combustion", Frank E. Huggins, Gerald P. Huffman, William P. Linak, C. Andrew Miller, submitted to *Environmental Science & Technology*.

32. "Assessment of x-ray scattering, diffraction, and spectroscopy for determining the structure of diesel soot", A. Braun, N. Shah, F.E. Huggins, K. Kelly, A. Sarofim, C. Jacobsen, S. Wirick, H. Francis, G.E. Thomas, G.P. Huffman, submitted to *Environmental Science & Technology*.

33. "Size-range analysis of diesel soot with ultra-small angle X-ray scattering", Artur Braun, Frank E. Huggins, Sönke Seifert, Jan Ilavsky, Naresh Shah, Kerry E. Kelly, Adel Sarofim , and Gerald P. Huffman, submitted to *Combustion & Flame*.

34. "A study of Diesel PM with X-ray Microspectroscopy", Artur Braun, Naresh Shah, Frank E. Huggins, Gerald P. Huffman, Sue Wirick, Christopher Jacobsen, Kerry Kelly, and Adel F. Sarofim, submitted to *Fuel*.

Recent presentations made at several national and international conferences are listed below.

**International Conference on Materials Engineering for Resources, Akita, Japan, Oct., 2001**

29. F.E. Huggins and G.P. Huffman, "X-ray absorption Fine Structure (XAFS) Spectroscopic Characterization of Emissions from Combustion of Fossil Fuels" (invited plenary talk).

**Air Quality III, Arlington, VA, September 9-12, 2002**

30. G.P. Huffman, F.E. Huggins, A. Braun, N. Shah, A.F. Sarofim, K.E. Kelly, J.R. Kyger, J.D. Robertson, C. Jacobsen, S. Wirick, W. Linak, and C.A. Miller, "New approaches for investigating the molecular structure of $PM_{2.5}$: leaching-enhanced XAFS and STXM",

Proceedings of Air Quality III, available from the University of North Dakota Energy and Environmental Research Center, Grand Forks, ND.

31. Artur Braun, Naresh Shah, Frank E. Huggins, Gerald P. Huffman, Sue Wirick, Christopher Jacobsen, Kerry Kelly, and Adel F. Sarofim, "Investigation of fine PM from a diesel engine using scanning transmission x-ray microspectroscopy", ibid.
32. G.S. Casuccio, S.F. Schlaegle, T.L. Lersch, G.P. Huffman, Y. Chen, and N. Shah, "Measurement of Fine Particulate Matter Using Electron Microscopy Techniques", ibid.

**Synchrotron Environmental Science II, Argonne National Laboratory, May 6-8, 2002**

37. F.E. Huggins and G.P. Huffman, "XAFS investigation of metals and sulfur in fine particulate from combustion sources" (invited presentation).

**Canadian Light Source Annual Users' Meeting, Saskatoon, SK, Canada, Nov. 15-15, 2002**

38. F.E. Huggins et al., "Application of XAFS Spectroscopy and other synchrotron-based methods for investigation of fine airborne particulate matter from combustion sources" (invited presentation).